

AN ANALYSIS OF PERMANENT MAGNET SYNCHRONOUS
MOTOR DRIVE

CENTRE FOR NEWFOUNDLAND STUDIES

**TOTAL OF 10 PAGES ONLY
MAY BE XEROXED**

(Without Author's Permission)

SAAD MUFTAH ZEID



INFORMATION TO USERS

This manuscript has been reproduced from the microfilm master. UMI films the text directly from the original or copy submitted. Thus, some thesis and dissertation copies are in typewriter face, while others may be from any type of computer printer.

The quality of this reproduction is dependent upon the quality of the copy submitted. Broken or indistinct print, colored or poor quality illustrations and photographs, print bleedthrough, substandard margins, and improper alignment can adversely affect reproduction.

In the unlikely event that the author did not send UMI a complete manuscript and there are missing pages, these will be noted. Also, if unauthorized copyright material had to be removed, a note will indicate the deletion.

Oversize materials (e.g., maps, drawings, charts) are reproduced by sectioning the original, beginning at the upper left-hand corner and continuing from left to right in equal sections with small overlaps.

Photographs included in the original manuscript have been reproduced xerographically in this copy. Higher quality 6" x 9" black and white photographic prints are available for any photographs or illustrations appearing in this copy for an additional charge. Contact UMI directly to order.

**Bell & Howell Information and Learning
300 North Zeeb Road, Ann Arbor, MI 48106-1346 USA**

UMI[®]
800-521-0600



**National Library
of Canada**

**Acquisitions and
Bibliographic Services**

**395 Wellington Street
Ottawa ON K1A 0N4
Canada**

**Bibliothèque nationale
du Canada**

**Acquisitions et
services bibliographiques**

**395, rue Wellington
Ottawa ON K1A 0N4
Canada**

Your file Votre référence

Our file Notre référence

The author has granted a non-exclusive licence allowing the National Library of Canada to reproduce, loan, distribute or sell copies of this thesis in microform, paper or electronic formats.

The author retains ownership of the copyright in this thesis. Neither the thesis nor substantial extracts from it may be printed or otherwise reproduced without the author's permission.

L'auteur a accordé une licence non exclusive permettant à la Bibliothèque nationale du Canada de reproduire, prêter, distribuer ou vendre des copies de cette thèse sous la forme de microfiche/film, de reproduction sur papier ou sur format électronique.

L'auteur conserve la propriété du droit d'auteur qui protège cette thèse. Ni la thèse ni des extraits substantiels de celle-ci ne doivent être imprimés ou autrement reproduits sans son autorisation.

0-612-42466-9

Canada

**An Analysis of Permanent Magnet Synchronous
Motor Drive**

By

©SAAD MUFTAH ZEID

**A thesis submitted to the School of Graduate Studies in
partial fulfillment of the requirements for the degree of
Master of Engineering**

**Faculty of Engineering and Applied Science
Memorial University of Newfoundland**

December 1998

St. John's

Newfoundland

Canada

Abstract

Permanent magnet (PM) excited synchronous machines have shown increasing popularity in recent years for the industrial drive applications due to the recent developments in magnetic materials, power converters, and digital signal processors. The control of a high performance permanent magnet synchronous motor drive for general industrial application has received wide spread interest of the researchers. Interior permanent magnet synchronous motor drives are widely used in high performance applications. In these applications, the drive speed should follow accurately a certain command trajectory and recover from sudden load disturbances very fast. The precise control of the permanent magnet synchronous motor is necessary where the dynamic responses greatly affect the quality of the products.

In this thesis, a complete permanent magnet synchronous motor (PMSM) drive system fed by a PWM voltage source inverter is developed. The design of multi-loop control for the interior permanent magnet synchronous motor drive for high performance application is introduced. Speed controller using synchronous reference frame proportional integral (PI) regulator is employed as an outer loop. Moreover, two synchronous frame PI regulators are employed as inner loops to control the direct and quadrature axis current components of the motor. Implementation of the current controllers in the synchronous reference frame ensures independency of the controllers on the cross coupling between the d-q axis and gives superior performance. The controllers are based on the indirect field oriented control. A systematic mathematical formulation is presented for designing motor controllers. The control scheme is implemented using a high speed digital signal processor (DSP). The experimental results validate the theoretically simulated speed responses with different dynamic operating conditions. These results illustrated the efficacy of the proposed multi-loop control of the PMSM drive.

Acknowledgements

I would like to express my most sincere gratitude and appreciation to my supervisor Professor M. A. Rahman for his guidance, encouragement, advice and active support throughout the preparation of this thesis. I am very grateful for his training which will be a valuable resource in my professional career.

My special thanks to Dr. T. Radwan and Mr. N. Uddin for the many discussions, useful suggestions and their cooperation throughout the course of my study.

Help from all friends of the Faculty of Engineering at the Memorial University of Newfoundland is gratefully acknowledged. Appreciation is also expressed to the technicians for their help.

I also wish to thank the General Secretariat of Education and Scientific Research, Libya, for funding my studies and stay here at the Memorial University of Newfoundland.

Finally, I would like to thank my wife, my daughter, my parents, as well as my brothers and sisters for their encouragement, understanding, patience and support.

Contents

Abstract	ii
Acknowledgement	iii
Contents	iv
List of Figures	vii
List of Symbols	xii
1 Introduction	1
1.1 General review of electric motor drives.....	2
1.2 Permanent Magnet Synchronous Motors.....	3
1.2.1 General.....	3
1.2.2 Classification of PMS motor.....	4
1.2.3 permanent magnet materials.....	7
1.3 Thesis organization.....	8
2 Literature survey and Thesis objective	9
2.1 Literature survey.....	9
2.2 Thesis Objective.....	16
3 Analysis and Modeling of PMSM	18
3.1 Analysis.....	18

3.1.1 Machine winding and air-gap MMF.....	18
3.1.2 Winding Inductances and Voltage Equations.....	21
3.2 Modeling.....	27
3.2.1 Motor modeling.....	27
3.2.2 Park's equation.....	29
3.2.3 Relationship between 3-phase and orthogonal quantity in stationary and synchronous reference frame.....	34
3-2-4 Torque expression of PMSM.....	37
4 System description and control structure	39
4.1 General	39
4.2 Inverter model.....	41
4.3 Sinusoidal Pulse Width Modulation	43
4.4 The sine Triangle Comparison.....	45
4.5 Vector Space and Control Strategies	47
4.6 Controllers structure and design	50
4.7 Current controller design.....	52
4.7 Speed controller design.....	54
5 Simulation and real time implementation	56
5.1 Simulation.....	56
5.2 Simulation results.....	60
5.3 Real-time implementation.....	87
5.3.1 Experimental set up.....	87
5.3.2 Experimental results.....	89

6 Conclusion	95
References	97
Appendices	102
A. Permanent magnet synchronous motor design data	102
B. Subsystem description	103
C. dSPACE DS1102 controller board	112
D. C programs on DSP board	115
E. Program listing	116

List of Figures

1.1	Cross-section of surface mounted PM motor.....	5
1.2	Cross-section of interior type PM motor	6
1.3	Cross-section of inset PM motor.....	6
1.4	Permanent magnet characteristics.....	8
2.1	Direct method of vector control.....	13
2.2	Indirect method of vector control	13
2.3	Current controller scheme.....	17
2.4	Hybrid current controller scheme	17
3.1	2-pole, 3-phase, wye-connected, salient-pole synchronous machine	20
3.2	Sinusoidal distribution, (a) Equivalent distribution of as winding and (b) MMF due to equivalent as winding.....	20
3.3	Park's model of PMSM: (a) d-axis (b) q-axis.....	33
3.4	Stationary d-q axis to synchronously rotating d^r - q^r axes transformation.....	36
4.1	Schematic diagram of the PMSM drive system	40
4.2	Power circuit for the PMSM drive system.....	42
4.3	Sinusoidal pulse-width modulation for three-phase inverter.....	44
4.4	Circuit scheme for generation of the triangular carrier wave.....	46
4.5	Implementation of SPWM using sine triangular comparison in a three-phase	

inverter.....	46
4.6 Basic vector diagram of PMSM (a) general vector diagram (b) vector diagram with $I_d = 0$	49
4.7 Multi-loop control structure of PMSM drive.....	51
4.8 Current controller design	52
4.9 Speed controller structure.....	55
5.1 Structure of the PMSM mathematical model.....	58
5.2 Simulink model of the PMSM drive system	59
5.3 Drive responses at full load with speed command of 180 rad./sec., (a) speed response and (b) motor phase current.....	61
5.3 Drive responses at full load with speed command of 180 rad./sec, (c) Steady state voltage command and (d) motor phase voltage.....	62
5.3 Drive responses at full load with speed command of 180 rad./sec., (e) q-axis current, and (f) d-axis current.....	63
5.4 Drive responses at no load with speed command of 180 rad./sec., (a) speed response, and (b) motor phase current.....	64
5.4 Drive responses at no load with speed command of 180 rad./sec., (c) steady state voltage command and (d) motor phase voltage.....	65
5.4 Drive responses at no load with speed command of 180 rad./sec., (e) q-axis current and (f) d-axis current	66
5.5 Drive responses at full load with speed command of 150 rad./sec., (a) speed response and (b) motor phase current.....	67
5.5 Drive responses at full load with speed command of 150 rad./sec., (c) motor	

phase voltage and (d) voltage command.....	68
5.5 Drive responses at full load with speed command of 150 rad./ sec., (e)q-axis and current and (f) d-axis current.....	69
5.6 Drive responses at no load with speed command of 150 rad./sec., (a) speed response and (b) motor phase current.....	70
5.6 Drive responses at no load with command speed of 150 rad./sec., (c) steady state voltage command and (d) motor phase voltage.....	71
5.6 Drive responses at no load with speed command of 150 rad./sec., (e) q-axis current and (f) d-axis current.....	72
5.7 Drive responses for the step change in the reference speed at full load, (a) speed response and (b) motor phase current.....	74
5.7 Drive responses for the step change in the reference speed at full load, (c) q-axis current and (d) d-axis current.....	75
5.7 Drive responses for the step change in the reference speed at full load, (e) motor phase current during speed increase and (f) motor phase current during speed decrease.....	76
5.7 Drive responses for the step change in the reference speed at full load, (g) voltage command during step increase in speed and (h) voltage command during step decrease in speed.....	77
5.7 Drive responses for the step change in the reference speed at full load, (j) motor phase voltage during the step increase of speed and (l) motor phase voltage during the decrease of speed.....	78
5.8 Drive responses for step change in the reference speed at no load,(a) speed	

response and (b) q-axis current.....	79
5.8 Drive responses for the step change in the reference speed at no load, (c) voltage command during step increase of speed and (d) voltage command during step decrease of speed.....	80
5.9 Drive responses for the step change in the load with speed command of 188 rad./sec., (a) speed response and (b)q-axis current	82
5.9 Drive responses for the step change in load with speed command of 188 rad./sec., (c) phase voltage command and (d) motor phase current.....	83
5.10 Drive responses for the step change in load with speed command of 150 rad./sec., (a) speed response and (b)q-axis current.....	84
5.10 Drive responses for the step change in load with speed command of 150 rad./sec., (c) phase voltage command and (d) motor phase current.....	85
5.11 Drive responses for the speed reversal with speed command of 180rad./sec to -180 rad./sec., (a) speed response and (b) q-axis current.....	86
5.12 Experimental set up for PMSM.....	88
5.13 Drive responses at full load with speed command of 150 rad./sec., (a) speed response(speed scale 66.67rad./sec/div) and (b)motor phase voltage (voltage scale 100 volt/div).....	90
5.14 Drive responses for the step change in the speed command. At half load, (a) speed response (speed scale 66.67 rad./sec/div) and (b) q-axis current (current scale 1.25 A/div).....	91
5.15 Drive responses for step change in the command speed at full load,(a)	

speed response(speed scale 66.67rad./sec/div) and (b)motor phase current (current scale 3A/div).....	92
5.16 Drive responses for step change in load with speed command of 150 rad./sec., (a) speed response(speed scale 66.67 rad./sec/div) and (b) motor phase current (current scale 3A/div).....	93
5.17 Drive responses for change in load with speed command of 180 rad. / sec., (a) speed response (speed scale 66.67 rad. /sec./div) and (b) motor phase current (current scale 3A/div).....	94
B.D Simulink model of the PMSM drive system	104
B.D ₁ Multi-loop control.....	105
B.D ₂ Voltage V_command subsystem.....	106
B.D ₃ Comparator.....	107
B.D ₄ Block diagram of the inverter	108
B.D ₅ Block diagram of the coordinate transformation	109
B.D ₆ Block diagram of the PMSM voltage equation.....	110
B.D ₇ Block diagram of Park's transformation.....	111
C. 1 Block diagram of the DS1102 DSP board	114

List of Symbols

θ_r	: rotor angular displacement
ϕ_s	: stator angular displacement
ϕ_r	: relative angular displacement of the rotor
N_{as}	: number of turns of the “as” winding
as	: a phase of stator winding
N_p	: maximum conductor density expressed in turn/radian
N_s	: number of turns of the equivalent sinusoidal distributed winding
i_{as}, i_{bs}, i_{cs}	: stator phase currents
α_1, α_2	: constants used in minimum and maximum air-gap
H	: magnetic field intensity
B_r	: magnetic flux density
μ_0	: permeability of free space
μ_r	: relative permeability
Φ	: flux linking a single turn
l	: length of the air gap
r	: mean radius of the air gap
ξ	: dummy variables of integration

λ_{as}	: total flux linkage in stator phase "as"
L_{ls}	: stator leakage inductance
$L_{asas}, L_{bsbs}, L_{cses}$: stator self inductances
λ_{asbs}	: the mutual flux linkage in as winding due to current in bs winding
$M_{asbs}, M_{bscs}, M_{ascs}$: stator mutual inductances
λ_{fd}	: total flux linkage in the field
L_{fdfd}	: field self inductance
$M_{asfd}, M_{bsfd}, M_{csfd}$: field mutual inductances
λ_m	: flux linkage due to permanent magnet
v_{as}, v_{bs}, v_{cs}	: stator phase voltages
r_{as}, r_{bs}, r_{cs}	: stator phase resistances
p	: operator d/dt
I_d^r, I_q^r	: direct and quadrature axis currents in the rotor reference frame
I_d^s, I_q^s	: direct and quadrature axis currents in the stationary reference frame
V_d^r, V_q^r	: direct and quadrature axis voltages in the rotor reference frame
V_d^s, V_q^s	: direct and quadrature axis voltages in the stationary reference frame
λ_d^r, λ_q^r	: direct and quadrature axis flux linkages in the rotor reference frame
L_{mg}	: d-axis magnetizing inductance
L_{mq}	: q-axis magnetizing inductance
P	: number of pair poles
ω_r	: rotor angular speed
v_a, v_b, v_c	: phase voltages

P_{in}	: input power in Watt
T_{em}	: electromechanical torque
L_q	: q-axis inductance
L_d	: d-axis inductance
J_m	: moment of inertia
B_m	: friction coefficient
T_l	: load torque
V_B	: inverter dc input voltage
K_I	: integral constant
K_p	: proportional constant
K_t	: torque constant
ω_r^*	: speed command
i_d^*, i_q^*	: d-q axis current commands

Chapter 1

Introduction

A significant technological change has occurred in motor drive system in recent years. The main feature of the drive system refers to its capability to operate within the given speed and torque limits. Other desirable features of variable speed drives include low space requirement, low maintenance, and capability of the speed or torque to follow the speed or torque command. Recent developments in magnetic materials, semiconductor and microprocessor technology have made significant impact on the design and control of electric motors. The uses of dc, ac induction, and conventional wire-wound excited synchronous motor drives are being increasingly replaced by the permanent magnet synchronous motor (PMSM) drives. Increasing interest has been shown in using permanent magnet synchronous motors with variable-frequency inverters in adjustable-speed drive, taking advantage of increased efficiency and power factor product to reduce volt-ampere requirement [1]. The PMS motor offers several advantages over other motors. The control of PMS motors is done entirely through the stator side and there is no rotor side excitation control. Vector control is used for the variable speed PMS motor drives where the speed and rotor position are used as feedback control of the drive. Vector controlled permanent magnet synchronous motor drive offers

a number of attractive features such as smooth operations at a wide range of speeds, high torque capability, and high efficiency along with higher power factor.

1.1 General review of electric motor drives

DC motors were used for variable speed applications and they offer various control features of simplicity to control due to the decoupled nature of the field and armature magnetomotive force (MMF). DC motor drives were proven to be excellent in both transient and steady state performances [2]. However, disadvantages of dc motors such as high cost, the mechanical friction between the commutators and the brushes that require high maintenance, frequent changing of the brushes and the sparking that occurs by the brushes limit the power rating of the motor. These reasons make the dc drive system less attractive.

Induction motors have been known to be rugged, reliable, simple in construction and economical for a long time. However, they have some limitations associated with their use in high performance variable speed drive applications. One of the limitations that induction motors always operate at lagging power factor because of their rotor induced current is supplied from the stator side. Secondly, the induction motor always runs at speeds lower than the synchronous speed, so the control of these induction motors is very complex. Thirdly, additional slip dependent power losses and torque pulsation due to higher harmonics originated from the power converters are considered to be major problems in inverter-fed induction motor drives. Fourthly, the real time implementation of the induction motor drive requires sophisticated modeling and estimation of machine parameters with complex control circuitry.

Ac motors have been favoured for constant speed applications. The dynamic control of the ac drives is complex compared to the dc motor drive, but the recent developments in power electronics and in very large scale integrated [VLSI] circuits have simplified the system complexity to a large extent, leading to tremendous growth of ac drive technology. Synchronous motors of wire-wound rotor type are common in high power ac drive systems because the field current can be controlled from the rotor side. However, the presence of the field coil, dc supply and slip rings, makes these drives less efficient. Due to the significant technological advancement that has occurred in motor drive in recent years arising from the concurrent development of permanent magnet materials and power semiconductor switching device technologies, the PMS motors are becoming increasingly popular in varied drive applications.

1.2 Permanent Magnet Synchronous Motors

1.2.1 General

A permanent magnet synchronous motor consists of a stator with three phase windings and a rotor mounted with permanent magnets to provide the field flux. The permanent magnet synchronous motor is not subjected to the limitation of dc, ac induction and wire-wound excited synchronous motors as previously discussed. It does not need an external supply to excite the rotor field and hence the field winding and slip rings are eliminated. The absence of the field winding reduces the cost and eliminates the power losses associated with this winding. The permanent magnet synchronous motor occupies less space than field winding for a given size, which leads to more compact design. Unlike in induction motor there is no slip dependent rotor copper loss in a

permanent magnet synchronous motor. The permanent magnet synchronous motor is more efficient and has a larger torque to inertia ratio and power density when compared to the induction motor. In addition, for the same output capacity the PMS motor is smaller in size and lower in weight. It is preferable for certain high performance applications like in machine tools and aerospace.

1.2.2 Classification of PMS motor

The rotor of a PMS motor has a special design to give the required characteristics. Numerous rotor geometries of permanent magnet synchronous motors have been developed. Depending on the orientation of the magnetization, the rotor can be classified into two types, radially oriented type and circumferential type [3]. In radially oriented type, the rotor magnets are oriented such that the direction of magnetization of the permanent magnets in the machine is radial. Thus, the air gap flux density above the magnets is approximately the same as the magnetic flux density. This type of rotor construction using low residual flux density magnetic material such as ferrite magnets, results in very low air gap flux density. However, with the development of high-energy permanent magnet materials such as neodymium boron iron (NdBFe) efficient motor design using this type of construction is possible due to their high residual flux density and large coercivity. The circumferential type is suitable for motors with large number of poles and using magnets with low residual flux density.

Depending on the location of the magnets in the rotor, the permanent magnet motor can be classified into three different configurations, namely the surface mounted, interior, and inset types [4,5,6]. The motor with surface magnets as shown in Figure 1.1 is essentially non-salient type. It has a large air gap and is popularly used in a brushless dc

motor drive as for example in computer hard disk drives. The large air gap weakens the armature reaction effect, and therefore the operation is essentially restricted to low speed and constant torque region. The inset permanent magnet motor as shown in Figure 1.2 has a small but relatively smooth air gap. The interior permanent magnet motor as shown in Figure 1.3 overcomes the above drawbacks of surface magnet type because of its narrow and smooth air gap. Moreover, the motor torque is contributed by reluctance component due to the difference between direct and quadrature axis reactances as well as the permanent magnet field component. Unlike surface mounted magnet type, it has advantages for high-speed applications.

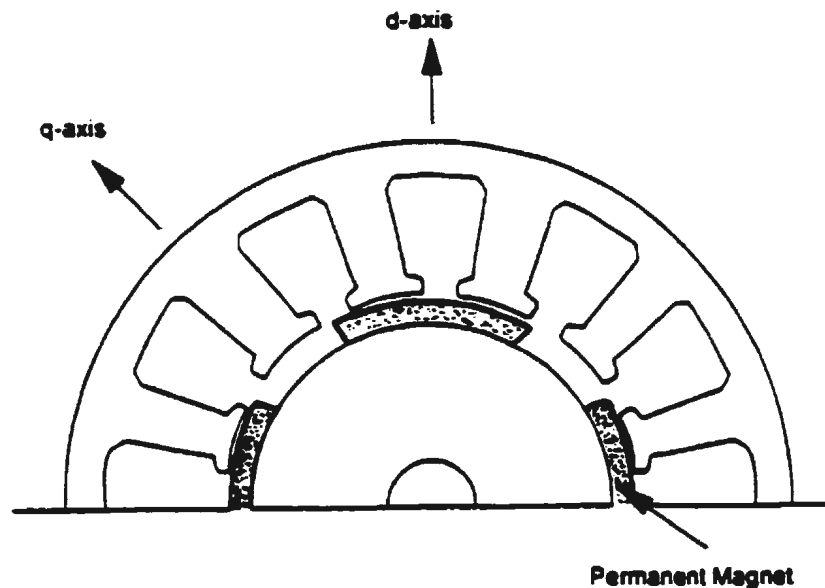


Figure 1.1: Cross-section of surface mounted PM motor

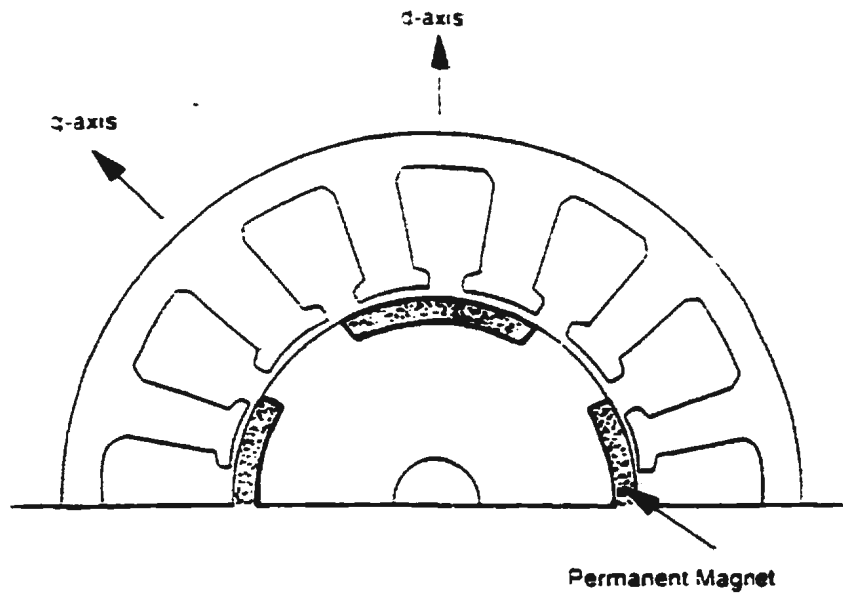


Figure 1.2: Cross-section of inset type PM motor

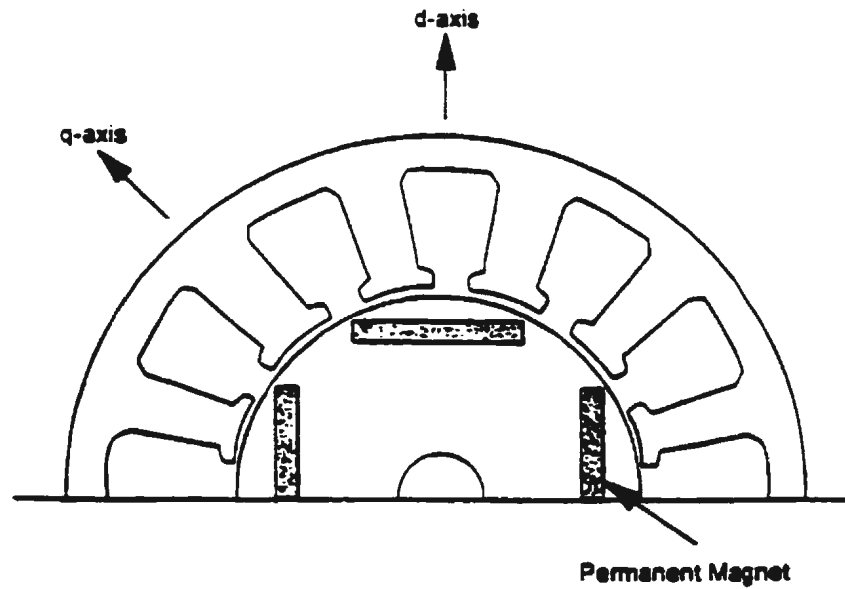


Figure 1.3: Cross-section of interior PM motor

1.2.3 Permanent magnet materials

The development of a permanent magnet motor is directly related to the recent advances of the permanent magnet materials technology over the past two decades [7]. The characteristics of the demagnetization curves for some permanent magnet materials are shown in Figure 1.4. The materials are compared on the basis of the residual flux density, coercive force and cost. The Alnicos are alloys of iron with aluminum, nickel, copper, and cobalt which were developed by Nishima in 1932. Alnico materials have relatively high residual flux density B_r , high service temperature tolerance, and good thermal stability, but may be easily demagnetized due to low value of coercive force H_c [8]. Barium and strontium ferrite materials were introduced in 1951 and 1963 respectively, which are low in cost and have excellent demagnetization linearity, limited by their low maximum energy product $(BH)_{max}$. This is due to the lower value of residual flux density B_r [9]. Permanent magnet machines using these ferrite materials tend to be bulky because of low remnance. Compared to Alnico magnets, ferrite materials are highly resistant to demagnetization and are low in cost. Cobalt-Samarium, first introduced in 1963, has a higher energy product and excellent temperature insensitivity than the ferrite [10,11]. However, its high cost restricts its use for application and may require care in handling since the ground powder air mixture is pyrophoric and magnetic force is strong. The Neodymium-Boron-Iron magnet (NdBFe) which has been introduced recently (1983), has maximum remnance and coercive force. Its cost is lower than Cobalt-samarium. Therefore, it will be used greatly for applications in permanent magnet motors. This material, however, has some temperature sensitivity, which must be taken into consideration during machine design. The NdBFe magnet has

large energy product $(BH)_m$ in excess of 80 MGO_e. This material is quite ductile and easily machineable. The NdBF_e magnet is susceptible to oxidation unless protected by a non-oxidation coating.

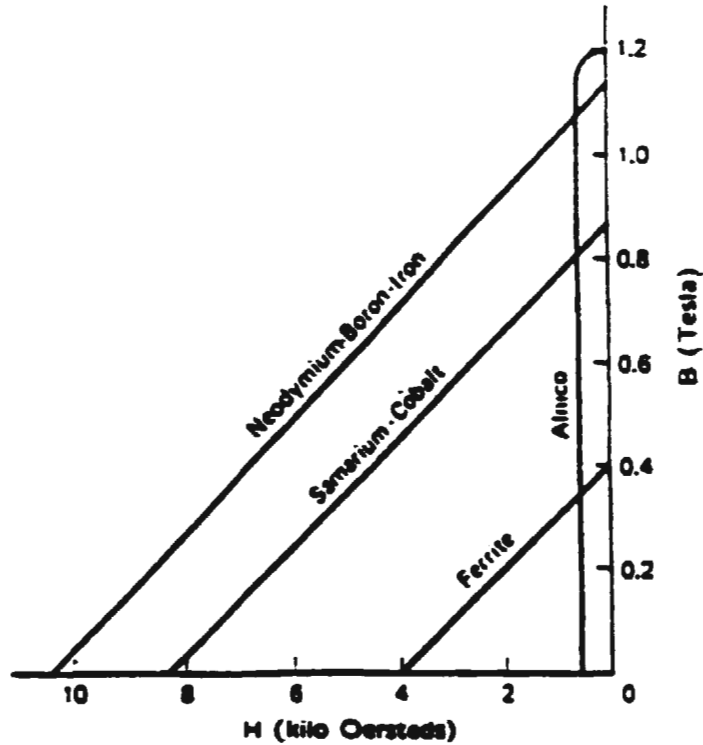


Figure 1.4: Permanent magnet characteristics

1.3 Thesis organization

This thesis consists of six chapters: The introduction has been given in the chapter one. Chapter two provides the literature survey of vector control techniques for ac motor drive and provides a brief thesis objective. Chapter three provides the theoretical analysis and modeling of PMS motor. Chapter four includes system description and controller structure design. Chapter five includes the simulation and real time experimental implementation. Chapter six includes the conclusion.

Chapter 2

2.1 Literature survey

With the advancement of technology, the area of applications for electric motors increases in a versatile manner. Recent developments in magnetic materials, semiconductor and microprocessor technology have made revolutionary advancements on the design and control of electric motors. Ac drives in industrial applications are rapidly increasing. It will replace the dc motors in motion control applications and possibly make dc motors relatively obsolete by the beginning of the next century. The dynamics and control of ac drives are very complex, and their complexity increases for higher performance requirements. Many different control techniques of varying degree of complexity have appeared on the nature of drive applications.

The simple open-loop volt/hertz (v/f) control method has been popularly used for long time in low performance drives. Closed-loop with flux control, torque control, slip control, and angle control have been used where better drive performance is demanded, but these scalar control techniques have drawbacks due to non-linearity of the motor model and inherent coupling between the direct and quadrature axis quantities. This causes sluggish responses which are unacceptable for high-performance drive applications with fast and precise torque response. In order to achieve these required

characteristics, several methods have been proposed to obtain fast response. The vector or field oriented control techniques are being accepted almost universally for control of ac drive. Vector control technique displays excellent performance for variable speed ac drive, particularly in the case of permanent magnet synchronous motors employing modern static inverters. In vector control techniques both the phase angle and the magnitude of the current have to be controlled. These control techniques were developed in Germany in the early of 1970's. Blaschke [12] and Hasse [13] invented the indirect method. At that time, it was very difficult to implement such control techniques because of their complexity. With the advancements of microcomputer era, VLSI, and high switching devices, such control is no longer a problem. The principle of vector control is to eliminate the coupling between the direct (d) and quadrature (q) axes. This can be achieved by coordinate transformation, and then the ac motor behaves like a separately excited dc motor. As for dc machines, torque control in ac machines is also achieved by controlling the motor current. However, in contrast to the dc machines, in an ac machine both the magnitude and phase angle of the stator current need to be controlled. This is achieved by defining a time-varying vector which corresponds to a sinusoidal flux wave moving in the air gap of the machine. When referring the mmf wave of the stator current to this flux wave, it is realized that only the quadrature axis component of the mmf wave is contributing to the torque, whereas the direct axis component affects the magnitude of the flux. Hence, the stator current phasor is defined in a frame of reference defined by the time-varying field or in field coordinates. This indicates a close correspondence to the dc machines, with the direct axis component of the stator current vector being analogous to the field current and the quadrature axis component to the armature current.

Vector control can be performed in a reference frame fixed to the stator-flux, rotor flux or magnetizing-flux space vector. The direct and quadrature axis stator currents are obtained in the corresponding reference frame. Based on which reference frame is chosen, vector control can be classified as: rotor flux oriented control, stator flux oriented control and magnetizing flux oriented control [14]. Out of these three methods, rotor flux oriented control is the most popular one in ac drives. The reason for this is that in the other two cases there exists a coupling between the torque-producing stator current component and the stator magnetizing current. In rotor flux oriented control a natural decoupling exists between the two components.

Based on the control signals, vector control is classified as direct and indirect methods. The principle implementation of the direct method of vector control is shown in Figure 2.1. The method depends on the direct measurement of the stator (or rotor) flux. By using flux sensors, the flux components ψ_{dm}^s and ψ_{qm}^s can be measured directly. The unit vectors, $\cos\omega_e t$, and $\sin\omega_e t$ are generated from the d and q components of the air gap flux so that $\cos\omega_e t$ and $\sin\omega_e t$ are co-phasal to ψ_{dm}^s and ψ_{qm}^s , respectively. With the help of unit vectors, the principal control parameters i_{ds}^* and i_{qs}^* , which are dc quantities and proportional to flux and torque commands, respectively are converted to a stationary reference frame. These control parameters are then converted to phase current commands for the inverter. On the other hand, in the indirect method of field oriented control the unit vectors, $\cos\theta_e$ and $\sin\theta_e$ are calculated from the information of the rotor position. Figure 2.2 explains the principle of this method. This technique of vector control is more sensitive to parameter variation and the parameters must be known

accurately. Pillay and Krishnan presented modeling, simulation, analysis and controller design of high performance vector controlled PMSM drives [15-19]. The d-q axis model of the PMSM has been used to examine the transient and steady state behaviors of a high performance vector controlled drive.

Recent advancements in microelectronics and VLSI technology led to the practical utilization of the microprocessors which brought a new dimension in motion control technology. The microprocessors make it possible to realize very complicated control strategy. Bose and Szczesny proposed a microcomputer-based control of an interior PMSM drive system [20]. In microprocessor application, the computational time is critical for faster dynamics of the system implementation. In this respect, the uniprocessor based motor control is limited in offering higher computing speed. In recent years, multiprocessor-based motor control systems have received considerable attention. This allows faster systems to be controlled. One of the typical applications using multiprocessor for field-oriented control was developed in 1985 by F. Harashima, et. al. [21]. Another application using multiprocessor for field-oriented control was proposed by T. Liu, et. al. [22]. In this proposal, two microprocessors were used, in which one microprocessor was used to execute controller algorithms, and the other microprocessor was used to execute the current controller to generate firing signals for the inverter transistors.

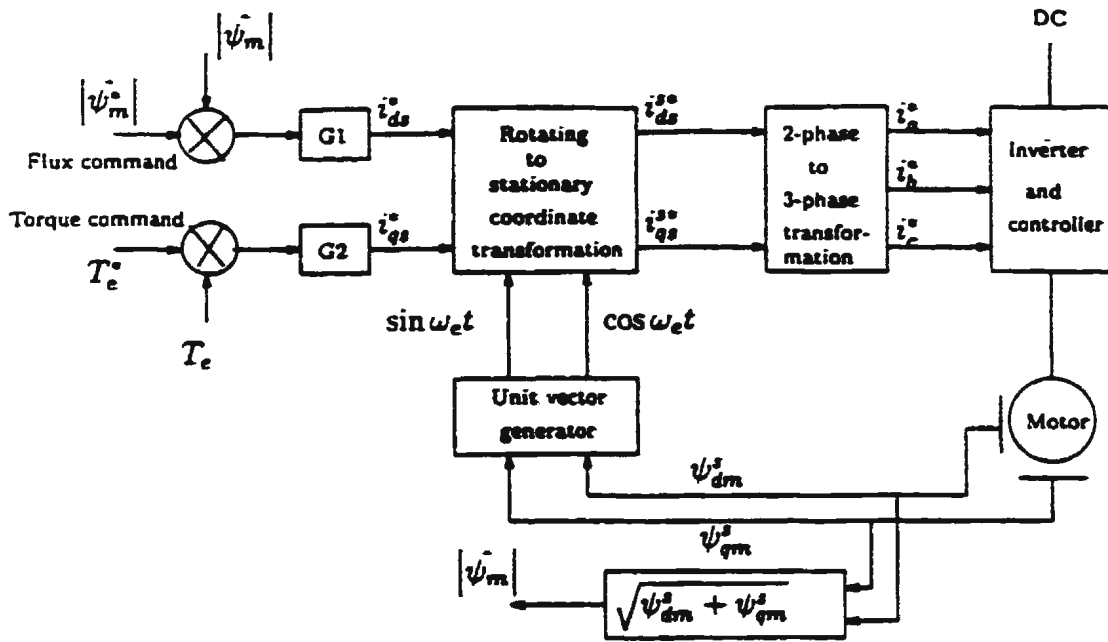


Figure 2.1: Direct vector control of PMSM

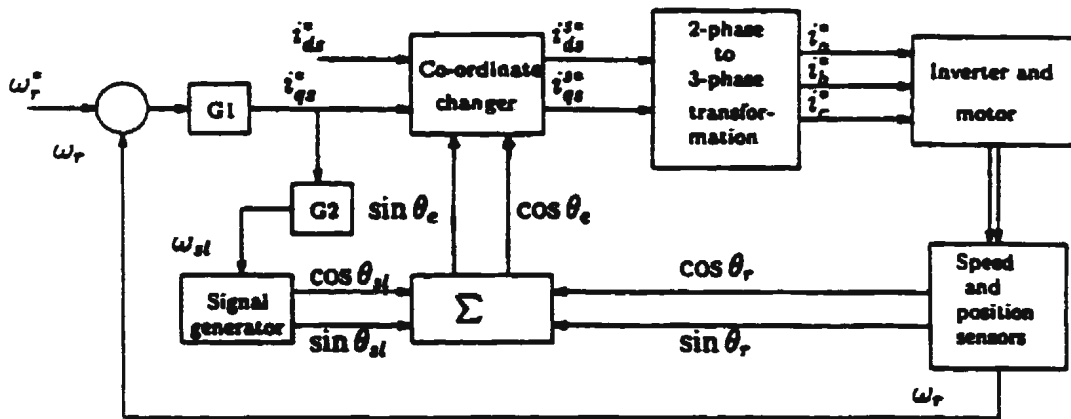


Figure 2.2: Indirect vector control of PMSM

Now-a-days, digital signal processors (DSP) have been introduced in the area of ac drives in order to give general solution. This type of processor has been developed for signal processing applications requiring high-speed and real-time computation, often for communications systems, but also applicable to digital control. Architecturally they are often quite different from normal microprocessors, and they have a separate program bus for instructions. For speed, the arithmetic logic unit (ALU) will have a hardware multiplier array, which can carry out its function in a single instruction cycle. The DSP starts at 16-bits; and 24-bits and 32-bits devices are also available. Because of their numerical capabilities, as well as the fact that very little peripheral hardware is required, DSPs are currently being considered for real-time implementation of vector control. Pillay, et. al. [23] proposed a design of DSP-based vector control scheme for the PMSM drive.

Current controlled voltage source inverters (VSI) play an important role in improving the motor system dynamics in high performance ac drive systems under vector control techniques. In such systems, the current controller has direct influence on the drive performance and its design requires particular considerations. The basic requirements from the controllers are low harmonics to reduce losses and noise in the motor, and fast response to provide high dynamic performances. Performance of various current control schemes for the VSI fed PMSM drive have been investigated and reported [24-26]. However, each current control scheme has its own advantages and drawbacks with regard to accuracy and dynamic response over the entire speed ranges.

The hysteresis controller is used to control the load current by forcing it to follow the reference current. This is achieved by the switching action of the inverter to keep the current within the hysteresis band. A simplified diagram of a typical three-phase hysteresis current controller is shown in Figure 2.3 with the switching “SW” off. The load currents are sensed and compared to the respective command current using three independent hysteresis comparators having hysteresis band H . The output signals of the comparators are used to activate the inverter power switches. The advantages of hysteresis current controller are its simplicity, fast response and good accuracy. However, the hysteresis controller has some drawbacks, because it generates random PWM switching pattern in order to achieve concurrence between the reference and feedback currents [27]. As a result switching frequency varies over the fundamental period.

In the ramp comparator control scheme, the motor currents are sensed and compared to the references, which are generated from the field oriented controller. The error signals are compared to a triangular waveform to produce constant frequency pulse width modulated drive signals for the inverter switches as shown in Figure 2.3 with switching “SW” on and reducing the hysteresis band to zero. This switching frequency is limited to that of the triangular waveform. This is the main advantage of the ramp comparator controller. Moreover, the amplitude and phase errors are introduced in the motor line currents. Good performance can be obtained at low and medium speeds. At high speeds, the amplitude and phase errors introduced by the ramp comparator may become unacceptable for certain applications, especially high performance applications.

To overcome the drawbacks of the current controllers, a hybrid current scheme has been proposed [28]. The principle of the hybrid scheme is shown in Figure 2.4. It is shown from the figure that the controller has two modes of operation, the hysteresis mode and ramp comparator mode. This gives better response over the entire speed ranges. Current controlled VSI gives fast response. This type of control is usually implemented in the stationary reference frame. This makes the controller response dependent on the motor parameters which are not constant and affected by the operating conditions

2.2 Thesis Objective

The objective of this thesis is to develop and implement a complete PMSM drive system for high performance application. Design of the multiple loop control scheme for an interior permanent magnet synchronous motor drive system. Speed control using synchronous frame PI regulator employed as outer loop. On the other hand, two synchronous PI regulators are proposed to be employed as inner loops to control the direct and quadrature axis current components of the motor. Implementation of the current controllers in the rotor synchronous reference frame ensures independency of the controllers on the cross coupling between the d-q axis quantities and gives excellent terminal performances of the drive system.

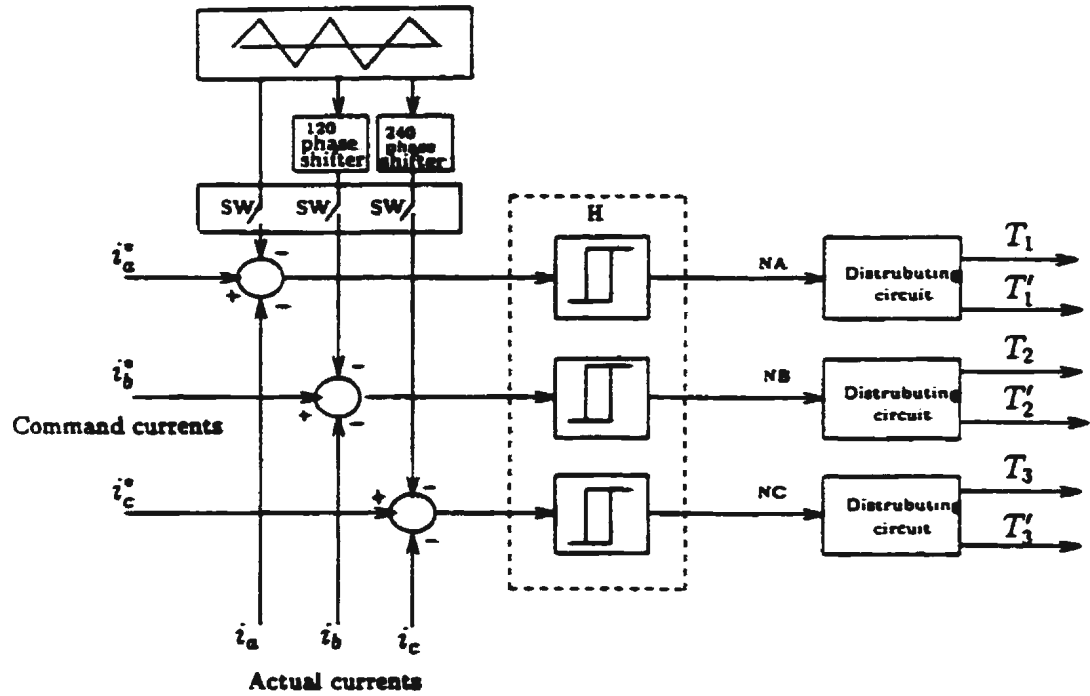


Figure 2.3 Current controller scheme

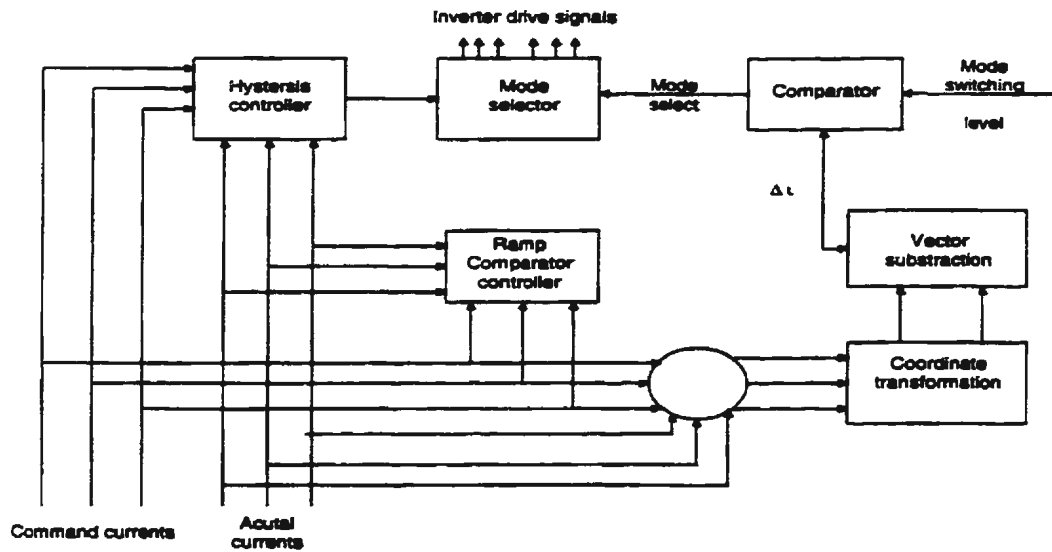


Figure 2.4 Hybrid current controller scheme

Chapter Three

Analysis and Modeling of PMSM

3.1 Analysis

The permanent magnet synchronous motor is the same as the field excited synchronous motor from the analytical point of view. The only exception is that the rotor field due to permanent magnet excitation gives a constant flux. A two pole, three phase, wye-connected salient pole machine is chosen for this analysis as shown in Figure 3.1 [29].

3.1.1 Machine winding and air-gap MMF

The stator windings of the synchronous machine are embedded in slots around the inside circumference of the stator yoke. The stator winding is displaced 120° with respect to each other as illustrated in Figure 3.1. This winding produces an air-gap MMF which is a closely sinusoidal air-gap MMF with respect to the angular displacement about the air gap. The angular displacement of the stator is denoted by ϕ_s . The angular displacement of the rotor is θ_r , and the angular velocity of the rotor is ω_r . For a given angular displacement relative to the given axis we can relate ϕ_s , ϕ_r , and θ_r as.

$$\phi_s = \phi_r + \theta_r \quad (3.1)$$

The analysis may be simplified by considering only one of the stator windings at a time and assuming that the winding may be approximated as a sinusoidally distributed winding.

A sinusoidally distributed winding and a sinusoidal air-gap MMF_s are depicted in Figure 3.2. The distribution of the winding may be written as

$$N_{as} = N_p \sin \phi_s \quad 0 \leq \phi_s \leq \pi \quad (3.2)$$

$$N_{as} = -N_p \sin \phi_s \quad \pi \leq \phi_s \leq 2\pi \quad (3.3)$$

Where N_p is the maximum conductor density expressed in turns/radian. If N_s represents the number of turns per phase of the equivalent sinusoidally distributed winding, then

$$N_s = \int_0^\pi N_p \sin \phi_s d\phi_s = 2 N_p \quad (3.4)$$

$$N_p = N_s / 2 \quad (3.5)$$

The phase 'as' winding is expressed as

$$N_{as} = -(N_s / 2) \sin \phi_s \quad (3.6)$$

The air-gap MMF waveform is also shown in Figure 3.2b. The MMF waveform of the equivalent phase "as" winding (letter 'a' stands for phase a and 's' stands for stator) is

$$\text{MMF}_{as} = (N_s/2) i_{as} \cos \phi_s \quad (3.7)$$

Similarly for the other two phases "bs" and "cs" it can be written as

$$\text{MMF}_{bs} = (N_s/2) i_{bs} \cos (\phi_s - 2\pi/3) \quad (3.8)$$

$$\text{MMF}_{cs} = (N_s/2) i_{cs} \cos (\phi_s + 2\pi/3) \quad (3.9)$$

The total air-gap MMF_s produced by the stator currents can be obtained by adding the equations (3.7-3.9) as

$$\text{MMF}_s = N_s/2 [i_{as} \cos \phi_s + i_{bs} \cos (\phi_s - 2\pi/3) + i_{cs} \cos (\phi_s + 2\pi/3)] \quad (3.10)$$

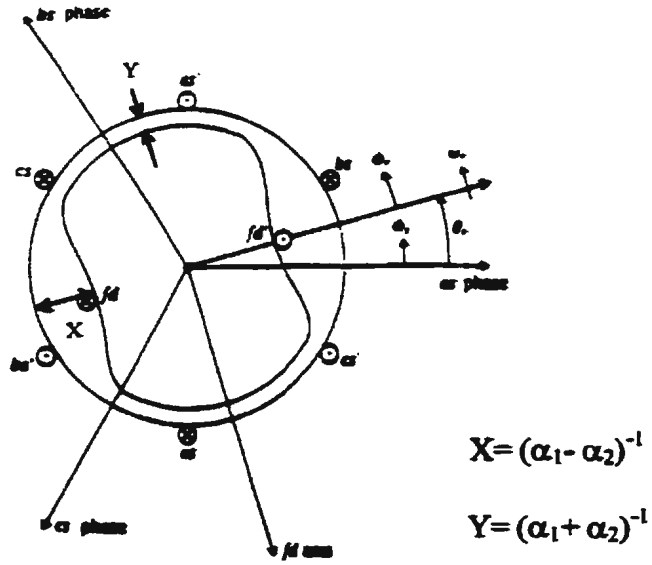


Figure.3.1 2-pole, 3-phase, wye-connected, salient-pole synchronous machine

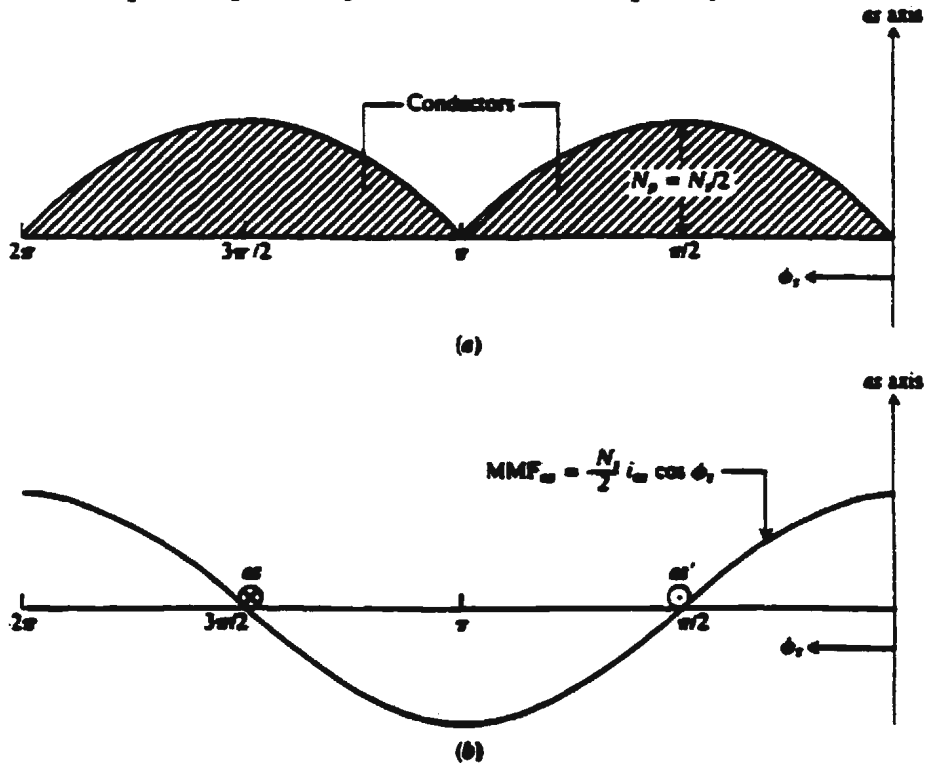


Figure3.2 Sinusoidal distribution. (a) Equivalent distribution of "as" winding. (b) MMF due to equivalent "as" winding

3.1.2 Winding Inductances and Voltage Equations

As shown in Figure 3.1 the winding is shown as sinusoidally distributed one. In a magnetically linear system the self-inductance of a winding is the ratio of the flux linked by a winding to the current flowing in the winding with all other winding currents zero. Mutual inductance is the ratio of flux linked by one winding due to current flowing in a second winding with all other winding currents zero including the winding for which the flux linkages are being determined. In this analysis it is assumed that the air gap length may be approximated as [30].

$$g(\phi_r) = \frac{1}{\alpha_1 - \alpha_2 \cos 2\phi_r} \quad (3.11)$$

and,

$$g(\phi_s - \theta_r) = \frac{1}{\alpha_1 - \alpha_2 \cos 2(\phi_s - \theta_r)} \quad (3.12)$$

Where the minimum air gap length is $1/(\alpha_1 + \alpha_2)$ and the maximum is $1/(\alpha_1 - \alpha_2)$

The air gap magnetomotive force (MMF) can be expressed as

$$\text{MMF} = H \times g = \frac{B_r}{\mu_r \mu_0} g \quad (3.13)$$

Where H is the magnetic field intensity, B_r is the magnetic flux density and μ_0 is the permeability of free space and is given by $4\pi \times 10^{-7}$ H/m, and μ_r is the relative permeability.

Since the MMF is a function of ϕ_s , the equation (3.13) can be modified as

$$\text{MMF}(\phi_s) = H \times g = \frac{B_r(\phi_s, \theta_r)}{\mu_r \mu_0} g(\phi_s - \theta_r) \quad (3.14)$$

The air gap flux density due to current in the “as” winding with all other currents zero, can be obtained by substituting (3.7) and (3.12) into (3.14).

$$B_r(\phi_s, \theta_r) = \mu_0 \mu_r \frac{\text{MMF}_{as}(\phi_s)}{g(\phi_s - \theta_r)} \quad (3.15)$$

$$= \mu_0 \mu_r \frac{N_s}{2} i_{as} \cos \phi_s [\alpha_1 - \alpha_2 \cos 2(\phi_s - \theta_r)] \quad (3.16)$$

Similarly the flux density with all currents zero except i_{bs} is

$$B_r(\phi_s, \theta_r) = \mu_0 \mu_r \frac{N_s}{2} i_{bs} \cos(\phi_s - 2\pi/3) [\alpha_1 - \alpha_2 \cos 2(\phi_s - \theta_r)] \quad (3.17)$$

and the flux density with all currents zero except i_{cs} is

$$B_r(\phi_s, \theta_r) = \mu_0 \mu_r \frac{N_s}{2} i_{cs} \cos(\phi_s + 2\pi/3) [\alpha_1 - \alpha_2 \cos 2(\phi_s - \theta_r)] \quad (3.18)$$

Assuming that the field winding is sinusoidally distributed with N_f equivalent turns.

Thus, the air gap MMF due to direct axis field current i_{fd} flowing in the “fd” winding may be expressed as.

$$\text{MMF}_{fd} = -(N_f / 2) i_{fd} \sin \phi_r \quad (3.19)$$

Therefore, the air gap flux density due to i_{fd} with all other currents zero may be expressed as.

$$B_r(\phi_r) = -\mu_0 \mu_r \frac{N_f}{2} i_{fd} \sin \phi_r (\alpha_1 - \alpha_2 \cos 2\phi_r) \quad (3.20)$$

To determine the self inductance and mutual inductance it is necessary to compute the flux linking due to its own current and due to current flowing in another winding. The flux linkages of a single turn of a stator winding located at ϕ_s angle and whose span length is π radian, is given by

$$\Phi(\phi_s, \theta_r) = \int_{\phi_s}^{\phi_s + \pi} B_r(\xi, \theta_r) r l d\xi \quad (3.21)$$

Where Φ is the flux linking a single turn, l is the axial length of the air gap of the machine, r is the mean radius of the air gap, and ξ is a dummy variable of integration. To obtain the flux linkage of an entire winding the flux linked by each turn must be summed. This summation may be accomplished by integration over all coil sides carrying current. The total flux linkage of the “as” winding due to current flowing only in the “as” winding becomes.

$$\lambda_{as} = L_{ls}i_{as} + \int N_{as}(\phi_s)\Phi(\phi_s, \theta_r)d\phi_s \quad (3.22)$$

$$= L_{ls}i_{as} + \int N_{as}(\phi_s) \int_{\phi_s}^{\phi_s+\pi} B_r(\xi, \theta_r)rl d\xi d\phi_s \quad (3.23)$$

Where L_{ls} is the stator leakage inductance due to the leakage flux at the end turns. By substituting (3.3) with N_p replaced by $N_s/2$ and (3.16) for $B_r(\xi, \theta_r)$ into (3.23) we get the expression for a phase stator flux linkage λ_{as} as

$$\lambda_{as} = L_{ls}i_{as} - \int_{\pi}^{2\pi} (N_s/2) \sin\phi_s \int_{\phi_s}^{\phi_s+\pi} \mu_r\mu_0(N_s/2) \cos\xi[\alpha_1 - \alpha_2 \cos 2(\xi - \theta_r)]rl d\xi d\phi_s \quad (3.24)$$

$$\lambda_{as} = L_{ls}i_{as} + (N_s/2)^2 \pi\mu_r\mu_0rl(\alpha_1 - (\alpha_2/2) \cos 2\theta_r)i_{as} \quad (3.25)$$

Now, we can get the equation for the self inductance of the “as” winding. In a magnetically linear system the self inductance of the winding is the ratio of the flux linked by winding to the current flowing in the winding with other winding currents zero.

$$L_{as} = \frac{\lambda_{as}}{i_{as}} \quad (3.26)$$

Thus,

$$L_{as} = L_{ls} + \frac{N_s^2}{4} \pi\mu_r\mu_0rl(\alpha_1 - \frac{\alpha_2}{2} \cos 2\theta_r) \quad (3.27)$$

The self inductances for the other stator phase windings “bs” and “cs” are similar to the winding “as” and may be expressed respectively as

$$L_{bs} = L_{ls} + \frac{N_s^2}{4} \pi \mu_r \mu_0 r l \left(\alpha_1 - \frac{\alpha_2}{2} \cos 2\left(\theta_r - \frac{2\pi}{3}\right) \right) \quad (3.28)$$

$$L_{cs} = L_{ls} + \frac{N_s^2}{4} \pi \mu_r \mu_0 r l \left(\alpha_1 - \frac{\alpha_2}{2} \cos 2\left(\theta_r + \frac{2\pi}{3}\right) \right) \quad (3.29)$$

The mutual flux linkage in “as” winding due to current in “bs” winding is found in a similar manner, but in this case, the flux density will be taken due to I_{bs} and can be written as

$$\lambda_{as} = \int N_{as}(\phi_s) \int_{\phi_s}^{\phi_s + \pi} B_r(\xi, \theta_r) r l d\xi d\phi_s \quad (3.30)$$

By substituting (3.3) and (3.17) into (3.30) we obtain λ_{asbs} as

$$\lambda_{asbs} = -\frac{N_s^2}{4} \frac{\pi}{2} \mu_r \mu_0 r l \left[\alpha_1 + \alpha_2 \cos 2\left(\theta_r - \frac{\pi}{3}\right) \right] i_{bs} \quad (3.31)$$

Therefore, the mutual inductance between “as” and “bs” windings is obtained by dividing equation (3.31) by i_{bs} .

$$M_{asbs} = -\frac{N_s^2}{4} \frac{\pi}{2} \mu_r \mu_0 r l \left[\alpha_1 + \alpha_2 \cos 2\left(\theta_r - \frac{\pi}{3}\right) \right] \quad (3.32)$$

The self inductance of the field winding may be obtained as following.

$$\lambda_{fd} = L_{lfd} i_{fd} - \int_{\pi/2}^{3\pi/2} \left(\frac{N_f}{2} \right) \cos \phi_r \int_{\phi_r}^{\phi_r + \pi} \mu_r \mu_0 \left(\frac{N_f}{2} \right) i_{fd} \sin \xi \left(\alpha_1 - \alpha_2 \cos 2\xi \right) r l d\xi d\phi_r \quad (3.33)$$

then,

$$\lambda_{fd} = L_{lfd} i_{fd} + \frac{N_f^2}{4} \pi \mu_r \mu_0 r l \left[\alpha_1 + \frac{\alpha_2}{2} \right] i_{fd} \quad (3.34)$$

then, the self inductance of the field winding is given as

$$L_{fd} = L_{lfd} + \frac{N_f^2}{4} \pi \mu_r \mu_0 r l \left[\alpha_1 + \frac{\alpha_2}{2} \right] \quad (3.35)$$

where L_{lfd} is the leakage inductance of the field winding.

The mutual flux linkage between the stator phase “as” and rotor d-axis field “fd” windings is determined by substituting (3.20) expressed in terms of $(\phi_s - \theta_r)$ into (3.30),

$$\lambda_{as} = -\frac{N_s N_f}{4} \pi \mu_r \mu_0 r l \left(\alpha_1 + \frac{\alpha_2}{2} \right) \sin \theta_r i_{fd} \quad (3.36)$$

Then dividing equation (3.36) by i_{fd} ,

$$M_{asfd} = -\frac{N_s N_f}{4} \pi \mu_r \mu_0 r l \left(\alpha_1 + \frac{\alpha_2}{2} \right) \sin \theta_r \quad (3.37)$$

Similarly the other mutual inductances can be obtained as

$$M_{ascs} = -\frac{N_s^2}{4} \frac{\pi}{2} \mu_r \mu_0 r l \left[\alpha_1 + \alpha_2 \cos 2\left(\theta_r + \frac{\pi}{3}\right) \right] \quad (3.38)$$

$$M_{bscs} = -\frac{N_s^2}{4} \frac{\pi}{2} \mu_r \mu_0 r l \left[\alpha_1 + \alpha_2 \cos 2(\theta_r + \pi) \right] \quad (3.39)$$

$$M_{bsfd} = \frac{N_s N_f}{4} \pi \mu_r \mu_0 r l \left(\alpha_1 + \frac{\alpha_2}{2} \right) \sin\left(\theta_r - \frac{2\pi}{3}\right) \quad (3.40)$$

$$M_{csfd} = \frac{N_s N_f}{4} \pi \mu_r \mu_0 r l \left(\alpha_1 + \frac{\alpha_2}{2} \right) \sin\left(\theta_r + \frac{2\pi}{3}\right) \quad (3.41)$$

We can modify these equations by the following expressions,

$$L_A = \left(\frac{N_s}{2}\right)^2 \pi \mu_0 \mu_r r l \alpha_1 \quad (3.42)$$

$$L_B = \frac{1}{2} \left(\frac{N_s}{2}\right)^2 \pi \mu_0 \mu_r r l \alpha_2 \quad (3.43)$$

$$L_{sfd} = \left(\frac{N_s}{2}\right) \left(\frac{N_f}{2}\right) \pi \mu_0 \mu_r r l \left(\alpha_1 - \frac{\alpha_2}{2} \right) \quad (3.44)$$

$$L_{mfd} = \left(\frac{N_f}{2}\right)^2 \pi \mu_0 \mu_r r l \left(\alpha_1 + \frac{\alpha_2}{2}\right) \quad (3.45)$$

Then, the machine inductances can be written in terms of the following equations as

$$L_{asas} = L_{ls} + L_A - L_B \cos 2\theta_r \quad (3.46)$$

$$L_{bsbs} = L_{ls} + L_A - L_B \cos 2\left(\theta_r - \frac{2\pi}{3}\right) \quad (3.47)$$

$$L_{csas} = L_{ls} + L_A - L_B \cos 2\left(\theta_r + \frac{2\pi}{3}\right) \quad (3.48)$$

$$L_{fdfd} = L_{lfd} + L_{mfd} \quad (3.49)$$

$$M_{asbs} = -\frac{1}{2}L_A - L_B \cos 2\left(\theta_r - \frac{\pi}{3}\right) \quad (3.50)$$

$$M_{ascs} = -\frac{1}{2}L_A - L_B \cos 2\left(\theta_r + \frac{\pi}{3}\right) \quad (3.51)$$

$$M_{bscs} = -\frac{1}{2}L_A - L_B \cos 2(\theta_r + \pi) \quad (3.52)$$

$$M_{asfd} = L_{sfd} \sin \theta_r \quad (3.53)$$

$$M_{bsfd} = L_{sfd} \sin\left(\theta_r - \frac{2\pi}{3}\right) \quad (3.54)$$

$$M_{csfd} = L_{sfd} \sin\left(\theta_r + \frac{2\pi}{3}\right) \quad (3.55)$$

Thus, we can express the inductances of the machine in matrix form as

$$[L] = \begin{bmatrix} L_{asas} & M_{asbs} & M_{ascs} & M_{asfd} \\ M_{bsas} & L_{bsbs} & M_{bscs} & M_{bsfd} \\ M_{csas} & M_{csbs} & L_{csas} & M_{csfd} \\ M_{fdas} & M_{fdbs} & M_{fdcs} & L_{fdfd} \end{bmatrix} \quad (3.56)$$

The relation between the flux linkages, inductances and currents is given as

$$[\lambda] = [L] \times [i] \quad (3.57)$$

thus, the flux linkage in phases a,b,c and field windings are given as

$$\begin{bmatrix} \lambda_{as} \\ \lambda_{bs} \\ \lambda_{cs} \\ \lambda_{fd} \end{bmatrix} = \begin{bmatrix} L_{asas} & M_{asbs} & M_{ascs} & M_{asfd} \\ M_{bsas} & L_{bsbs} & M_{bscs} & M_{bsfd} \\ M_{csas} & M_{csbs} & L_{cscs} & M_{csfd} \\ M_{fdas} & M_{fdbs} & M_{fdcs} & L_{fdfd} \end{bmatrix} \times \begin{bmatrix} i_{as} \\ i_{bs} \\ i_{cs} \\ i_{fd} \end{bmatrix} \quad (3.58)$$

Then, we can also write flux linkage for any phase individually as

$$\lambda_{as} = L_{asas}i_{as} + M_{asbs}i_{bs} + M_{ascs}i_{cs} + M_{asfd}i_{fd} \quad (3.59)$$

$$\lambda_{bs} = M_{bsas}i_{as} + L_{bsbs}i_{bs} + M_{bscs}i_{cs} + M_{bsfd}i_{fd} \quad (3.60)$$

$$\lambda_{cs} = M_{csas}i_{as} + M_{csbs}i_{bs} + L_{cscs}i_{cs} + M_{csfd}i_{fd} \quad (3.61)$$

$$\lambda_{fd} = M_{fdas}i_{as} + M_{fdbs}i_{bs} + M_{fdcs}i_{cs} + L_{fdfd}i_{fd} \quad (3.62)$$

3.2 Modeling

3.2.1 Motor modeling

The permanent magnet synchronous motor is very similar to the standard wire-wound synchronous motor except that it has no damper windings and no wire-wound dc field excitation. The excitation is provided by the permanent magnet instead of a field winding. The permanent magnet gives a constant flux λ_m . The flux linkage in the stator winding due to the permanent magnet rotor is given as.

$$[\lambda] = \begin{bmatrix} \lambda_{asfd} \\ \lambda_{bsfd} \\ \lambda_{csfd} \end{bmatrix} = \begin{bmatrix} \lambda_m \sin \theta_r \\ \lambda_m \sin(\theta_r - \frac{2\pi}{3}) \\ \lambda_m \sin(\theta_r + \frac{2\pi}{3}) \end{bmatrix} \quad (3.63)$$

Thus, we can rewrite the equations (3.59-3.61) as follows

$$\lambda_{as} = L_{asas}i_{as} + M_{asbs}i_{bs} + M_{ascs}i_{cs} + \lambda_m \sin \theta_r \quad (3.64)$$

$$\lambda_{bs} = M_{bsas} i_{as} + L_{bsbs} i_{bs} + M_{bscs} i_{cs} + \lambda_m \sin(\theta_r - \frac{2\pi}{3}) \quad (3.65)$$

$$\lambda_{cs} = M_{csas} i_{as} + M_{csbs} i_{bs} + L_{cscs} i_{cs} + \lambda_m \sin(\theta_r + \frac{2\pi}{3}) \quad (3.66)$$

In the matrix form we can write the equations (3.64-3.66) as

$$\begin{bmatrix} \lambda_{as} \\ \lambda_{bs} \\ \lambda_{cs} \end{bmatrix} = \begin{bmatrix} L_{asas} & M_{asbs} & M_{ascs} \\ M_{bsas} & L_{bsbs} & M_{bscs} \\ M_{csas} & M_{csbs} & L_{cscs} \end{bmatrix} \begin{bmatrix} i_{as} \\ i_{bs} \\ i_{cs} \end{bmatrix} + \lambda_m \begin{bmatrix} \sin \theta_r \\ \sin(\theta_r - \frac{2\pi}{3}) \\ \sin(\theta_r + \frac{2\pi}{3}) \end{bmatrix} \quad (3.67)$$

Now, the voltage equation for the permanent magnet synchronous motor can be written as the synchronous machine equations without the damper winding and field current dynamics

$$v_{as} = r_{as} i_{as} + \frac{d\lambda_{as}}{dt} \quad (3.68)$$

$$v_{bs} = r_{bs} i_{bs} + \frac{d\lambda_{bs}}{dt} \quad (3.69)$$

$$v_{cs} = r_{cs} i_{cs} + \frac{d\lambda_{cs}}{dt} \quad (3.70)$$

Equations (3.68- 3.70) can be written in matrix form as

$$\begin{bmatrix} v_{as} \\ v_{bs} \\ v_{cs} \end{bmatrix} = \begin{bmatrix} r_{as} & 0 & 0 \\ 0 & r_{bs} & 0 \\ 0 & 0 & r_{cs} \end{bmatrix} \begin{bmatrix} i_{as} \\ i_{bs} \\ i_{cs} \end{bmatrix} + p \begin{bmatrix} \lambda_{as} \\ \lambda_{bs} \\ \lambda_{cs} \end{bmatrix} \quad (3.71)$$

Where the operator $p = d/dt$ and λ is the flux linkage.

$$\begin{bmatrix} \lambda_{as} \\ \lambda_{bs} \\ \lambda_{cs} \end{bmatrix} = \begin{bmatrix} L_{asas} & M_{asbs} & M_{ascs} \\ M_{bsas} & L_{bsbs} & M_{bscs} \\ M_{csas} & M_{csbs} & L_{cscs} \end{bmatrix} \begin{bmatrix} i_{as} \\ i_{bs} \\ i_{cs} \end{bmatrix} + \lambda_m \begin{bmatrix} \sin \theta_r \\ \sin(\theta_r - \frac{2\pi}{3}) \\ \sin(\theta_r + \frac{2\pi}{3}) \end{bmatrix} \quad (3.72)$$

Where L_{asas} , L_{bsbs} , and L_{cscs} are the self inductances and M_{asbs} , M_{bscs} , and M_{csas} are the mutual inductances, respectively. These inductances are function of the rotor position θ_r and therefore a function of the rotor speed ω_r . Hence, the coefficients of the voltage equations are time varying except when the rotor is in the stalled condition. This makes the solution of the voltage equations difficult unless all the equations are transformed to the synchronously rotating frame. The transformation of the synchronous machine equations from a-b-c phase variables to the d-q-o variables forces all sinusoidally varying inductances in the a-b-c frame to become constant in the d-q-o frame. So, the machine inductances will no longer be dependent on the rotor position. The transformation not only facilitates the solutions of the equations but also facilitates the design of the controller. This transformation is done by Park's transformation.

3.2.2 Park's equation

Park's equations can be obtained in two stages. At first, the a-b-c phase variables are transformed into d-q frame, where both are in the stationary reference frame. Secondly, the variables in stationary d-q frame can be converted to the synchronously rotating rotor d^f-q^f frame. The superfix r denotes rotor reference frame.

The following assumptions are made in the derivation of rotor d^f-q^f model of the PMSM.

- 1- There is no squirrel cage in the rotor.
- 2- There are no field current dynamics.

- 3- Eddy currents and hysteresis effects are negligible.
- 4- The induced EMF is sinusoidal.
- 5- Saturation is neglected.

The 3-phase variables in any reference frame can be transformed to the orthogonal components by the following relationship.

$$[x_{qdo}] = [c_1] [x_{abc}] \quad (3.73)$$

Where c_1 is the coefficient matrix of transformation and is given as

$$[c_1] = \frac{2}{3} \begin{bmatrix} \cos \theta & \cos(\theta - \frac{2\pi}{3}) & \cos(\theta + \frac{2\pi}{3}) \\ \sin \theta & \sin(\theta - \frac{2\pi}{3}) & \sin(\theta + \frac{2\pi}{3}) \\ \frac{1}{2} & \frac{1}{2} & \frac{1}{2} \end{bmatrix} \quad (3.74)$$

and the inverse of c_1 is given as

$$[c_1]^{-1} = \begin{bmatrix} \cos \theta & \sin \theta & 1 \\ \cos(\theta - \frac{2\pi}{3}) & \sin(\theta - \frac{2\pi}{3}) & 1 \\ \cos(\theta + \frac{2\pi}{3}) & \sin(\theta + \frac{2\pi}{3}) & 1 \end{bmatrix} \quad (3.75)$$

In equation (3.73), the term x can represent any variable such as voltage, current or flux linkage. The voltage equations in the machine can be transformed to the orthogonal components of a rotating reference frame as

$$[v_{qdo}]^f = [c_1] [v_{abc}] \quad (3.76)$$

Thus,

$$[v_{qdo}]^f = [c_1] \{ [r_{abc}] [i_{abc}] + p[\lambda_{abc}] \} \quad (3.77)$$

Equation (3.77) can be simplified further by substituting equations of currents and flux linkages in the dqo frame as:

$$[V_{qdo}]^r = [c_1] \{ [r_{abc}] [c_1]^{-1} [i_{qdo}]^r + p [c_1]^{-1} [\lambda_{qdo}]^r \} \quad (3.78)$$

$$= [c_1] [r_{abc}] [c_1]^{-1} [i_{qdo}]^r + [c_1] p [c_1]^{-1} [\lambda_{abc}]^r + [c_1] [c_2]^{-1} p [\lambda_{abc}]^r \quad (3.79)$$

We can simplify the above equation by substituting the value of $[c_1]$, $[c_1]^{-1}$, and $[r_{abc}]$.

$$[V_{qdo}]^r = [r_{abc}] [i_{qdo}]^r + P\omega_r [\lambda_{dq}]^r + p[\lambda_{qdo}]^r \quad (3.80)$$

where P is the number of pole pairs. Equation (3.80) can be expressed in matrix form as

$$\begin{bmatrix} v_q^r \\ v_d^r \\ v_o^r \end{bmatrix} = \begin{bmatrix} r_a & 0 & 0 \\ 0 & r_b & 0 \\ 0 & 0 & r_c \end{bmatrix} \begin{bmatrix} i_q^r \\ i_d^r \\ i_o^r \end{bmatrix} + P\omega_r \begin{bmatrix} \lambda_d^r \\ -\lambda_q^r \end{bmatrix} + p \begin{bmatrix} \lambda_q^r \\ \lambda_d^r \\ \lambda_o^r \end{bmatrix} \quad (3.81)$$

By assuming that $r_a = r_b = r_c = r_s$ equation (3.81) can be re-written as

$$\begin{bmatrix} v_q^r \\ v_d^r \\ v_o^r \end{bmatrix} = \begin{bmatrix} r_s & 0 & 0 \\ 0 & r_s & 0 \\ 0 & 0 & r_s \end{bmatrix} \begin{bmatrix} i_q^r \\ i_d^r \\ i_o^r \end{bmatrix} + P\omega_r \begin{bmatrix} \lambda_d^r \\ -\lambda_q^r \end{bmatrix} + p \begin{bmatrix} \lambda_q^r \\ \lambda_d^r \\ \lambda_o^r \end{bmatrix} \quad (3.82)$$

Then the equation (3.82) can be expressed as

$$v_q^r = r_s i_q^r + P\omega_r \lambda_d^r + p\lambda_q^r \quad (3.83)$$

$$v_d^r = r_s i_d^r - P\omega_r \lambda_q^r + p\lambda_d^r \quad (3.84)$$

$$v_o^r = r_s i_o^r + p\lambda_o^r \quad (3.85)$$

We can determine λ_d^r , λ_q^r , and λ_o^r as

$$[\lambda_{qdo}]^r = [c_1] [\lambda_{abc}] \quad (3.86)$$

$$[\lambda_{qdo}]^r = [c_1] \{ [L] [i_{abc}] + [\lambda_f] \} \quad (3.87)$$

$$[\lambda_{qdo}]^r = [c_1] [L] [c_1]^{-1} [i_{qdo}]^r + [c_1] [\lambda_f] \quad (3.88)$$

By putting the value of $[c_1]$, $[c_1]^{-1}$, $[L]$ from equation (3.58) and $[\lambda_f]$ from equation (3.63)

in the equation (3.88) we obtain

$$\begin{bmatrix} \lambda_q^r \\ \lambda_d^r \\ \lambda_o^r \end{bmatrix} = \begin{bmatrix} L_{ls} + \frac{3}{2}(L_A - L_B) & 0 & 0 \\ 0 & L_{ls} + \frac{3}{2}(L_A + L_B) & 0 \\ 0 & 0 & L_{ls} \end{bmatrix} \begin{bmatrix} i_q^r \\ i_d^r \\ i_o^r \end{bmatrix} + \lambda_m \begin{bmatrix} 0 \\ 1 \\ 0 \end{bmatrix} \quad (3.89)$$

By defining the d-q axis magnetizing inductances in equation (3.89) as

$$L_{mq} = \frac{3}{2}(L_A - L_B) \quad (3.90)$$

$$L_{md} = \frac{3}{2}(L_A + L_B) \quad (3.91)$$

and putting $L_q = L_{ls} + L_{mq}$, and $L_d = L_{ls} + L_{md}$, we can get these equations:

$$\begin{bmatrix} \lambda_q^r \\ \lambda_d^r \\ \lambda_o^r \end{bmatrix} = \begin{bmatrix} L_q & 0 & 0 \\ 0 & L_d & 0 \\ 0 & 0 & L_{ls} \end{bmatrix} \begin{bmatrix} i_q^r \\ i_d^r \\ i_o^r \end{bmatrix} + \lambda_m \begin{bmatrix} 0 \\ 1 \\ 0 \end{bmatrix} \quad (3.91)$$

$$\lambda_q^r = L_q i_q^r \quad (3.92)$$

$$\lambda_d^r = L_d i_d^r + \lambda_m \quad (3.93)$$

and in rotor zero reference frame $\lambda_o^r = L_{l1} i_o^r$

Thus, equations (3.83-3.84) can be expressed as

$$v_q^r = (r_s + pL_q) i_q^r + P\omega_r L_d i_d^r + \omega_r \lambda_m \quad (3.94)$$

$$v_d^r = (r_s + pL_d) i_d^r - P\omega_r L_q i_q^r \quad (3.95)$$

Equations (3.94) and (3.95) can be written in matrix form as

$$\begin{bmatrix} v_q^r \\ v_d^r \end{bmatrix} = \begin{bmatrix} r_s + pL_q & P\omega_r L_d \\ -P\omega_r L_q & r_s + pL_d \end{bmatrix} \begin{bmatrix} i_q^r \\ i_d^r \end{bmatrix} + \begin{bmatrix} P\omega_r \lambda_m \\ 0 \end{bmatrix} \quad (3.96)$$

For dynamic simulation, the model of the PMSM may be expressed as

$$p i_q^r = (v_q^r - r_s i_q^r - p \omega_r L_d i_d^r + p \omega_r \lambda_m) / L_q \quad (3.97)$$

$$p i_d^r = (v_d^r - r_s i_d^r + p \omega_r L_q i_q^r) / L_d \quad (3.98)$$

By the equations (3.97-3.98) we can represent the PMSM in d-q axis with the equivalent circuit diagram as shown in Figure 3.3.

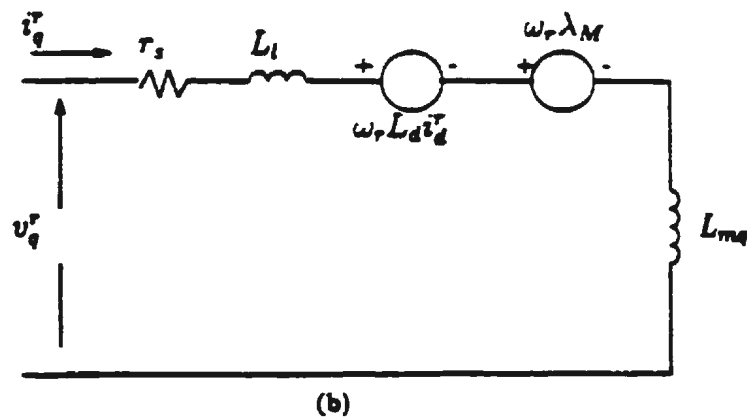
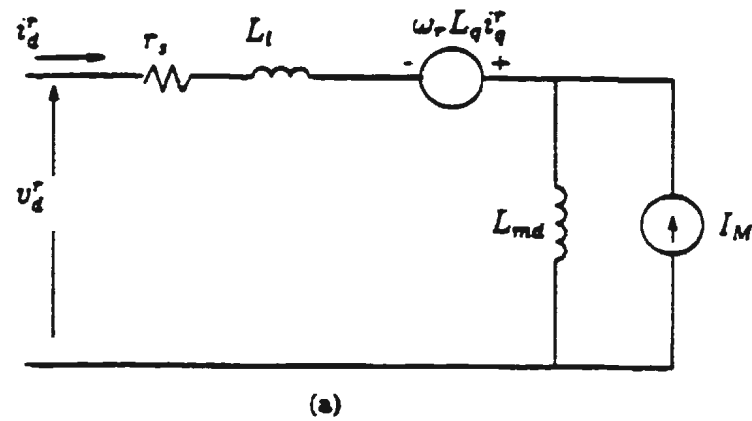


Figure 3.3. Park's model of PMSM: (a) d-axis (b) q-axis

3.2.3 Relationship between 3-phase and orthogonal quantity in stationary and synchronous reference frame.

The 3-phase machine equations can be transformed into d-q axis on the same stationary reference frame by using equation (3.73).

Thus,

$$[x_{abc}] = [c_1]^{-1} [x_{qdo}]^s \quad (3.99)$$

$$\begin{bmatrix} x_a \\ x_b \\ x_c \end{bmatrix} = \begin{bmatrix} \cos\theta & \sin\theta & 1 \\ \cos(\theta - \frac{2\pi}{3}) & \sin(\theta - \frac{2\pi}{3}) & 1 \\ \cos(\theta + \frac{2\pi}{3}) & \sin(\theta + \frac{2\pi}{3}) & 1 \end{bmatrix} \begin{bmatrix} x_q^s \\ x_d^s \\ x_o^s \end{bmatrix} \quad (3.100)$$

Where the term x may represent voltages, currents, or flux linkages. For a balanced three-phase system, zero sequence component does not exist. Also, it is convenient to set $\theta = 0$, so that the q-axis is coincident with the a-phase. Now, equation (3.100) can be simplified as

$$\begin{bmatrix} x_a \\ x_b \\ x_c \end{bmatrix} = \begin{bmatrix} 1 & 0 \\ -\frac{1}{2} & \frac{\sqrt{3}}{2} \\ -\frac{1}{2} & -\frac{\sqrt{3}}{2} \end{bmatrix} \begin{bmatrix} x_q^s \\ x_d^s \end{bmatrix} \quad (3.101)$$

Thus, we can write as

$$v_a = v_q^s \quad (3.102)$$

$$v_b = -\frac{1}{2} v_q^s - \frac{\sqrt{3}}{2} v_d^s \quad (3.103)$$

$$v_c = -\frac{1}{2}v_q^s + \frac{\sqrt{3}}{2}v_d^s \quad (3.104)$$

And we can also determine the d-q axis on the stationary reference frame from the three phases as

$$\begin{bmatrix} v_q^s \\ v_d^s \\ v_o^s \end{bmatrix} = \frac{2}{3} \begin{bmatrix} \cos\theta & \cos(\theta - \frac{2\pi}{3}) & \cos(\theta + \frac{2\pi}{3}) \\ \sin\theta & \sin(\theta - \frac{2\pi}{3}) & \sin(\theta + \frac{2\pi}{3}) \\ \frac{1}{2} & \frac{1}{2} & \frac{1}{2} \end{bmatrix} \begin{bmatrix} v_a \\ v_b \\ v_c \end{bmatrix} \quad (3.105)$$

Equation (3.105) can be simplified as

$$\begin{bmatrix} v_q^s \\ v_d^s \\ v_o^s \end{bmatrix} = \frac{2}{3} \begin{bmatrix} 1 & -\frac{1}{2} & -\frac{1}{2} \\ 0 & -\frac{\sqrt{3}}{2} & \frac{\sqrt{3}}{2} \\ \frac{1}{2} & \frac{1}{2} & \frac{1}{2} \end{bmatrix} \begin{bmatrix} v_a \\ v_b \\ v_c \end{bmatrix} \quad (3.106)$$

Thus, we can write as

$$\begin{aligned} v_q^s &= \frac{2}{3}(v_a - \frac{1}{2}v_b - \frac{1}{2}v_c) \\ &= \frac{2}{3}v_a - \frac{1}{3}v_b - \frac{1}{3}v_c \end{aligned} \quad (3.107)$$

and since $v_a + v_b + v_c = 0$, so we can write

$$v_a = -v_b - v_c \quad (3.108)$$

therefore,

$$v_q^s = v_a \quad (3.109)$$

$$v_d^s = \frac{2}{3}(-\frac{\sqrt{3}}{2}v_b + \frac{\sqrt{3}}{2}v_c) = \frac{1}{\sqrt{3}}v_b + \frac{1}{\sqrt{3}}v_c \quad (3.110)$$

The variables in the stationary d-q frame can be converted to the synchronously rotating d^r-q^r frame with the help of Figure 3.3 as follows:

$$\begin{bmatrix} v_q^r \\ v_d^r \end{bmatrix} = \begin{bmatrix} \cos(\theta_r) & -\sin(\theta_r) \\ \sin(\theta_r) & \cos(\theta_r) \end{bmatrix} \begin{bmatrix} v_q \\ v_d \end{bmatrix} \quad (3.111)$$

This equation can be inverted to define the relations of stationary frame variables in terms of rotating frame variables as follows:

$$\begin{bmatrix} v_q \\ v_d \end{bmatrix} = \begin{bmatrix} \cos(\theta_r) & \sin(\theta_r) \\ -\sin(\theta_r) & \cos(\theta_r) \end{bmatrix} \begin{bmatrix} v_q^r \\ v_d^r \end{bmatrix} \quad (3.112)$$

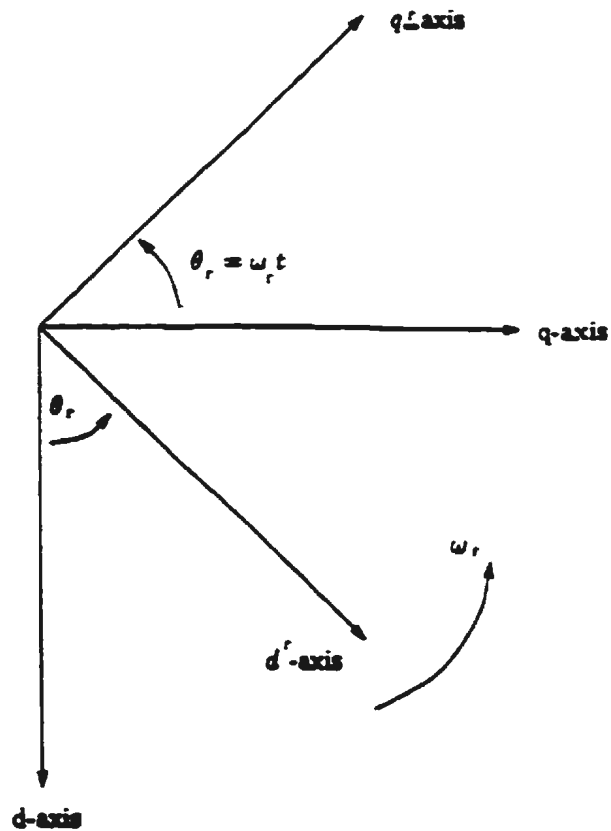


Figure 3.4: Stationary d-q axis to synchronously rotating d^r-q^r axis transformation.

3.2.4 Torque expression of PMSM

The expression for the electromagnetic torque developed by the machine can be obtained from the component of the input power that is transferred across the air gap.

The total input power into the machine is given by

$$P_{in} = v_a i_a + v_b i_b + v_c i_c \quad (3.113)$$

When the stator phase quantities are transformed to the rotor dqo reference frame that

rotates at a speed of $\omega_r = \frac{d\theta_r}{dt}$, equation (3.113) becomes

$$P_{in} = \frac{3}{2}(v_q^r i_q^r + v_d^r i_d^r) + 3v_o^r i_o^r \quad (3.114)$$

$$P_{in} = \frac{3}{2}(r_s(i_q^2 + i_d^2))^r + i_q^r \frac{d\lambda_q^r}{dt} + i_d^r \frac{d\lambda_d^r}{dt} + \omega_r(\lambda_d^r i_q^r - \lambda_q^r i_d^r) + 3i_o^2 r_o \quad (3.115)$$

Eliminating terms of the ohmic losses and the rate of change in magnetic energy, the above equation of the electromechanical power developed, P_{em} becomes

$$P_{em} = \frac{3}{2}\omega_r(\lambda_d^r i_q^r - \lambda_q^r i_d^r) \quad (3.116)$$

for a P- pair pole of machine, with $\omega_r = (P/2)\omega_{m}$, ω_{m} being the rotor speed in mechanical radians per second. Thus, equation (3.116) can be written as

$$P_{em} = \frac{3P}{2}\omega_{m}(\lambda_d^r i_q^r - \lambda_q^r i_d^r) \quad (3.117)$$

By dividing the electromechanical power by the mechanical speed of the rotor, we obtain the expression for electromechanical torque developed as

$$T_{em} = \frac{3P}{2}(\lambda_d^r i_q^r - \lambda_q^r i_d^r) \quad (3.118)$$

By substituting equations (3.92-3.93) in equation (3.118), we get

$$\begin{aligned}
T_{em} &= \frac{3P}{2} (L_d i_d^r i_q^r + \lambda_m i_q^r - L_q i_q^r i_d^r) \\
&= \frac{3P}{2} (\lambda_m i_q^r + (L_d - L_q) i_q^r i_d^r)
\end{aligned} \tag{3.119}$$

And the relationship between the electromechanical torque and the load torque is given as

$$T_{em} = J_m \frac{d\omega_r}{dt} + T_l + B_m \omega_r = J_m \frac{d^2\theta_r}{dt^2} + B_m \frac{d\theta_r}{dt} + T_l \tag{3.120}$$

where B_m is the friction coefficient, T_l is the load torque and J_m is the moment of inertia.

For simulation of the dynamic characteristics of the drive, we can rewrite equation

(3.120) in two first order equations as

$$p\omega_r = (T_{em} - T_l - B_m \omega_r) / J_m \tag{3.121}$$

$$p\theta_r = \omega_r \tag{3.122}$$

Chapter 4

System description and control structure

4.1 General

The basic configuration of the permanent magnet drive system consists of an interior permanent magnet synchronous motor fed by PWM voltage source inverter and connected with the load. The schematic diagram of the permanent magnet drive system is shown in Figure 4.1. All reference or command values are superscripted with a \cdot in the diagram. The optical incremental encoder is mounted on the rotor shaft. From the optical incremental encoder we get the actual position and the speed. The actual speed ω_r is compared with the reference speed ω_r^\cdot . The error between them is processed by the speed controller to generate the torque reference. This torque reference signal is processed through the torque current calculator to define the reference current I_q^\cdot . The actual current from the motor is converted by Park's transformation to generate the d-q axis currents I_d and I_q in rotating reference frame. The currents I_q and I_d are compared with the reference I_q^\cdot and I_d^\cdot , respectively. The error is utilized by the current controller to generate v_q^\cdot and v_d^\cdot voltage commands. This goes through the inverse Park's transformation to generate a, b, and c voltage commands. These commands are compared with the triangular waveform to generate the PWM signals, which will fire the power transistors to produce the actual voltages to the motor.

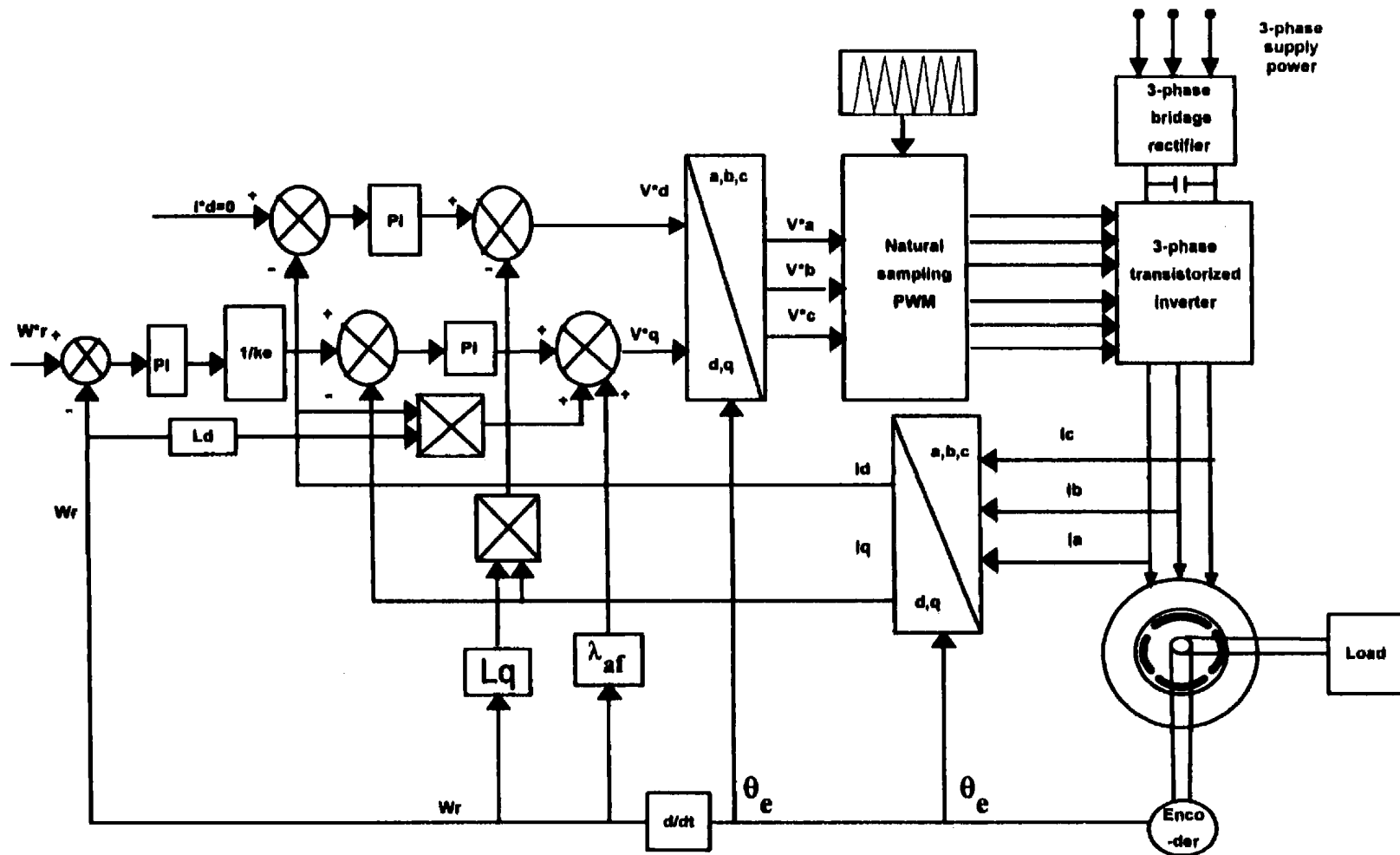


Figure 4.1: Schematic diagram of the PMSM drive system

4.2 Inverter model

The function of an inverter is to change a dc-input voltage to a symmetrical ac output voltage of desired magnitude and frequency. The output voltage could be fixed or variable at a fixed or variable frequency. A variable output voltage can be obtained by varying the input dc voltage and maintaining the gain of the inverter constant. On the other hand, if the dc input voltage is fixed and it is not controllable, a variable output voltage can be obtained by varying the gain of the inverter, which is normally accomplished by pulse-width-modulation (PWM) control within the inverter.

In the analysis of the inverter, it is assumed that the turn-off time of the transistor is negligible. As for high frequency, the switch turn-off time is approximately few microseconds. Figure 4.2 shows the six-pulse transistor inverter power circuit. At the instant switch T_1 is turned off, the current it was carrying is diverted to the diode in parallel with T_4 . The diode continues to conduct until the current decreases to zero. Once the current i_a reverses direction, it is carried by T_4 . This mode is generally referred to as the continuous voltage or continuous current mode. It is sometimes also called the 180° conduction mode. The inverter may also be operated in a discontinuous current mode wherein each phase current conducts for 120° . This mode is more suitable for the brushless dc motor drive where trapezoidal back EMF and rectangular shaped stator currents are needed to produce a constant torque. The 180° mode of operation is considered for sinusoidal PMSM drive. In this mode, the voltage v_{aG} as shown in Figure 4.2 is equal to the inverter voltage input v_{dc} , if T_1 or the diode in parallel with T_1 is conducting. It is zero when T_4 or the diode in parallel with T_4 is conducting. The output

voltage of the inverter can be represented as a function of switching logic of the transistors and the input voltage.

The inverter voltage vector is defined as [31]

$$\bar{v} = \frac{2}{3}(v_a + av_b + a^2v_c) \quad (4.1)$$

Where v_a , v_b , and v_c are phase voltages and the operator $a = 1 \angle 120^\circ$

The phase voltages v_a , v_b , and v_c may be expressed as a function of bus voltage V_B and logic variables as

$$v_{abcN} = \frac{1}{3} \begin{bmatrix} 2 & -1 & -1 \\ -1 & 2 & -1 \\ -1 & -1 & 2 \end{bmatrix} v_{abcG} \quad (4.2)$$

where v_{abcG} is:

$$v_{abcG} = \begin{bmatrix} NA \\ NB \\ NC \end{bmatrix} V_B \quad (4.3)$$

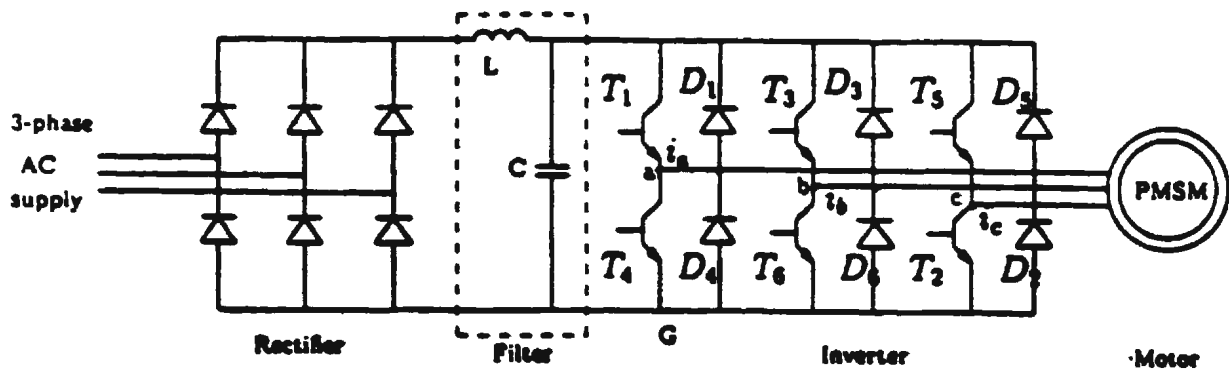


Figure 4.2: Power circuit for the PMSM drive system

4.3 Sinusoidal Pulse Width Modulation

The pulse width modulation (PWM) techniques in an inverter system can remove unwanted frequency components to a higher frequency region. The output waveform of a PWM inverter is generally improved by using a high ratio between the carrier frequency and the output fundamental frequency. The distortion factor and lower-order harmonics are reduced significantly. The inverter output voltage should be as nearly sinusoidal as possible. The three-phase reference should be sine wave reference, in order to give a PWM waveform in which the pulse width is sinusoidally modulated throughout the cycle. The gate signals as shown in Figure 4.3 [32] are generated by comparing a sinusoidal reference signal with a triangular carrier wave. This type of modulation is commonly used in industrial applications and abbreviated as SPWM. The frequency of the reference signal f_r determines the inverter output frequency f_o . The number of pulses per half-cycle depends on the carrier frequency. For large carrier ratios, the sinusoidal PWM inverter delivers a high quality output voltage waveform in which the dominant harmonics are of a higher order, being clustered around the carrier frequency and its harmonics. Smooth motor rotation is obtained, even at low speed, because the undesirable low-order harmonics and troublesome torque pulsation are minimized with the sinusoidal PWM supply.

The adjustable frequency operation of a sine PWM inverter for ac motor control requires the generation of a set of three-phase sine wave reference voltages of adjustable amplitude and frequency. If the motor is to operate at very low speeds, the reference waveform must have a corresponding low frequency capability.

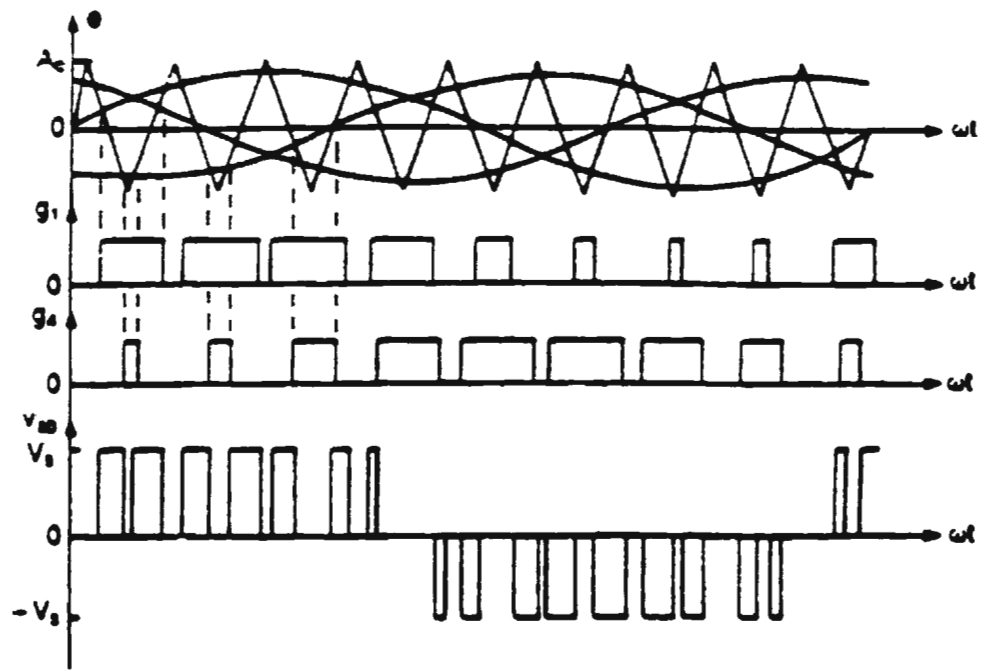


Figure 4.3 Sinusoidal pulse-width modulation for three-phase inverter

4.4 The Sine and Triangular waveforms Comparison

The generation of the triangular carrier voltage is shown in Figure 4.4 [33]. The principle employed here is that the integration of a square wave results in a triangular wave. The block labeled 1 in Figure 4.4 is a voltage controlled oscillator (VCO) chip. It is programmed to generate a pulse train whose frequency is twice the desired carrier frequency. The output of voltage control oscillator (VCO) may not be a symmetrical. Therefore, we use an edge triggered toggle flip flop. The output of the toggle flip flop in block 2 will therefore be a square wave. The square wave is integrated by using an operational amplifier as an integrator in block 3. The output of the integrator may not have the correct zero level. Therefore, we get to correct it by the level shifter. The output of the level shifter in block 4 will serve as the triangular wave.

The implementation of sine pulse width modulation (SPWM) using sine and triangular waves comparison in a three-phase inverter is shown in Figure 4.5. In this case, we use two voltage waveforms: (1) a three reference sinusoidal voltages with a phase shift of 120° and the same frequency as the inverter, which we call them the reference voltages and (2) high frequency voltages, which have triangular waveforms. The comparator chip will compare the two waveforms and implement SPWM. Figure 4.5 shows the timing instants of the six static switching elements of the inverter. The six timing voltage outputs shown in Figure 4.5 are numbered to correspond to the numbering of the six switches in the inverter topology. The triangular waveform has fixed amplitude and the amplitude of the reference sine wave is usually made adjustable. The modulation index M is given as

$$M = (\text{Amplitude of the reference wave}) / (\text{amplitude of the carrier})$$

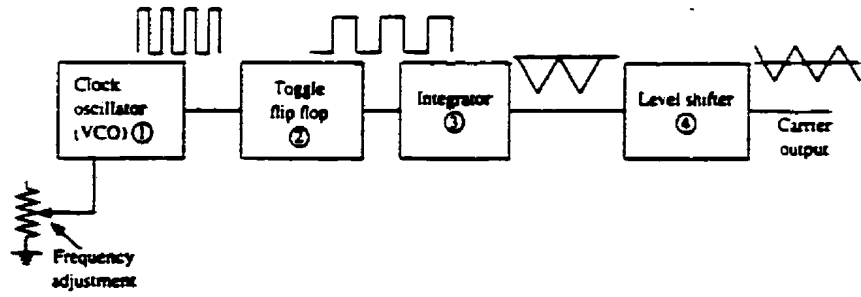


Figure 4.4 Circuit scheme for generation of the triangular carrier wave.

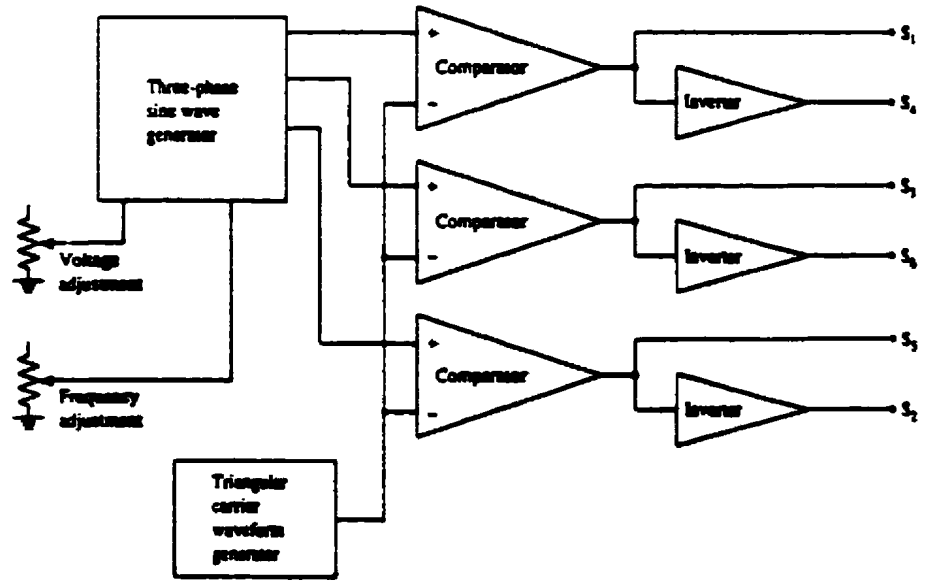


Figure 4.5 Implementation of SPWM using sine and triangular waves comparison in a three-phase inverter.

4.5 Vector Space and Control Strategies

Vector control techniques have been accepted as one of the most effective methods. Usually, the vector control strategy is formulated in the synchronously rotating reference frame. As is well known, the transformation of the synchronous machine equations from a-b-c phase variables to the d^f - q^f variables forces all sinusoidally varying variables in the a-b-c frame to become constant in the d^f - q^f frame. This concept facilitates the control tasks. The stator current phasor in the d^f - q^f axis synchronously rotating frame has two components, namely the magnetizing current component and torque producing current component. The generated torque is the product of two components. By keeping the magnetizing current component at constant value, the motor torque is linearly proportional to the torque producing component, which is similar to the control of a separately excited dc motor. The concept of the vector control can be understood with the help of the basic vector diagram of PMSM as in Figure 4.6(a). This vector diagram is obtained from equation (3.96). It is to be noted that the stator current can be adjusted by controlling the d^f - q^f axis current components. In order to achieve maximum torque per ampere with linear characteristics, i_d^f is forced to zero resulting orientation of all the linkage flux in the d^f -axis as shown in Figure 4.6(b). Electric torque equation is given as

$$T_{em} = \frac{3P}{2} (\lambda_m i_q^f + (L_d - L_q) i_d^f i_q^f) \quad (4.4)$$

The second term is made zero by forcing $i_d^f = 0$, the torque equation becomes

$$T_{em} = \frac{3P}{2} \lambda_m i_q^f \quad (4.5)$$

Hence the electric torque depends only on the quadrature axis current i_q . A constant torque can be obtained by ensuring that i_d^f is kept constant. The constant air gap flux

required up to rated speed, which is indicated by λ_m is provided by the magnet. If the air gap flux needs to be boosted (i_d^r in the same direction λ_m) or bucked (i_d^r in the opposite direction to λ_m), then the required i_d^r can be input into the machine.

For dynamic simulation the equations of the PMSM may be expressed in state space form as

$$p i_q^r = (v_q^r - r_s i_q^r - P \omega_r L_d i_d^r + P \omega_r \lambda_m) / L_q \quad (4.6)$$

$$p i_d^r = (v_d^r - r_s i_d^r + P \omega_r L_q i_q^r) / L_q \quad (4.7)$$

$$p \omega_r = (T_e - T_l - B_{\omega r}) / J \quad (4.8)$$

Where the d,q variables are obtained from a, b, c variables through the Park's transform as given below:

$$\begin{bmatrix} x_q \\ x_d \end{bmatrix} = \frac{2}{3} \begin{bmatrix} \cos(\theta_r) & \cos(\theta_r - 2\pi/2) & \cos(\theta_r + 2\pi/2) \\ \sin(\theta_r) & \sin(\theta_r - 2\pi/2) & \sin(\theta_r + 2\pi/2) \end{bmatrix} \begin{bmatrix} x_a \\ x_b \\ x_c \end{bmatrix} \quad (4.9)$$

Where element x may represent currents or voltages. According to the vector control principle, the direct axis current i_d is forced to zero in order to orient the linkage flux in the d-axis. This implies that $i_d = i_d^* = 0$. As a result, equations (4.6) to(4.8) can be simplified as:

$$p i_q^r = (v_q^r - r_s i_q^r + P \omega_r \lambda_m) / L_q \quad (4.10)$$

$$v_d^r = -(P \omega_r L_q i_q^r) / L_q \quad (4.11)$$

$$p \omega_r = (\frac{3}{2} \lambda_{afd} i_q - T_l - B_{\omega r}) / J \quad (4.12)$$

The above equations (4.10-4.12) are used to obtain the voltage commands v_d^* and v_q^* and for the design of PI regulator.

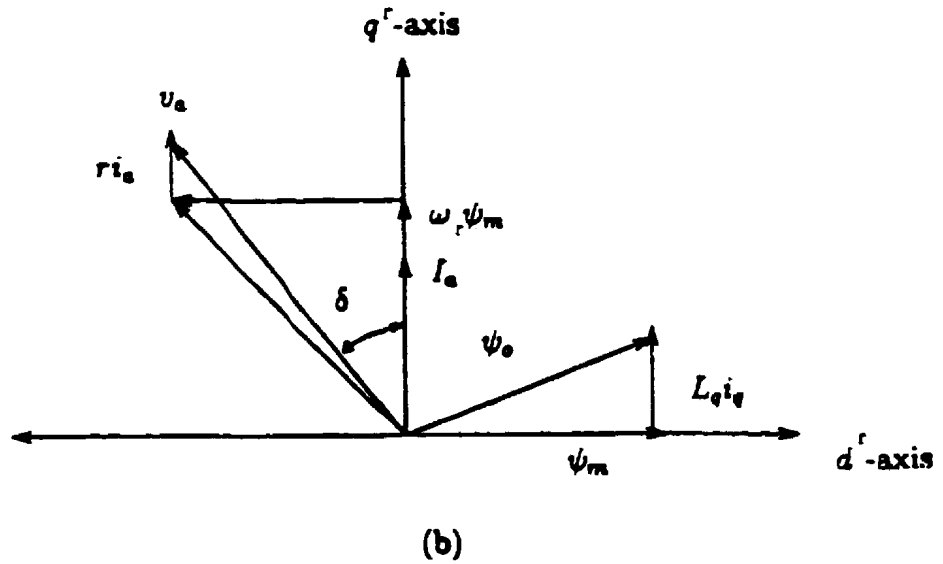
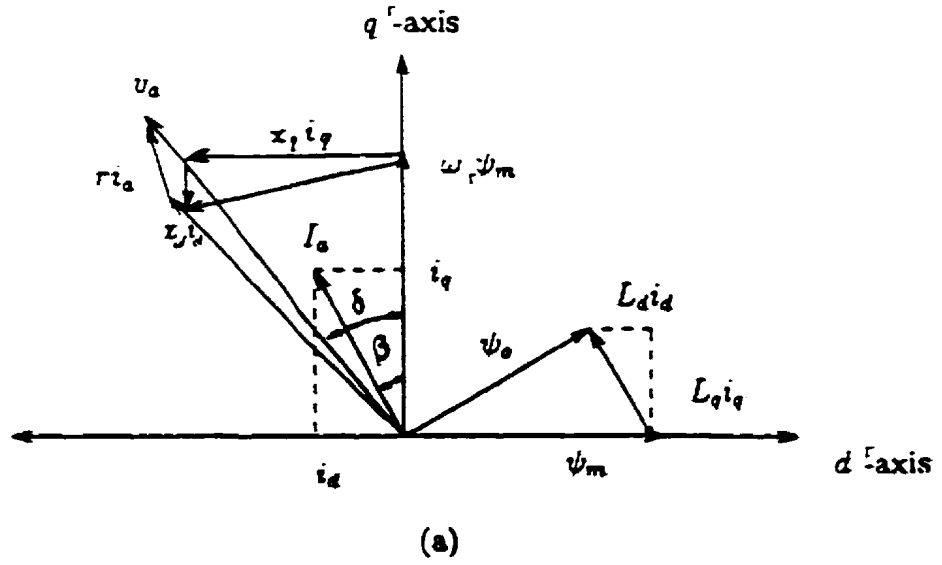


Figure 4.6: Basic vector diagram of PMSM (a) general vector diagram (b) vector diagram with $I_d = 0$

4.6 Controllers structure and design

The motor is controlled in d-q coordinates, which is guaranteed by the transformations described in chapter three. The drive is fed in such way that the q-axis current provides the desired torque. Since the d-axis of the current space vector points to the magnetization direction of the magnetic pole of the rotor, the d-axis current should be suppressed by the corresponding controller. Based on the vector control principle and current feedback control, the nonlinear dynamic model of the PMSM drive can be simplified and linearized as given in equations (4.10-4.12). Owing to the current feedback control, the inverter output voltages are fairly close to the reference voltage commands. Thus, in the d^f - q^f rotating frame the motor currents i_d^f and i_q^f are assumed to be equal to their respective references commands i_d^* and i_q^* . According to the vector control principle, the direct axis current i_d^f is forced to zero in order to orient all the linkage flux in the d-axis and to achieve maximum torque per ampere. Independent control of the field flux and torque is required for high performance applications. That is made possible by a decoupling controller. This decoupling controller will transform the torque and field flux commands into equivalent current commands to influence these variables independently. This is similar to the dc motor control.

For motor drive, the electrical dynamics are faster than the mechanical dynamics. The electrical state variables appear to have reached their equilibrium values when viewed by the slower mechanical states. On the other hand, the mechanical states are seen to be essentially constant at their initial values when viewed by the electrical sub-system. Usually, the mechanical time constant is many times greater than the electrical time

constant. The control system can be arranged as a multi-loop structure as shown in Figure 4.7. The inner loop is used to regulate the electrical dynamics. The current controller has the ability to force the motor current to follow their command values. Thus, under the control action, the equilibrium currents are actually equal to the command values. The current commands act as input for the speed loop. So, the outer control loop regulates the speed of the motor by issuing current commands to the inner control loop. The outer speed loop ensures that the actual speed is always equal to the command speed and any transient will be overcome within the system dynamics and without exceeding the motor and inverter capabilities. The inner current loop assures also fast current response within the drive system capabilities.

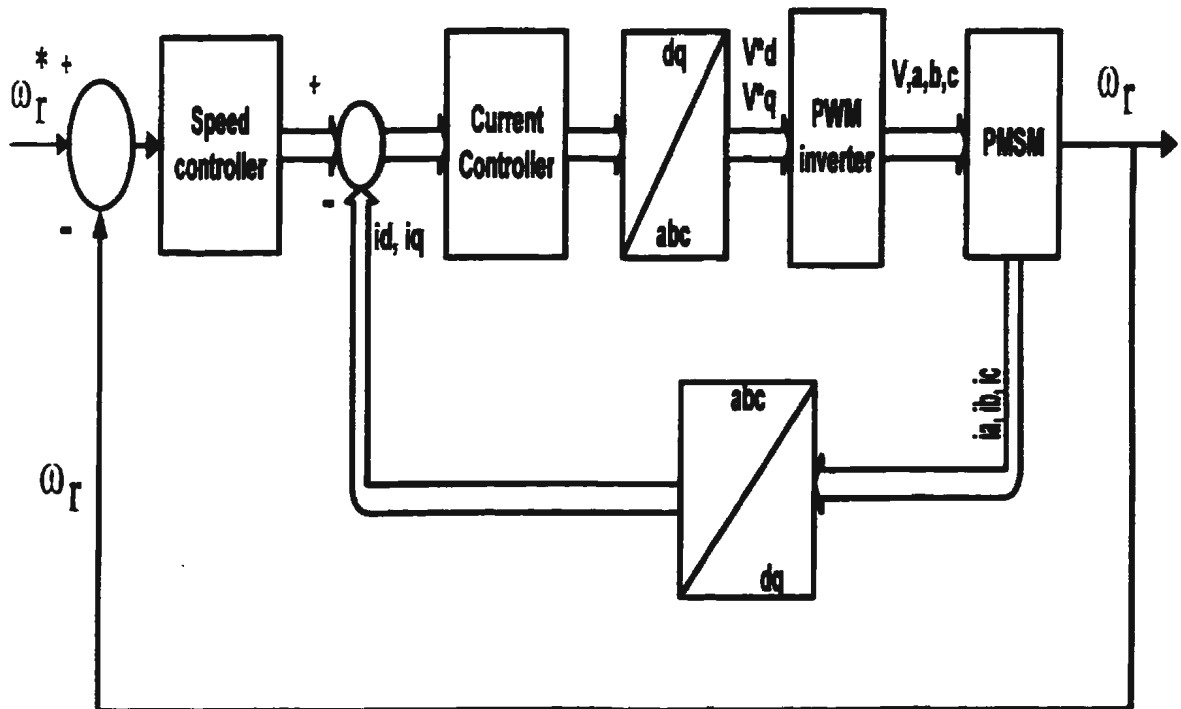


Figure 4.7 Multi-loop control structure of PMSM drive

4.7 Current controller design

The motor is controlled in d-q synchronous frame. This guarantees that the PI controller is operated by a dc error signal. The drive is fed in such a way that the q-axis current component provides the desired torque. Since the d-axis of the current space vector points to the magnetization direction of the magnetic pole of the rotor, the d-axis current component should be suppressed by the corresponding controller. The induced voltage and the coupling terms between the d and q-axis quantities of the motor are reconstructed by means of measured speed and currents. The values are necessary to make the control loop of the q-axis current independent on the speed and both the current loops to be decoupled to each other. To implement the current controllers, only the q-axis current controller is used to describe the system and to calculate the parameters. It is noted that current I_q controls the motor torque. The current controller structure is shown in Figure 4.8.

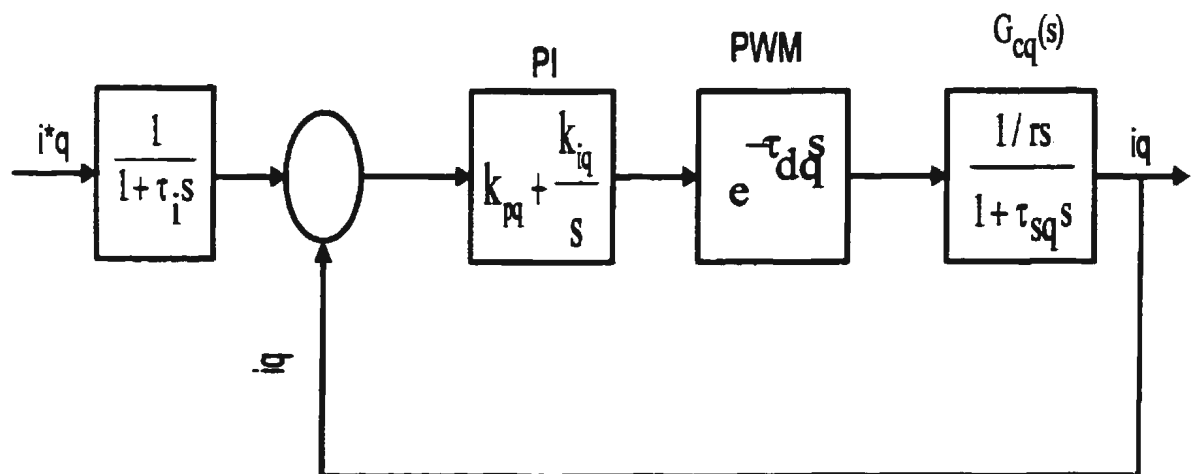


Figure 4.8 Current controller design

For the sake of clarity the decoupling part is omitted. The transfer function of the proportional plus integral (PI) controller is given as

$$P(s) = K_{pq} + \frac{K_{iq}}{s} = K_p \left(1 + \frac{1}{T_{qs}}\right) \quad (4.13)$$

Where K_p and K_i are the proportional and integral gain constants, respectively. The time constant is given as $T_q = K_p/K_i$

The q-axis of the stator dynamics is described by the first order function G_{sq} as

$$G_{sq}(s) = \frac{1/\tau_s}{1 + \tau_{sq}s} \quad (4.14)$$

Where $\tau_{sq} = (L_q/\tau_s)$ is the electrical time constant.

The PWM inverter is modeled by a delay element $e^{-\tau_{dq}s}$ with the delay time τ_{dq} .

The open loop transfer function for the current control system is described by the following equation.

$$G_{oq}(s) = \frac{K_{pq}s + K_{iq}}{s} e^{-\tau_{dq}s} G_{sq}(s) \quad (4.15)$$

The current control system closed loop transfer function is given as

$$G_{cq}(s) = \frac{G_{oq}(s)}{1 + G_{oq}(s)} \left(\frac{1}{1 + \tau_i s}\right) \quad (4.16)$$

Since the controller design is based on the symmetric optimum, the q-axis command current i_q^* is delayed via a first order lag with the parameter $\tau_i = 1.2\tau_q$, where $\tau_q = K_{iq}/K_{pq}$ is the time constant of the PI current controller.

The model of the direct axis current differs from that of the quadrature axis in that $L_d \neq L_q$.

The same design procedure can be used to design the d-axis current controller.

4.7 Speed controller design

The speed control structure is shown in Figure 4.9. The controller design is also based on the symmetric optimum. The outer speed loop ensures that the actual speed is equal to the command speed; and any transient is overcome within the shortest time without exceeding the motor and converter capabilities. The transfer functions of the various subsystems are described in the following way.

The transfer function of the proportional plus integral (PI) controller is given as

$$P(s) = K_{p\omega} + \frac{K_{i\omega}}{s} = K_p \left(1 + \frac{1}{T_{\omega s}}\right) \quad (4.17)$$

Where K_p and K_i are the proportional and integral gain constants, respectively. The time constant is given as $T_{\omega} = K_p/K_i$.

The rotor position and speed signals are generated by an optical incremental encoder. The output of the encoder is filtered to remove the ripples to provide position θ_r and the derivative of θ_r gives the speed ω_r . The transfer function of the speed feedback is given as

$$G_{\omega}(s) = \frac{1}{1 + \tau_{\omega}s} \quad (4.18)$$

The transfer function for the load and the torque constant is given as:

$$G_t(s) = \frac{K_t}{Js + B} \quad (4.19)$$

The transfer function of the closed loop current control is given in equation (4.16).

The open loop transfer function of the speed control system is given as

$$G_{\omega}(s) = \frac{K_{p\omega}s + K_{i\omega}}{s} G_{c\omega}(s) \left(\frac{K_t}{Js + B} \right) \quad (4.20)$$

And the close loop transfer function of the speed control system is given as

$$G_{\omega}(s) = \frac{G_{\omega}(s)}{1 + G_{\omega}(s)H(s)} \left(\frac{1}{1 + \tau_{\omega}s} \right) \quad (4.21)$$

where $H(s) = \frac{1}{1 + \tau_c s}$, τ_c is the time constant of the encoder and filter, and τ_{ω} is the delay

time of the speed command

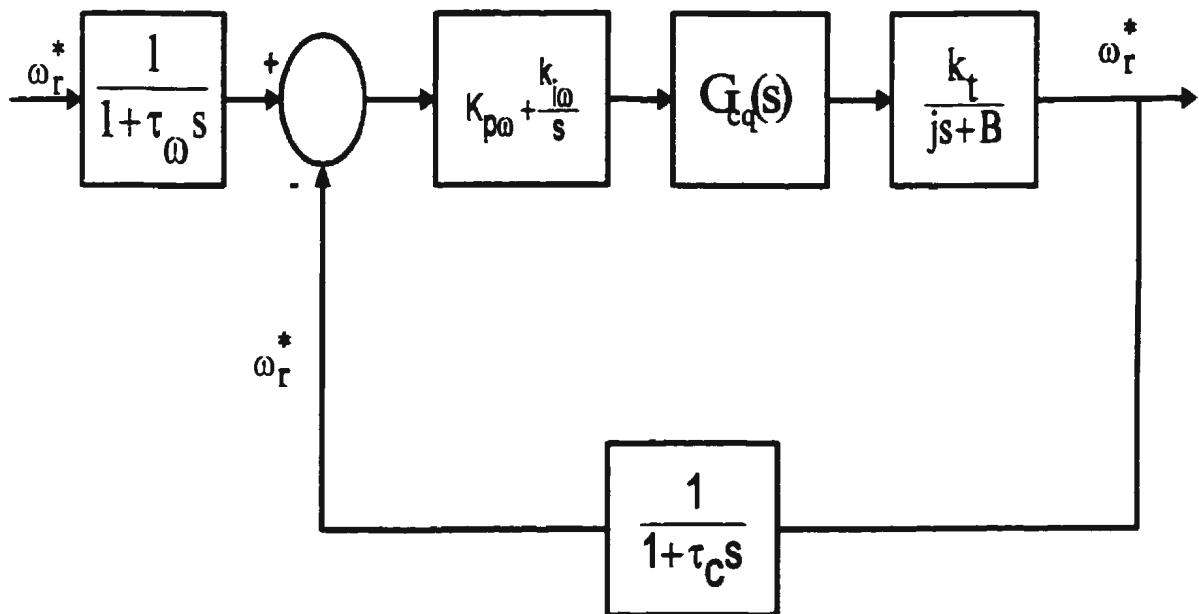


Figure 4.9 Speed controller structure

Chapter Five

Simulation and real time implementation

5.1 Simulation

It is a usual practice to simulate the drive system on the computer and predict the performance before real time implementation. A schematic of the simulated drive configuration consisting of the permanent magnet synchronous motor, the voltage source inverter as well as the control strategy is shown in Figure 5.1. The inverter's transistors are modeled as ideal controlled switches with instantaneous turn-on and turn-off. Therefore, the switches in each inverter leg have a complementary switching state. The assumption of ideal switches allows the blanking time, which is needed in practice to avoid cross conduction of the switches in the same inverter leg, to be neglected. Blanking time causes phase shift and additional ripple in the inverter output. In practice, this effect can be minimized by keeping the product of the switching frequency and the blanking time as small as possible [35]. There exist many softwares which can be helpful to simulate the dynamics of the system, such as electromagnetic transient program (EMTP), simulation of nonlinear system (SIMNON) and simulink [36]. The simulation enables an investigation of both the transient and the steady state performances of the system. Simulation input includes all the drive circuit parameters along with the command speed ω_r^* . The designed data and parameters of the PMSM drive are given in

Appendix A. The simulation outputs consist of the instantaneous currents, voltages, speed and torque waveforms. The simulink software, which uses the block diagram to represent a dynamic system, is used to simulate the entire drive system [9]. In order to obtain accurate and efficient simulation results with simulink, the equations describing the system are required to be arranged in the form of blocks. The following steps are considered in order to simulate the drive system by simulink.

- The structure of the PMSM mathematical model should be constructed in the form of block diagram as shown in Figure 5.2.
- From the simulink library, real-time switching model is used to represent the inverter.
- Built-in libraries for the PI controller, unit vectors generator and coordinate transformation are used after choosing the suitable parameters.
- Built-in Runge-Kutta algorithm is used to obtain the system performance.

The system shown in Figure 5.1 was modeled in Matlab using simulink. The schematic of this simulink is shown in Figure 5.2. Figure 5.2 contains different blocks such as multi-loop control, PMSM voltage equation, inverter, etc... These are known as the subsystems. Each subsystem includes many blocks, which represent specific tasks. A detail of each subsystem is given in Appendix B. The inputs for the control of the drive system are the references speed ω_r^* and the load torque. Any internal variables such as phase currents, inverter output voltages, etc... can be traced from corresponding subsystem block.

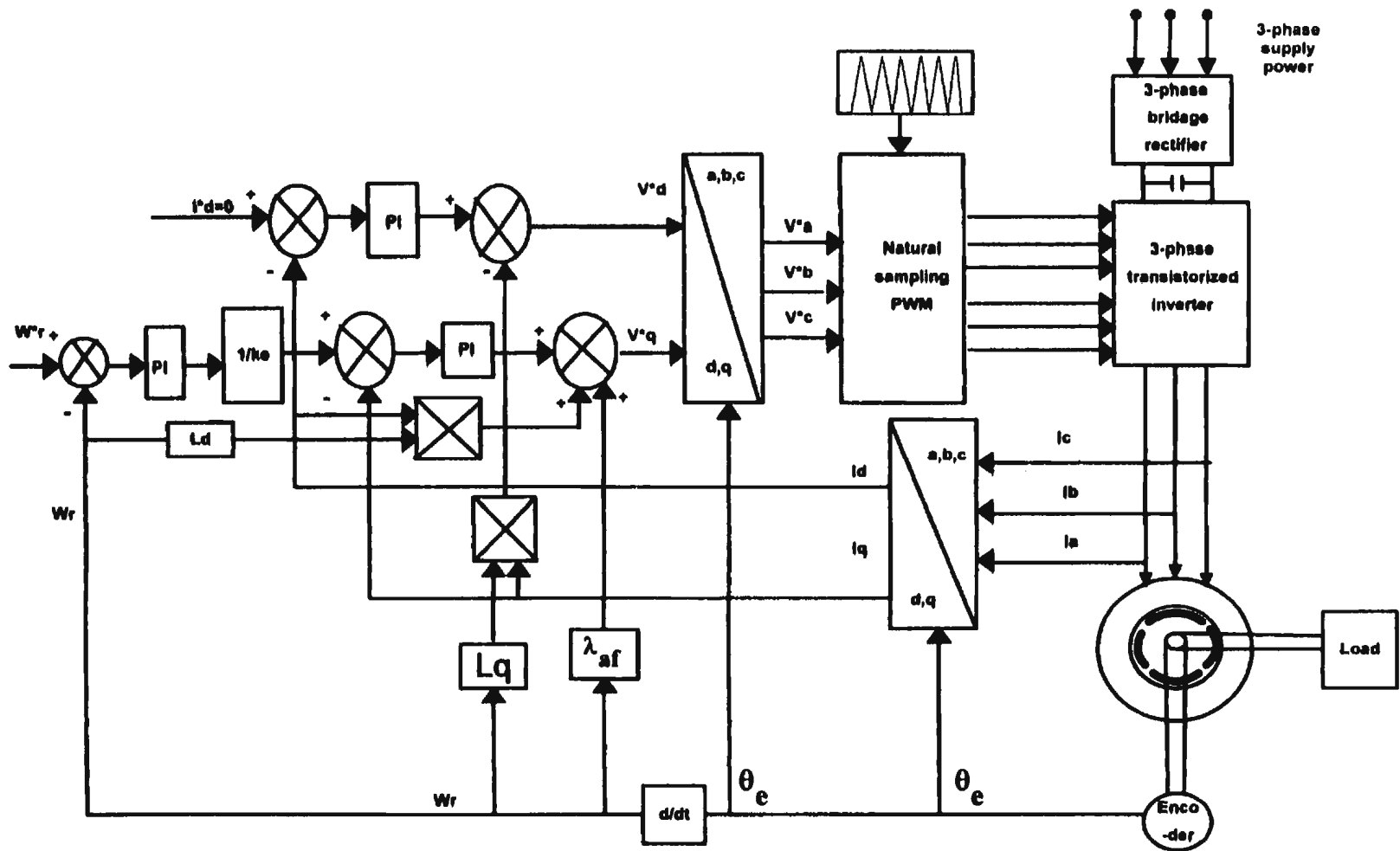


Figure 5.1: Structure of the PMSM mathematical model

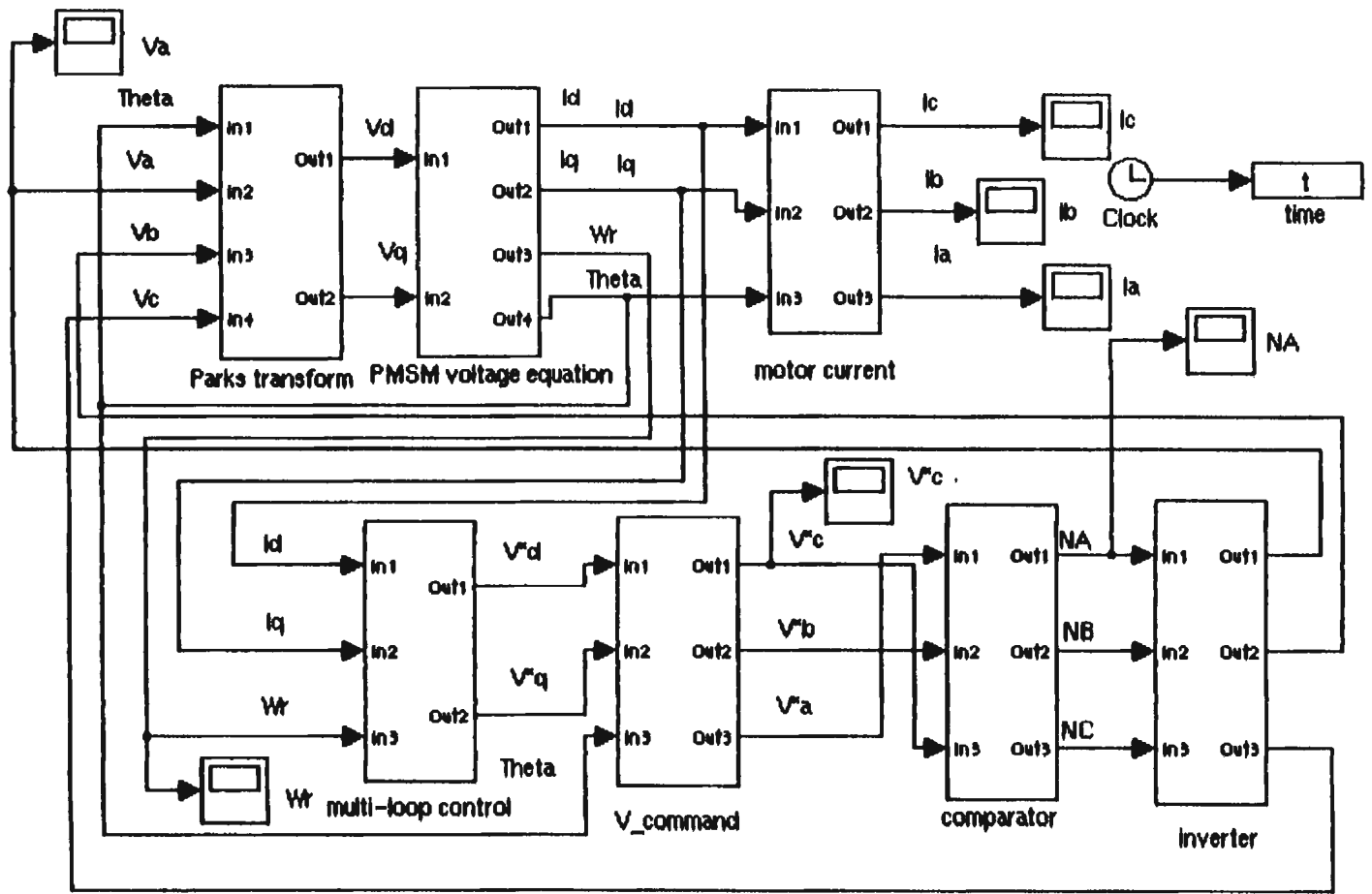


Figure 5.2: Simulink model of the entire drive system

5.2 Simulation results

For studying the starting and dynamic properties of multi-loop control of the PMSM drive, a series of simulations have been carried out. In these simulations, the dynamic responses of the control system for the following disturbances were studied: step change in the reference speed and step change in the load.

Figure 5.3 shows drive response for 180 rad./sec. command speed, from starting instant to the steady state instant at full load. It is seen from Figure 5.3 (a) that the rotor speed is accelerated smoothly and follows the speed command with accurate tracking of the motor speed with an acceptable overshoot and nearly zero steady state error. As the stator frequency is derived from the rotor position information, the motor is therefore always in synchronism. Figure 5.3 (b) shows the motor currents during the line start operation with fast responses. Figure 5.3 (c) shows the steady state voltage command. Figure 5.3 (d) shows the motor phase voltage. Figure 5.3 (e) shows the q-axis current component. Figure 5.3 (f) shows the d-axis current component. Since the $i_d = 0$ control method is used, it is noticed from the figure 5.3 (f) that the d-axis current is forced to oscillate around the zero value.

Similar results like those of Figure 5.3 were obtained for different operating conditions. The drive responses at no load with speed command of 180 rad./sec. are shown in Figure 5.4. The drive responses at full load with speed command of 150 rad./sec. are shown in Figure 5.5. The drive responses at no load with speed command of 150 rad./sec. are shown in Figure 5.6. These results show the accurate tracking of the motor speed and fast dynamic response of the PI regulators with minimum overshoots.

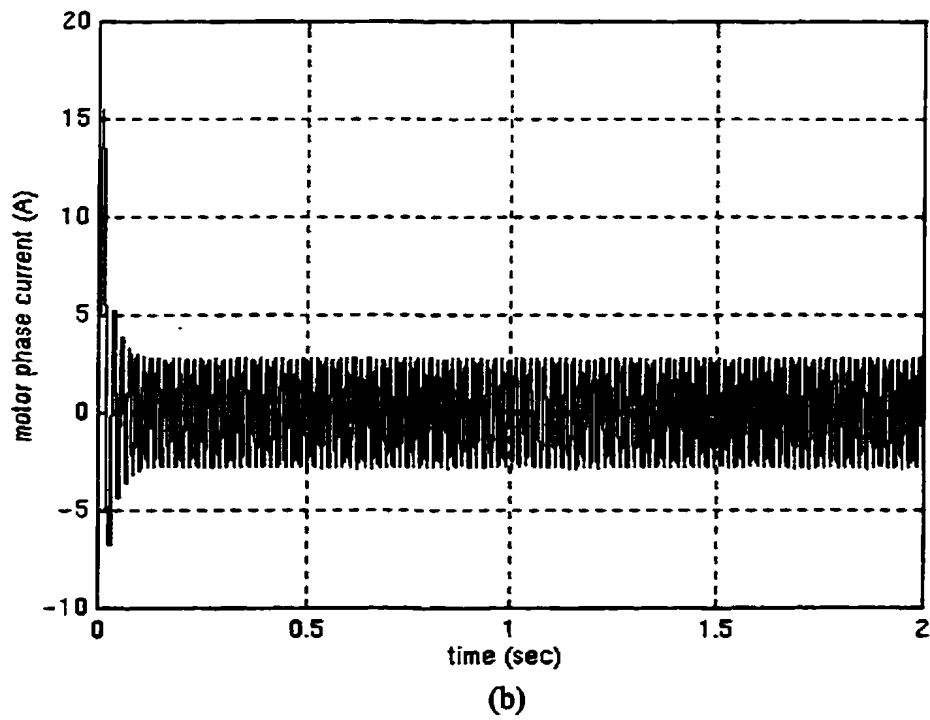
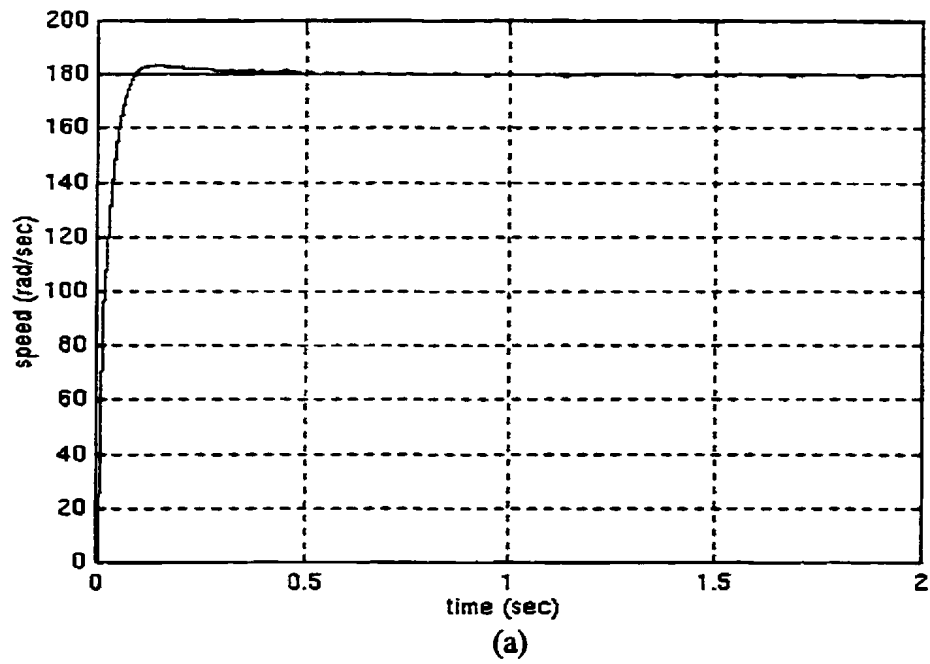


Figure 5.3: Drive responses at full load with speed command of 180 rad./sec., (a) speed response (b) motor phase current.

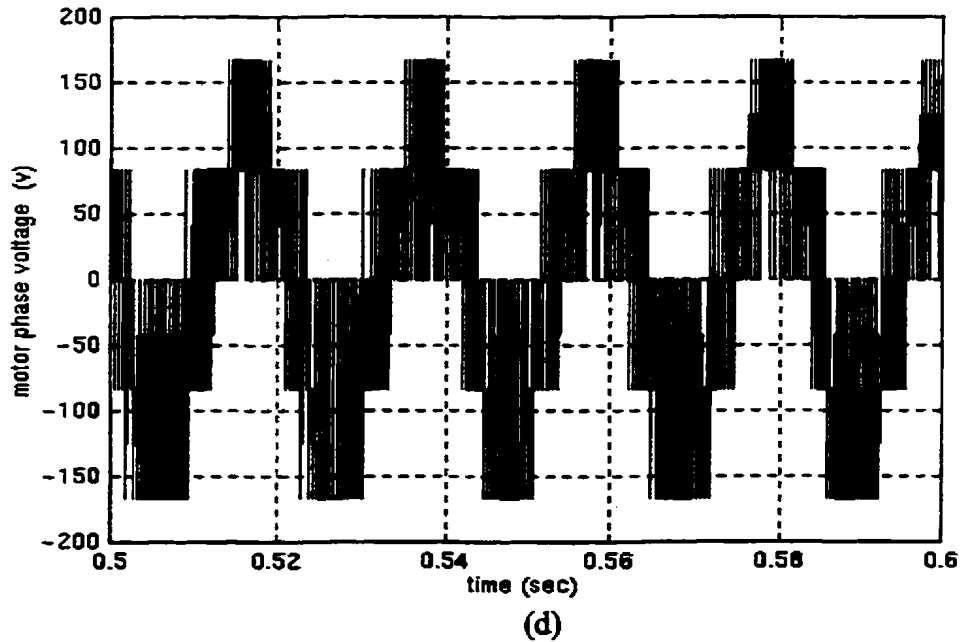
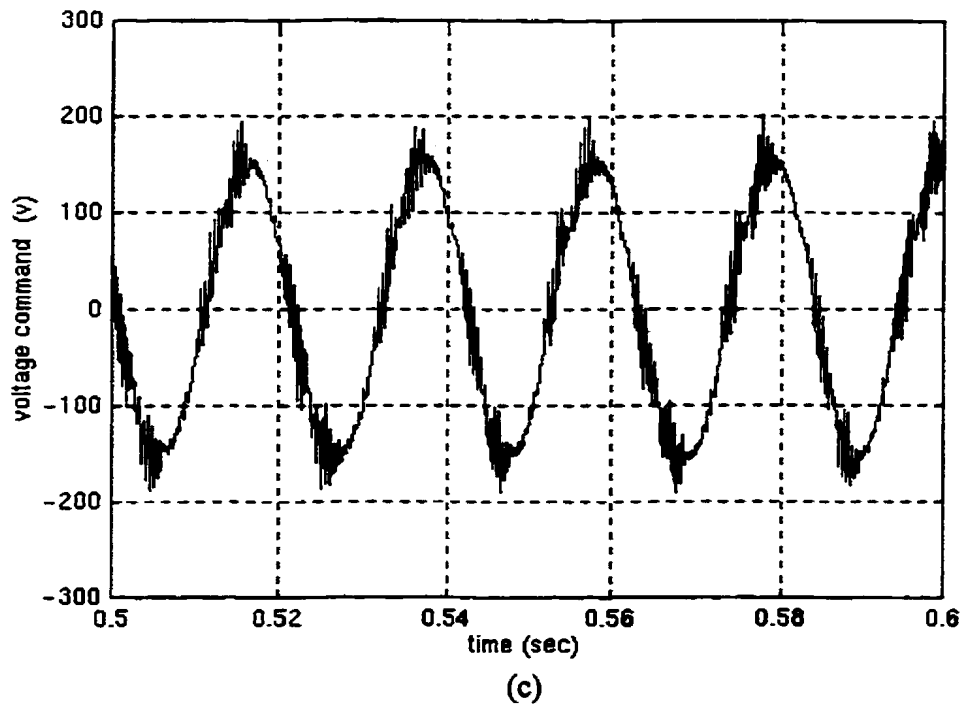


Figure 5.3: Drive responses at full load with speed command of 180 rad./sec., (c) Steady state voltage command (d) motor phase voltage

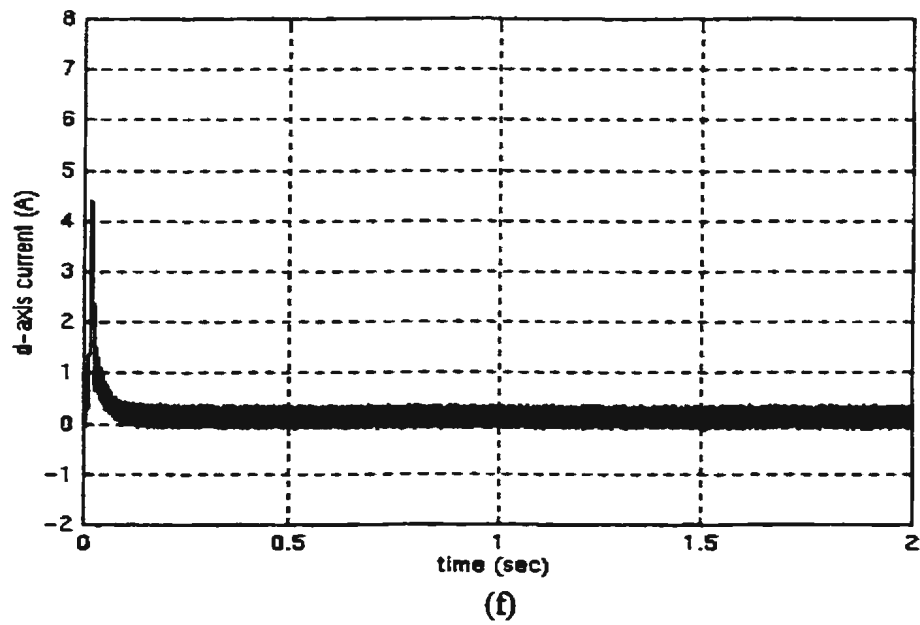
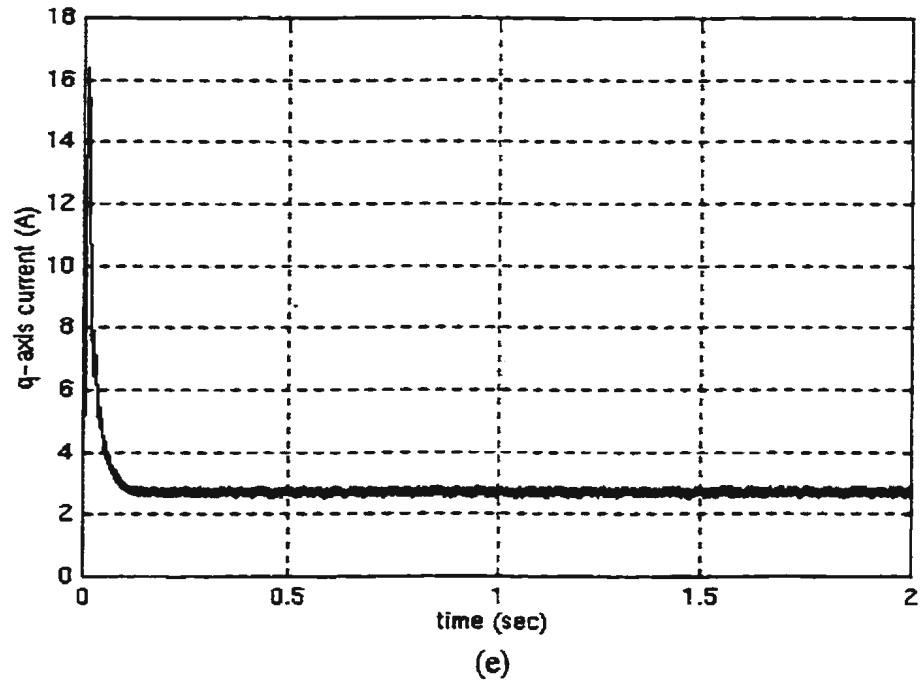
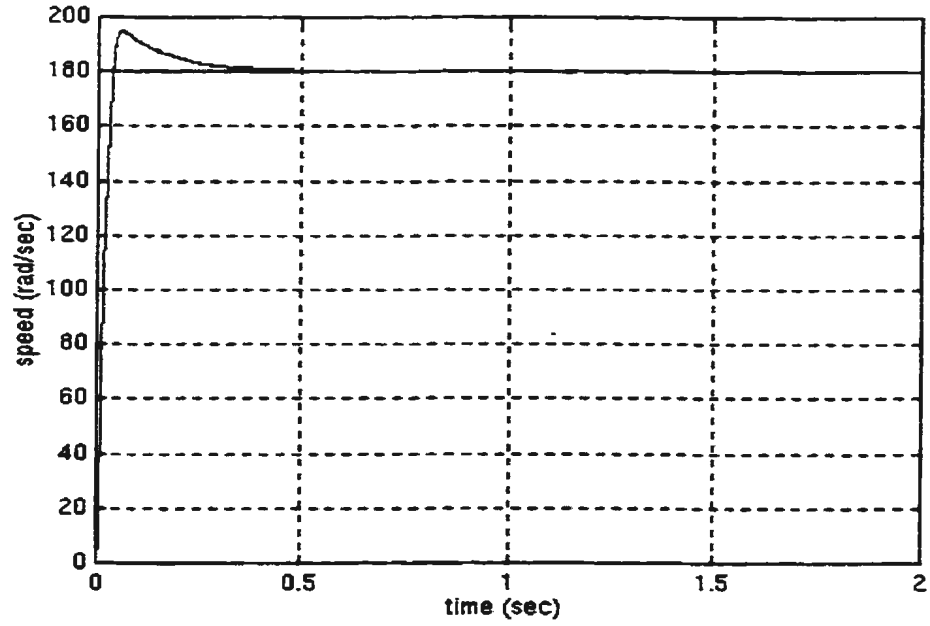
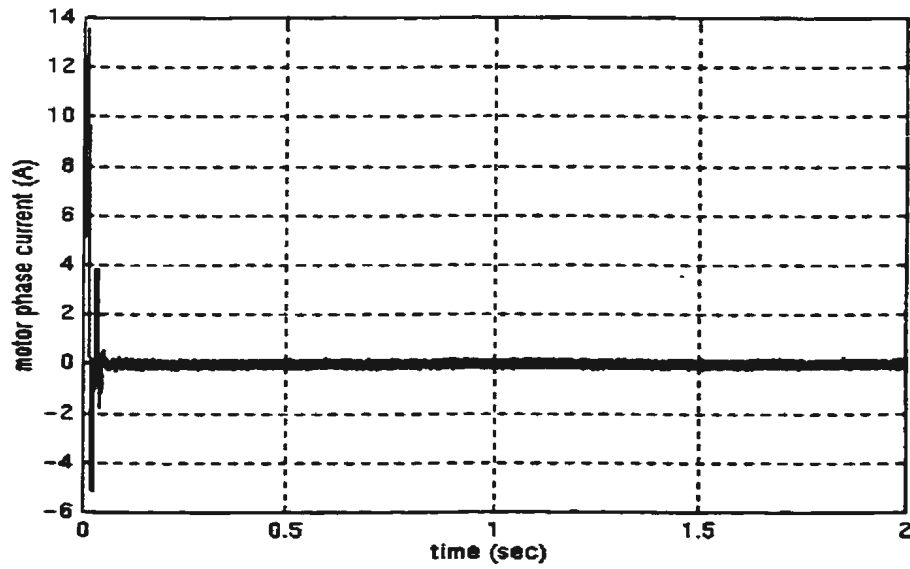


Figure 5.3: Drive responses at full load with speed command of 180 rad./sec., (e) q-axis current, and (f) d-axis current.

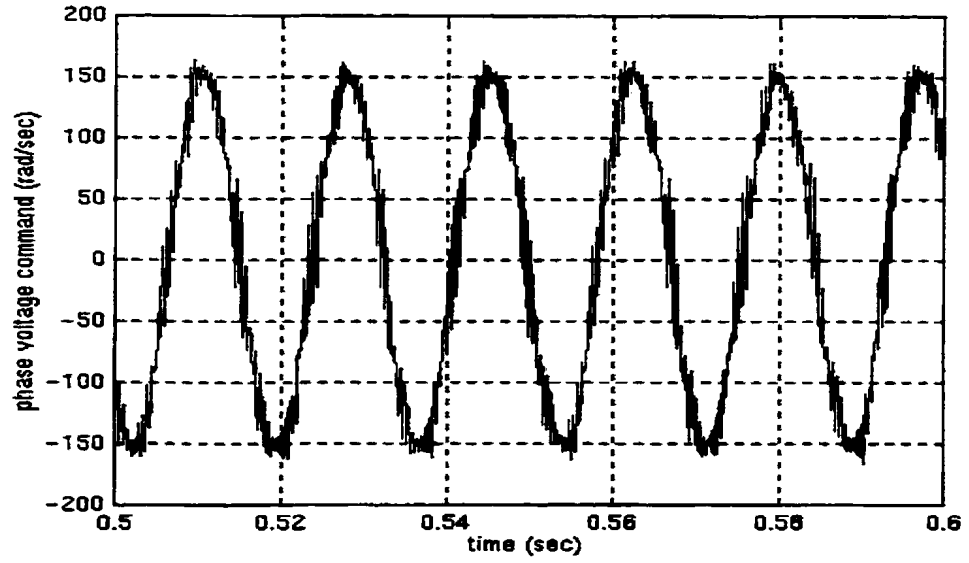


(a)

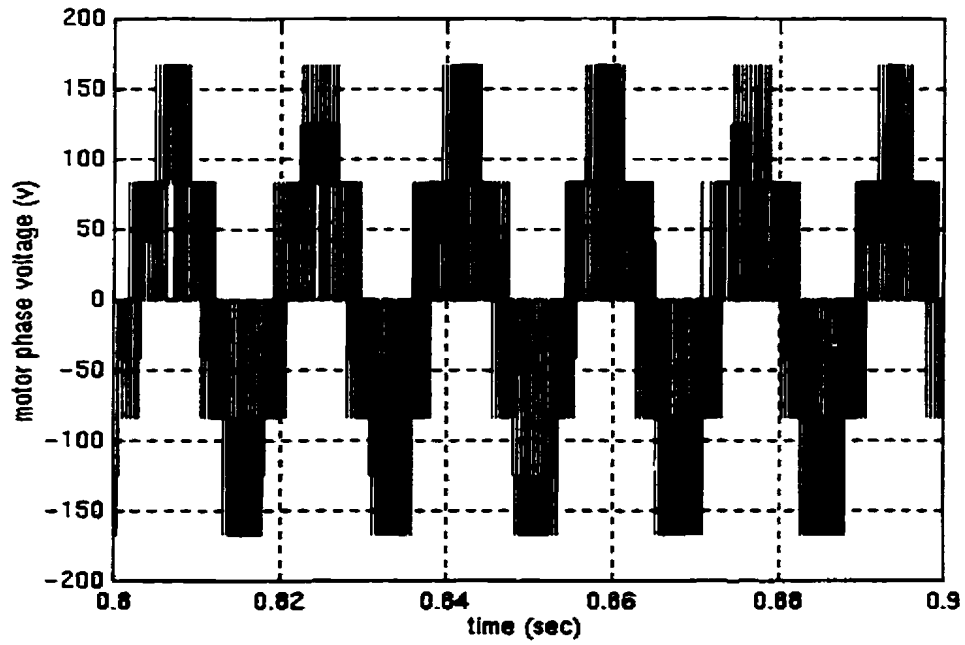


(b)

Figure 5.4: Drive responses at no load with speed command of 180 rad./sec., (a) speed response, and (b) motor phase current.



(c)



(d)

Figure 5.4: Drive responses at no load with speed command of 180 rad./sec., (c) steady state voltage command and (d) motor phase voltage.

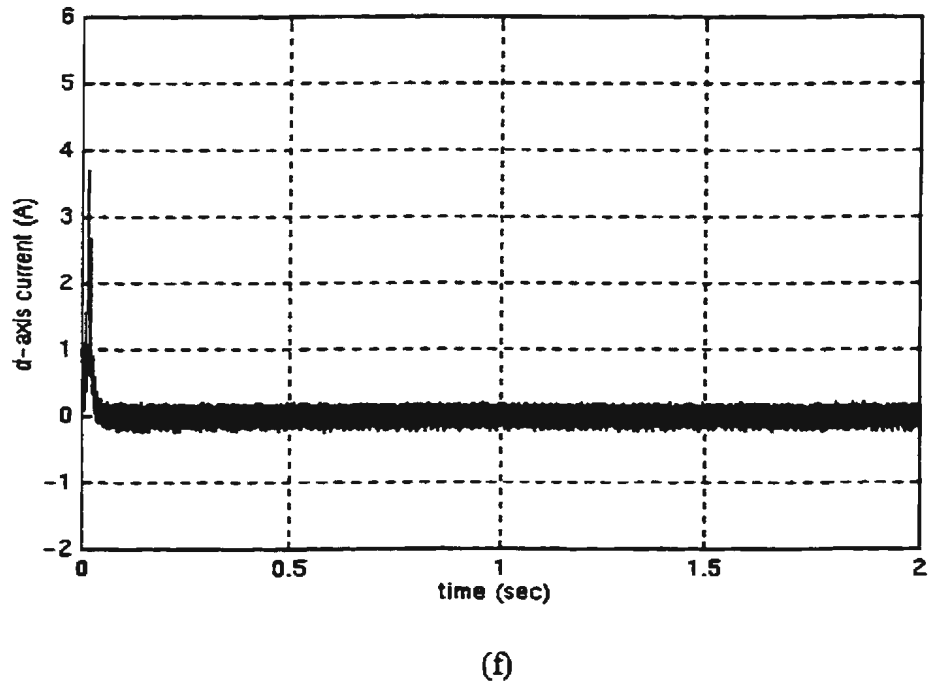
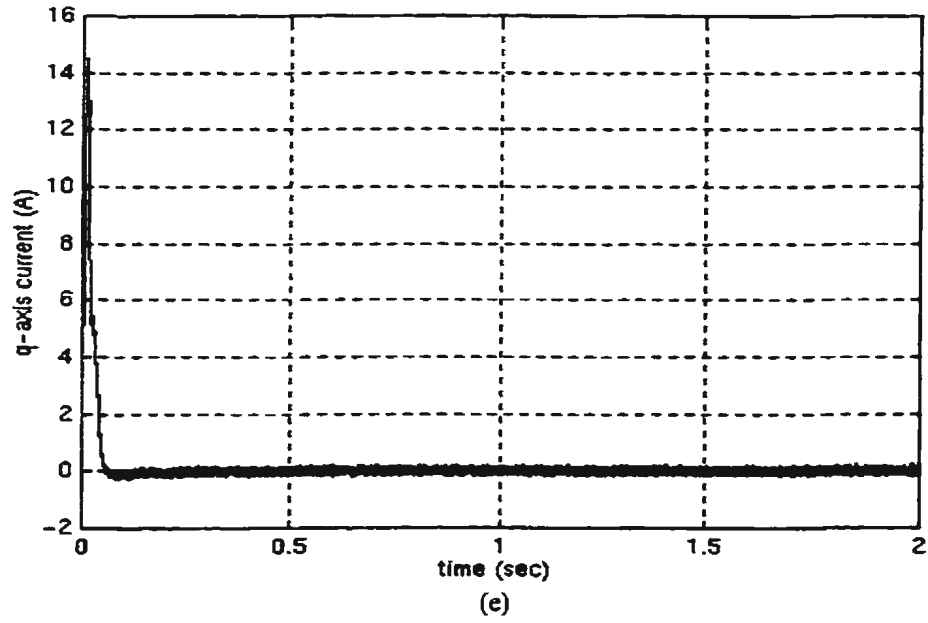


Figure 5.4: Drive responses at no load with speed command of 180 rad./sec., (e) q-axis current and (f) d-axis current.

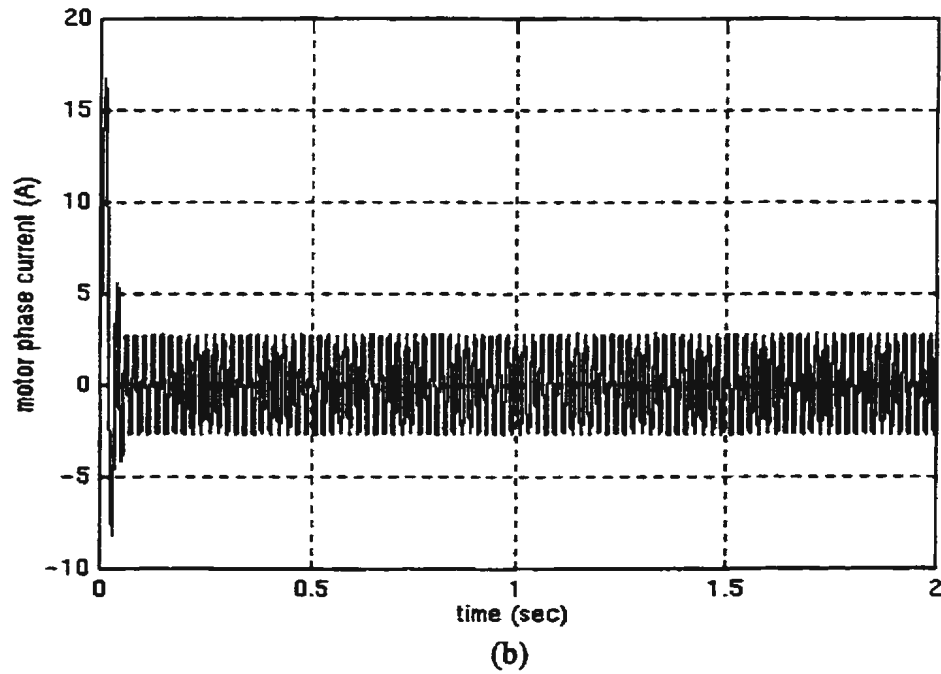
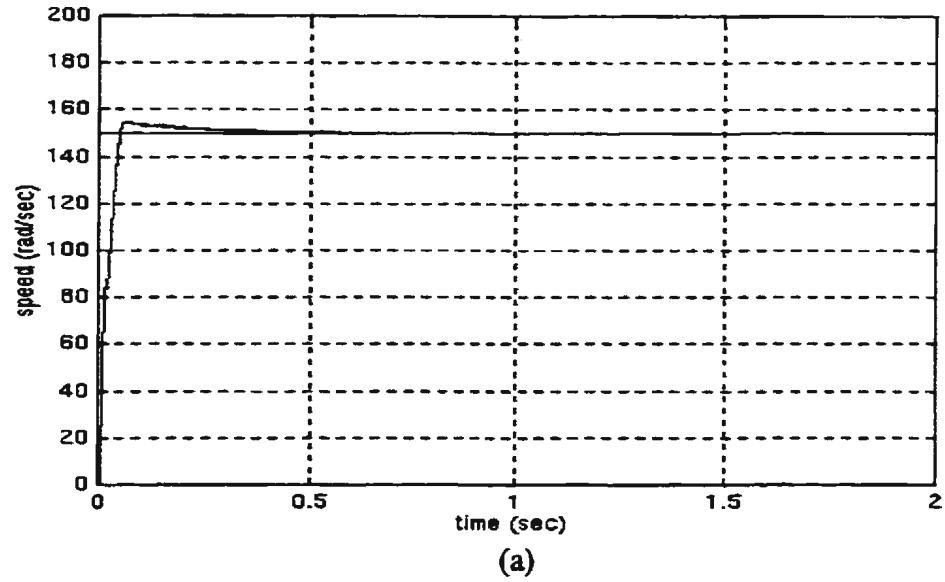


Figure 5.5: Drive responses at full load with speed command of 150 rad./sec., (a) speed response and (b) motor phase current.

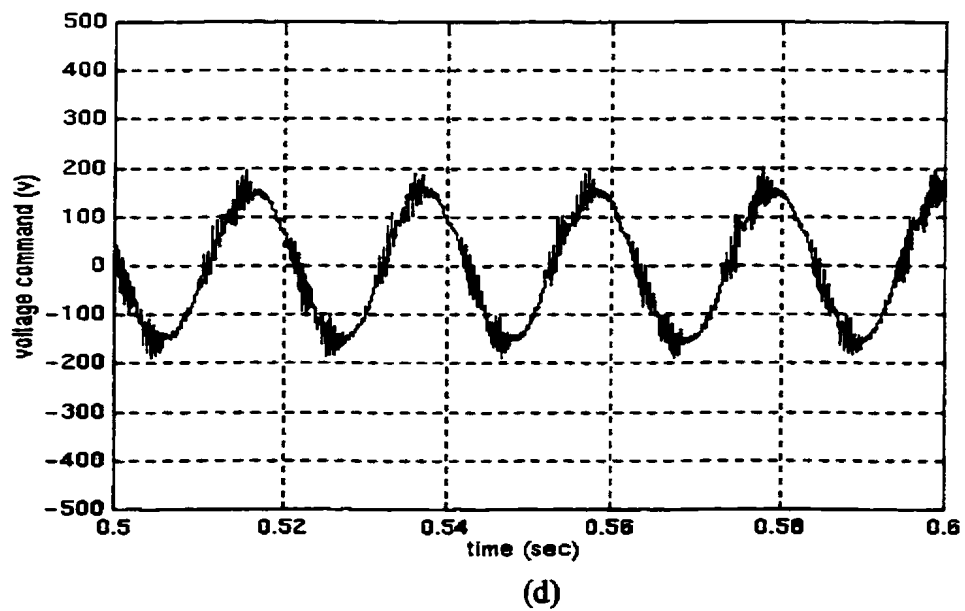
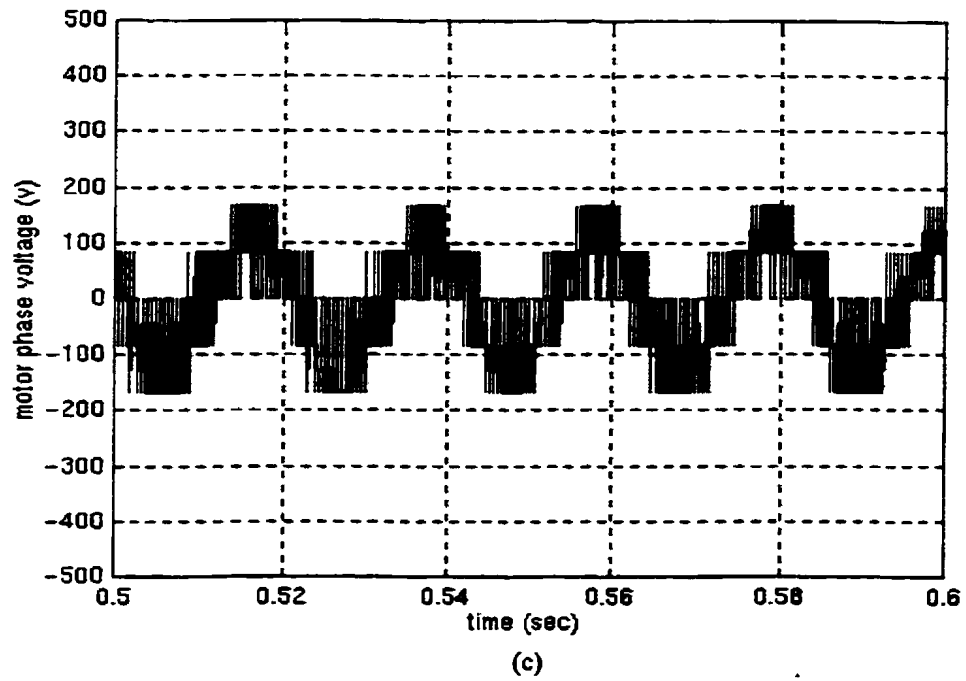


Figure 5.5: Drive responses at full load with speed command of 150 rad./sec., (c) motor phase voltage and (d) voltage command.

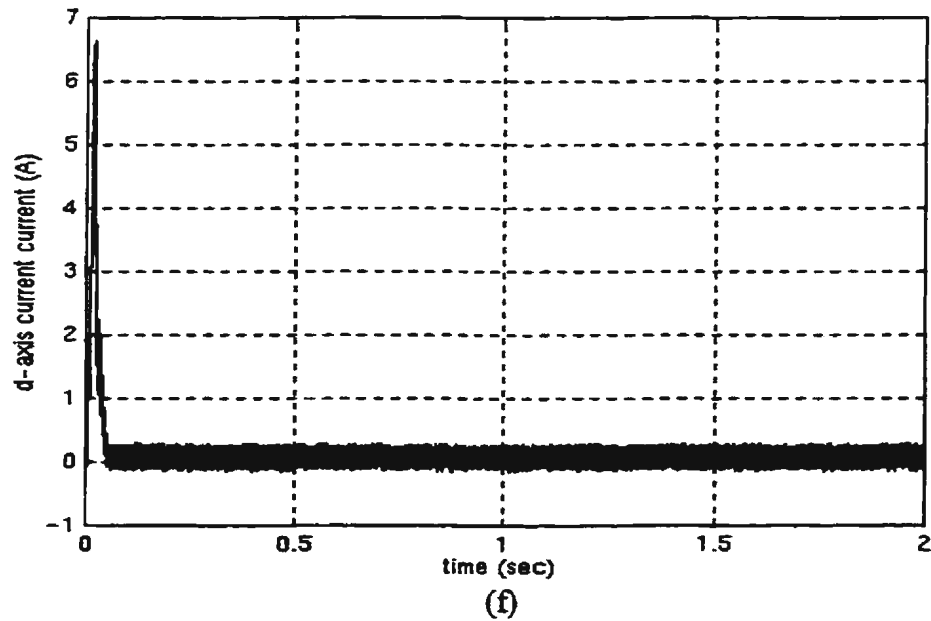
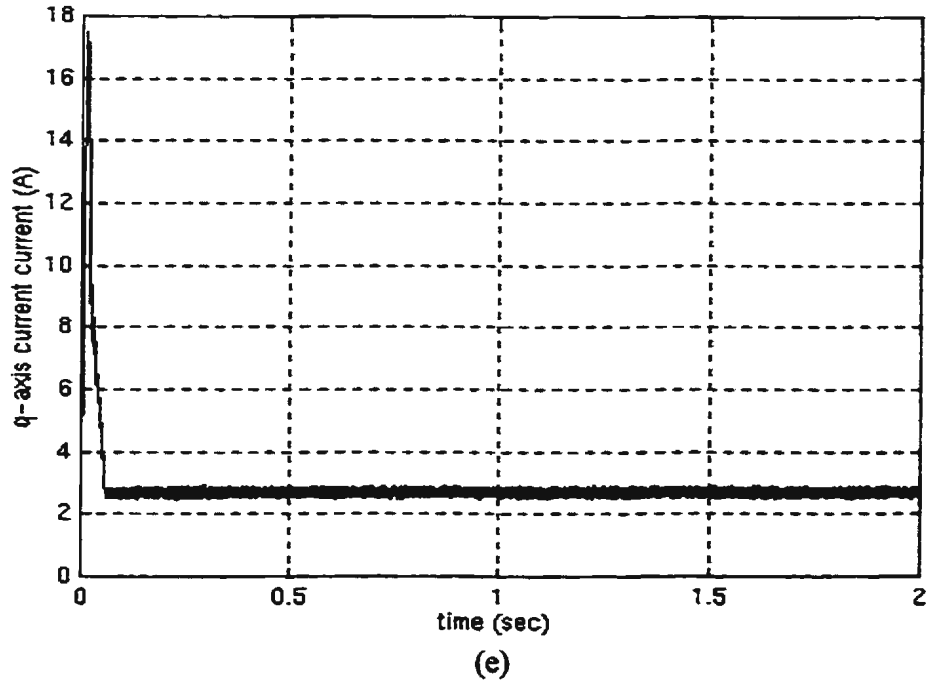


Figure 5.5: Drive responses at full load with speed command of 150 rad./sec., (e) q-axis and current and (f) d-axis current.

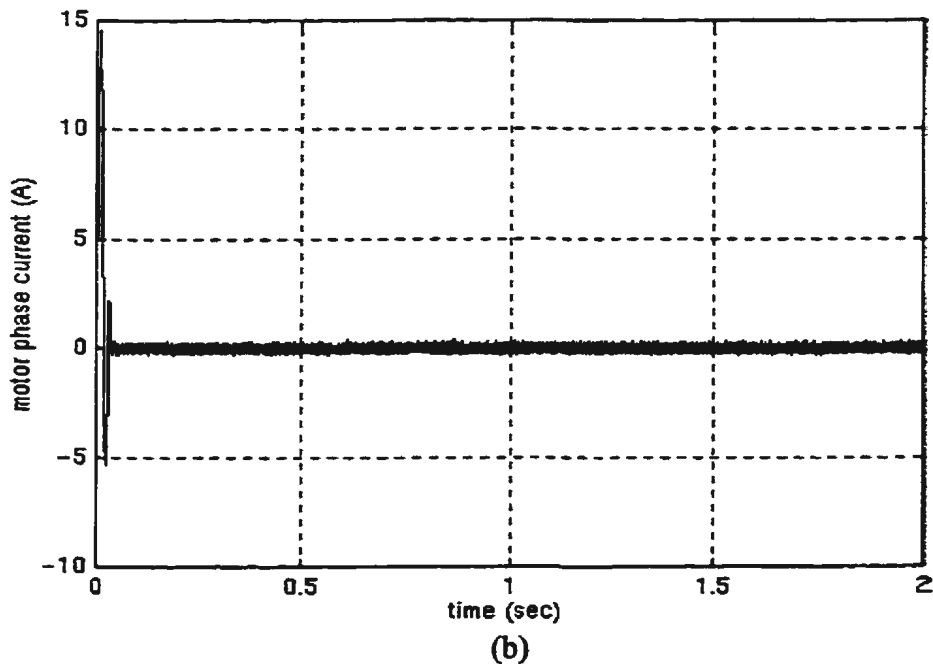
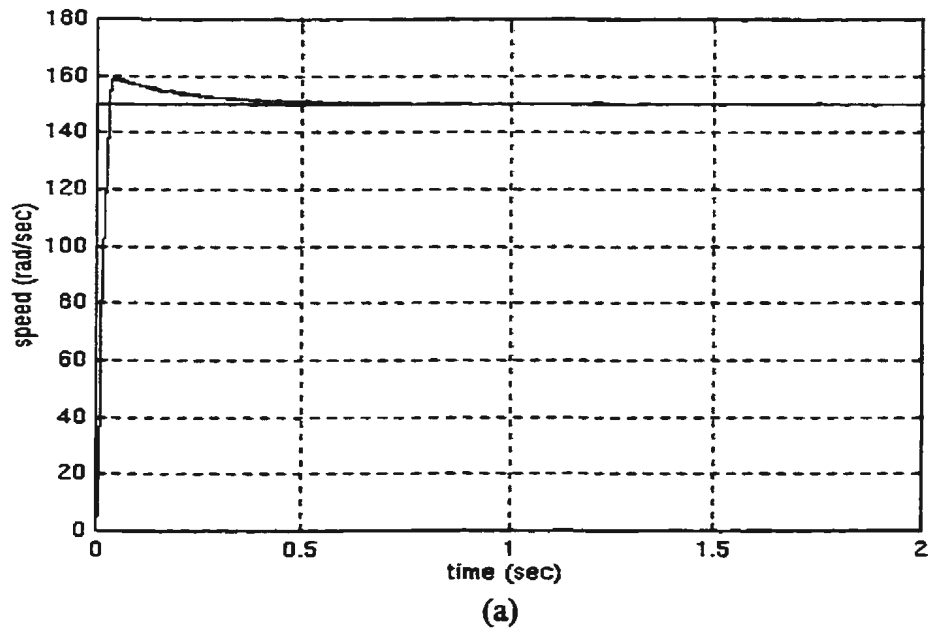


Figure 5.6: Drive responses at no load with speed command of 150 rad./sec., (a) speed response and (b) motor phase current.

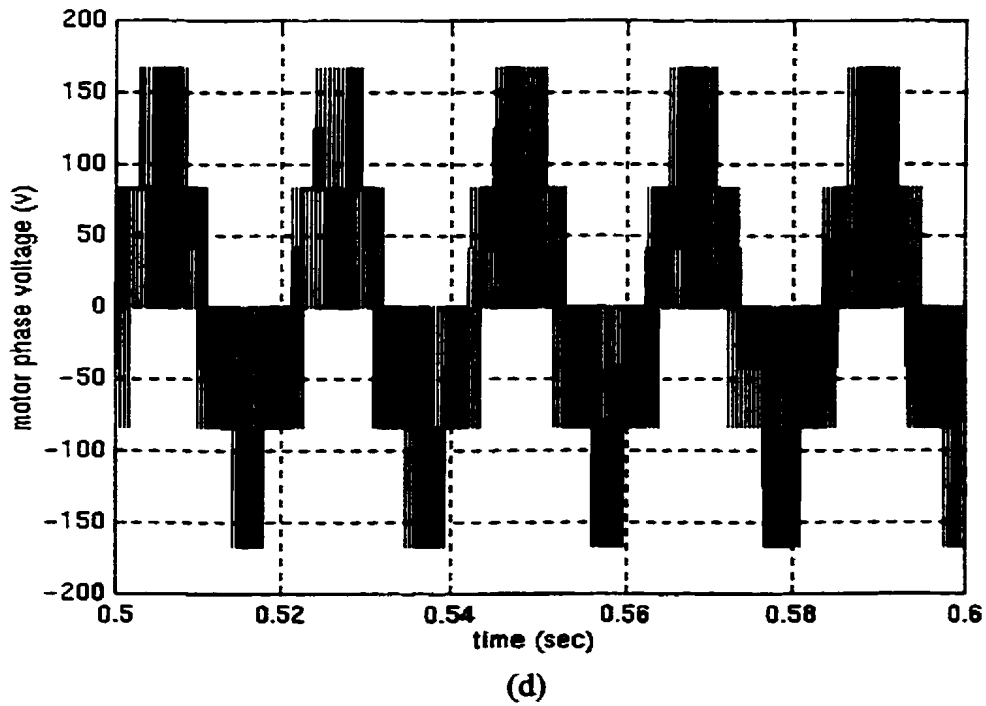
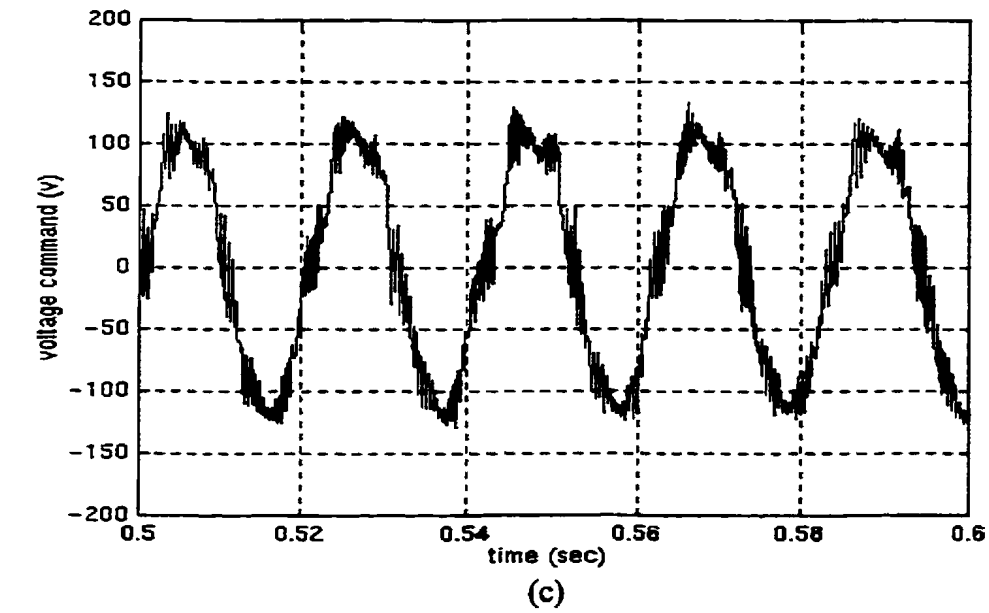


Figure 5.6: Drive responses at no load with command speed of 150 rad./sec., (c) steady state voltage command and (d) motor phase voltage.

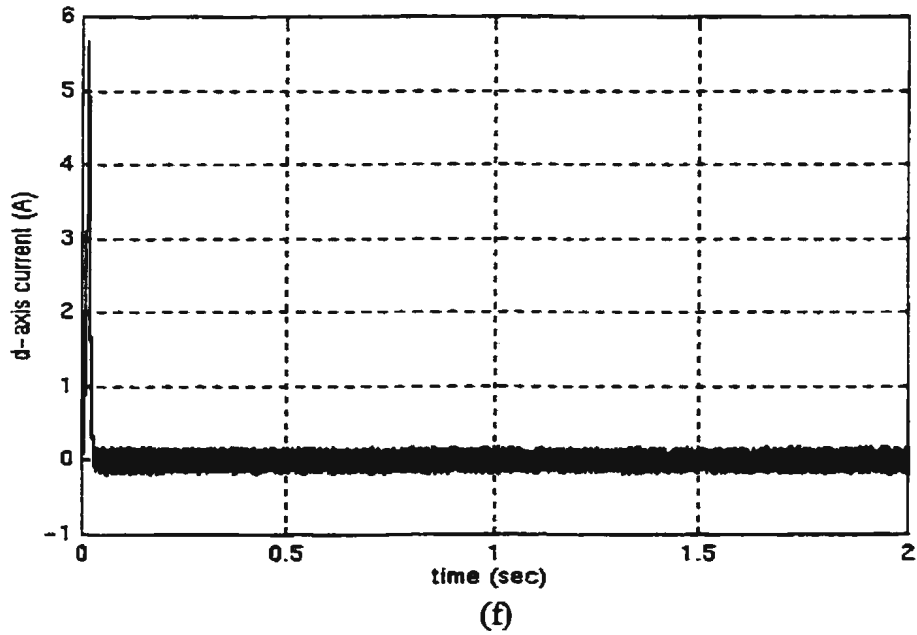
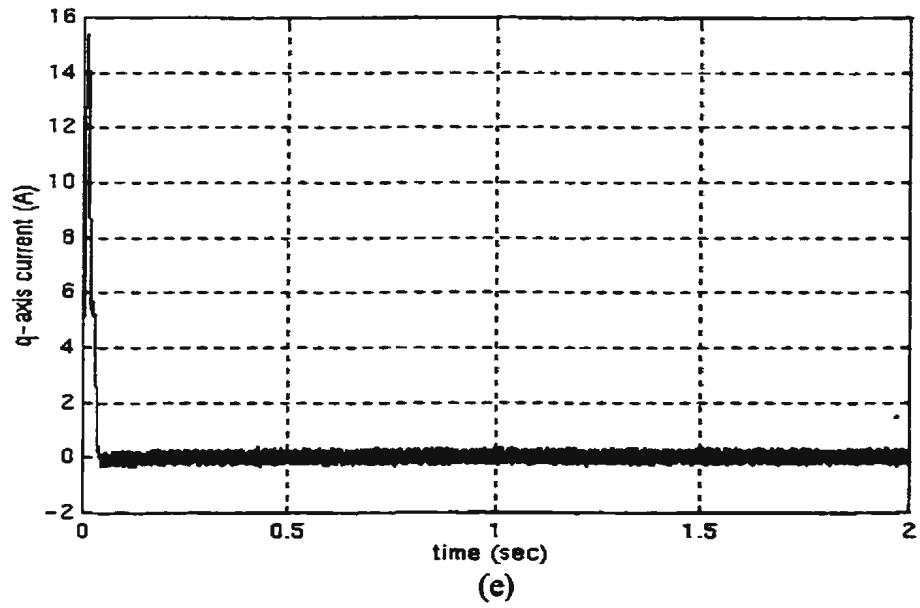
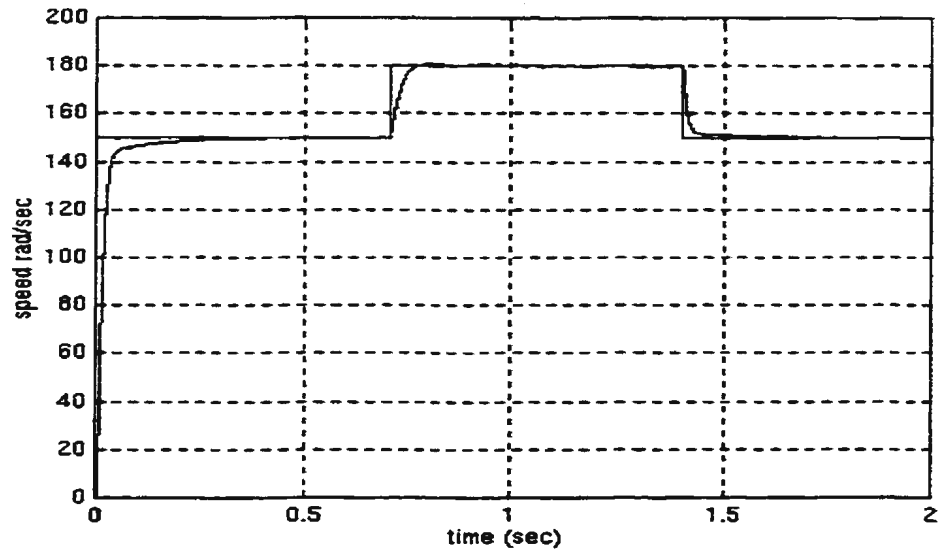


Figure 5.6: Drive responses at no load with speed command of 150 rad./sec., (e) q-axis current and (f) d-axis current.

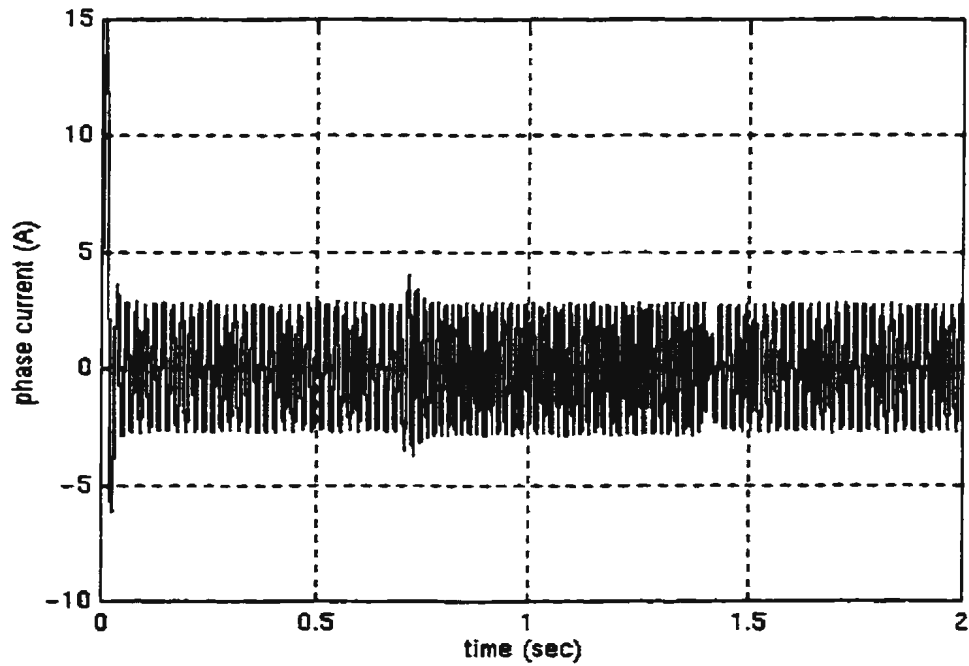
- Step change in the reference speed

The responses due to a step change command are used to evaluate the performances in terms of response time, overshoot, transient or steady state errors and stability.

The motor is subjected to step decrease and step increase in the reference speed under different loading conditions to evaluate its performance. Figure 5.7(a) shows the rotor speed response with a command speed of 150 (rad./sec.) at full load. At $t = 0.7$ second the speed reference has been changed to 180 (rad./sec.), and at $t = 1.4$ second the speed is changed back to 150 (rad./sec.). We can see that the rotor speed is accelerated and decelerated smoothly to follow its reference value with nearly zero steady state errors. Figure 5.7 (b) shows the motor phase current. The current shows corresponding increase and decrease during the step changes in the reference speed due to the dynamic states. Figures 5.7 (c) and (d) show the q-axis and d-axis current components, respectively. The q-axis and d-axis current components have changed momentarily and returned to their previous values quickly. Figure 5.7 (e) shows the phase current during the period from $t = 0.6$ sec. to 0.8 sec. This shows the increase in phase current at $t = 0.7$ sec. and the decrease in phase current quickly. The decrease and increase of the phase current during the period from $t = 1.35$ to 1.5 second are shown in Figure 5.7 (f). Figures 5.7 (g) and (h) show the increase and decrease of the voltage commands for the step increase and decrease in speed. These responses are shown in the periods of time from 0.6 sec. to 0.8 sec. and from 1.3 sec. to 1.5 sec., respectively. Figures 5.7 (j) and (l) show the motor phase voltage for the increase and decrease of the speed command. Similar results like those of Figure 5.7 were obtained at no load as shown in Figure 5.8.

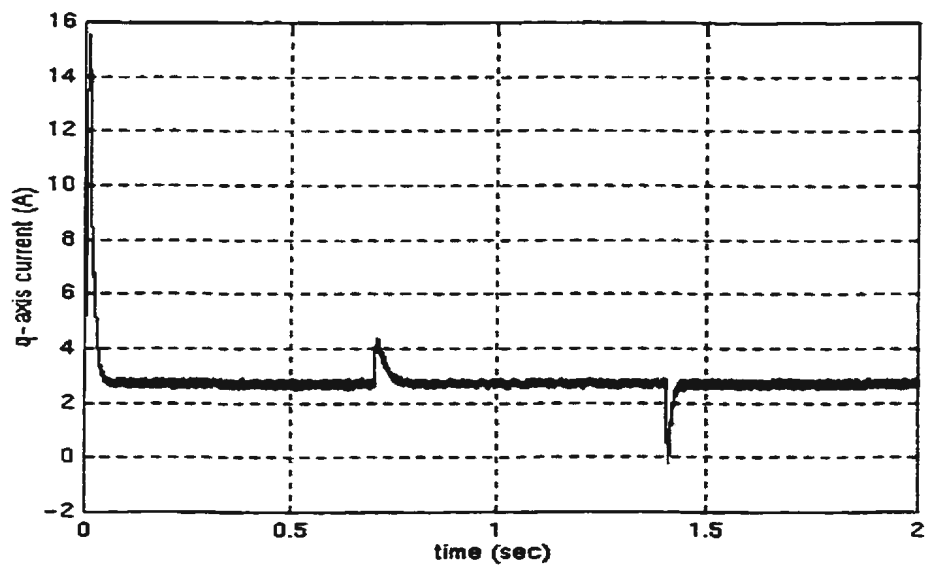


(a)

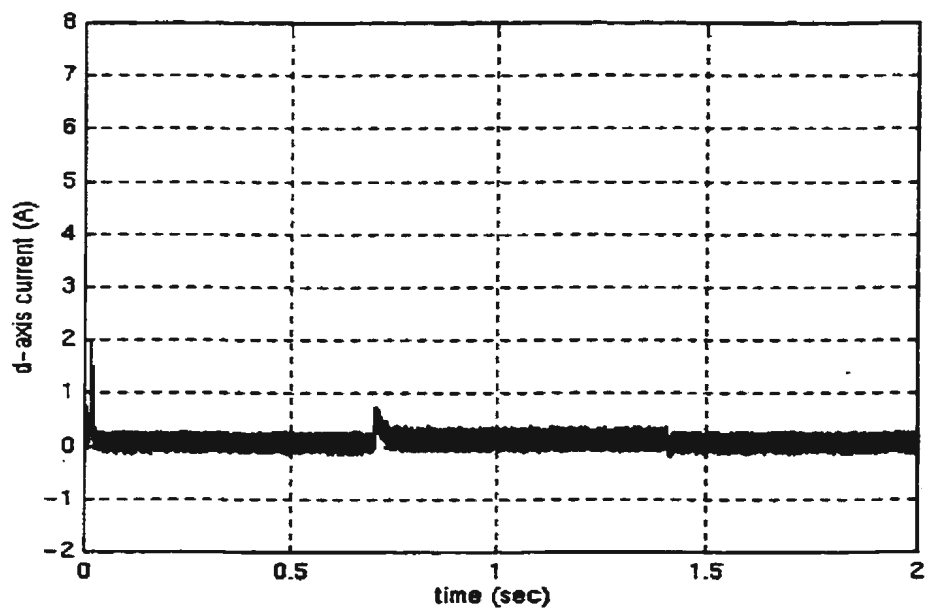


(b)

Figure 5.7 Drive responses for step change in the reference speed at full load, (a) speed response and (b) motor phase current.

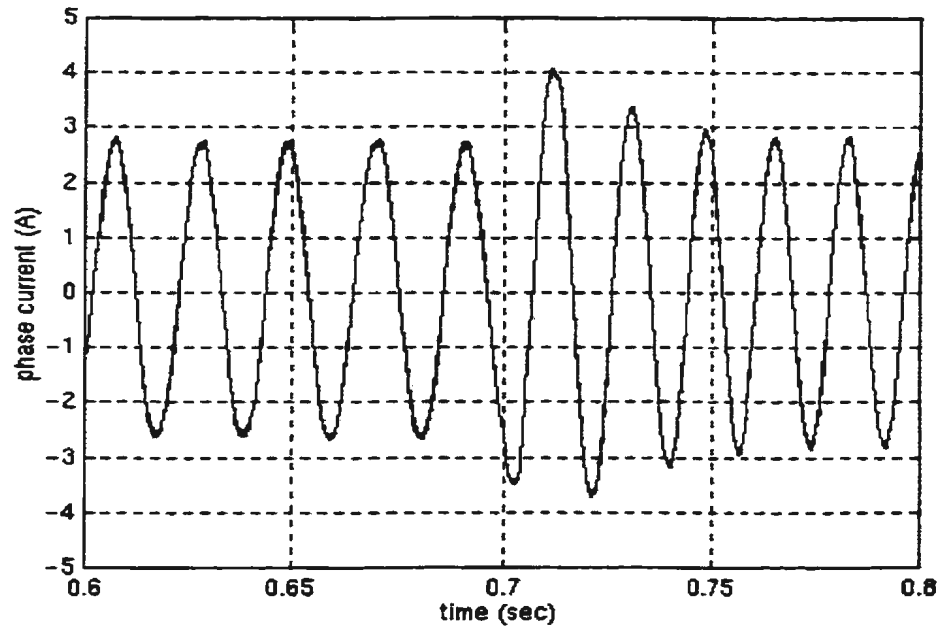


(c)

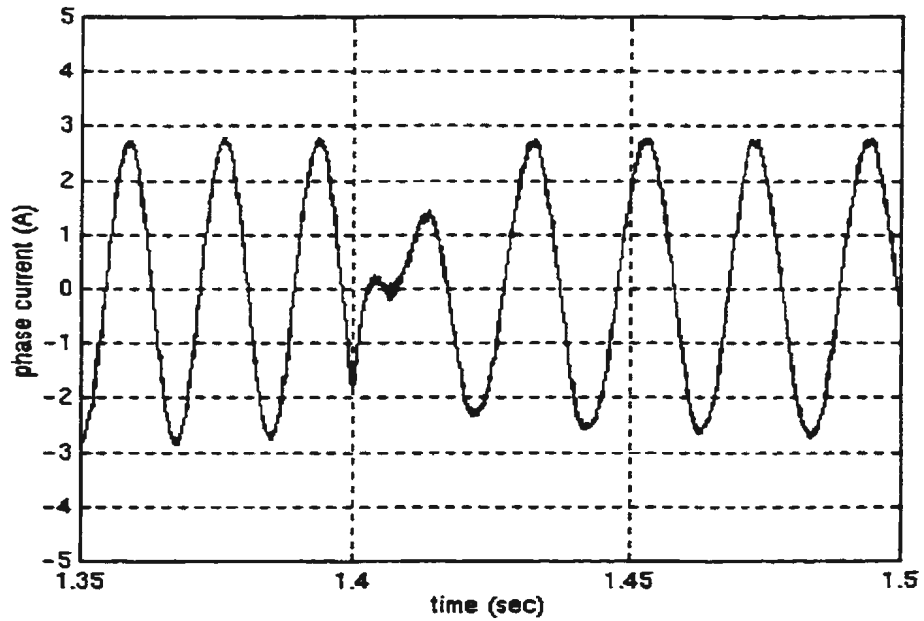


(d)

Figure 5.7: Drive responses for step change in the reference speed at full load, (c) q-axis current and (d) d-axis current.

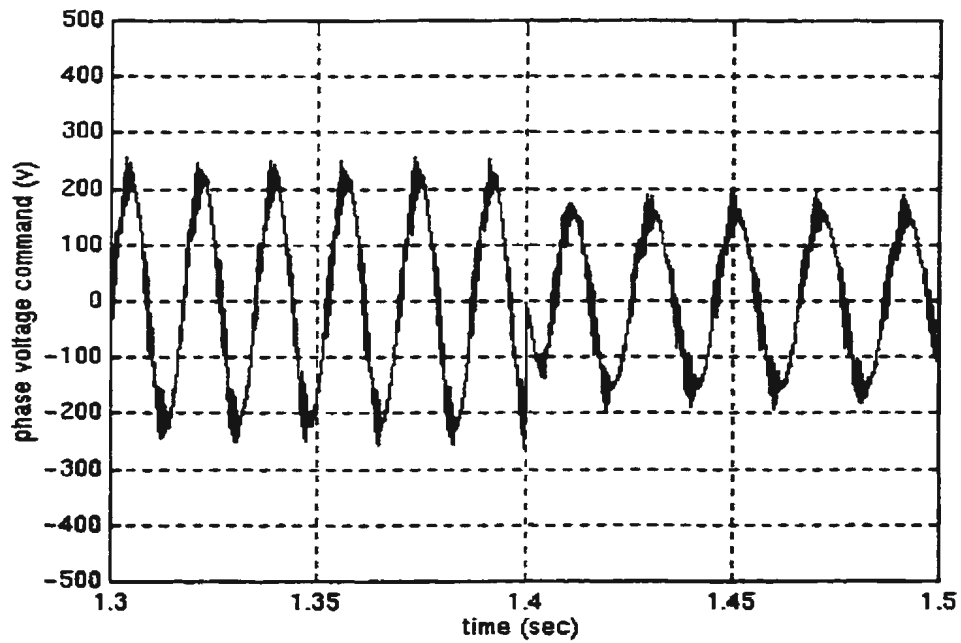
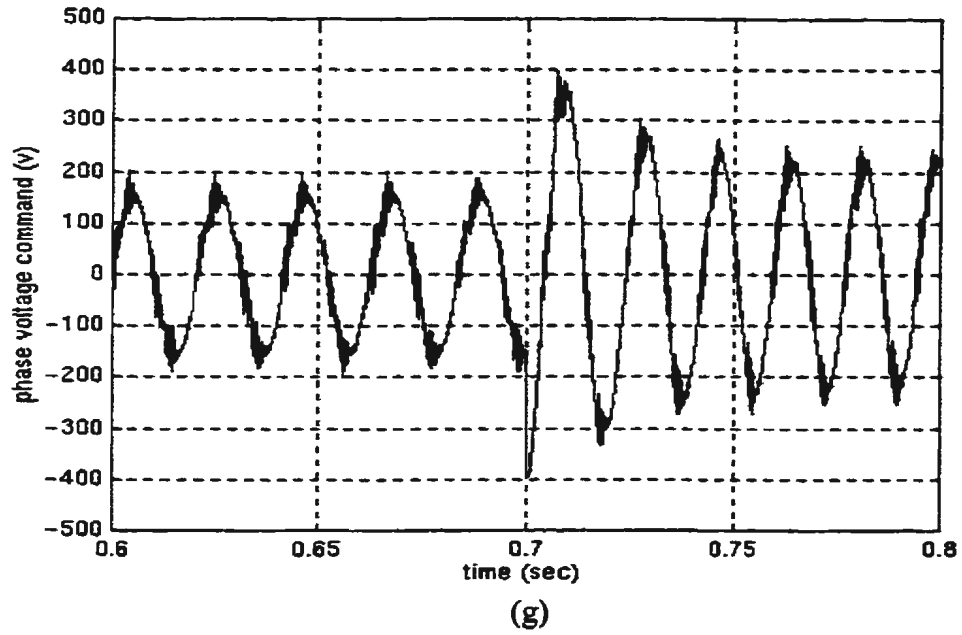


(e)



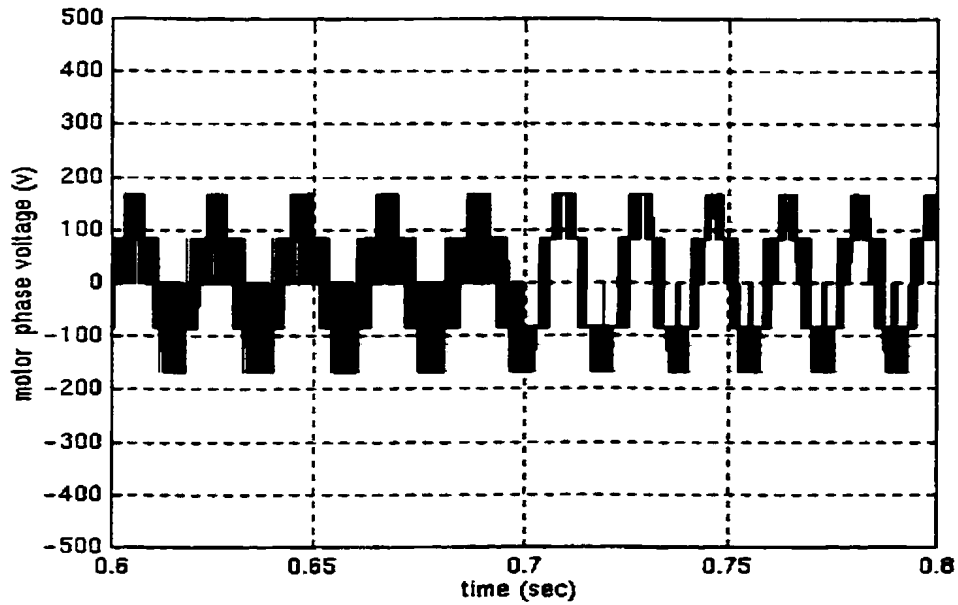
(f)

Figure 5.7: Drive responses for step change in the reference speed at full load, (e) motor phase current during speed increase and (f) motor phase current during speed decrease.

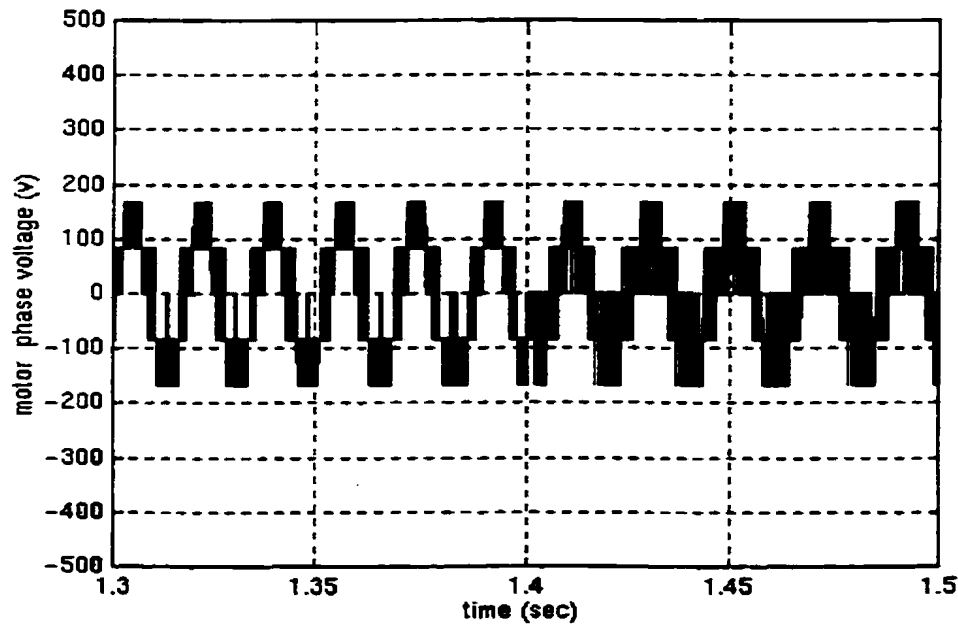


(h)

Figure 5.7: Drive responses for step change in the reference speed at full load, (g) voltage command during step increase in speed and (h) voltage command during step decrease in speed.

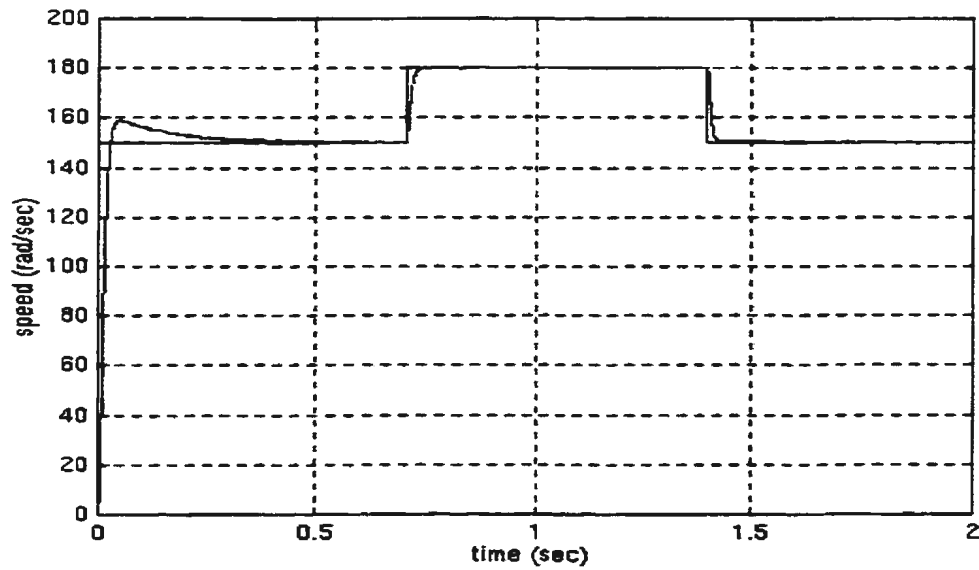


(j)

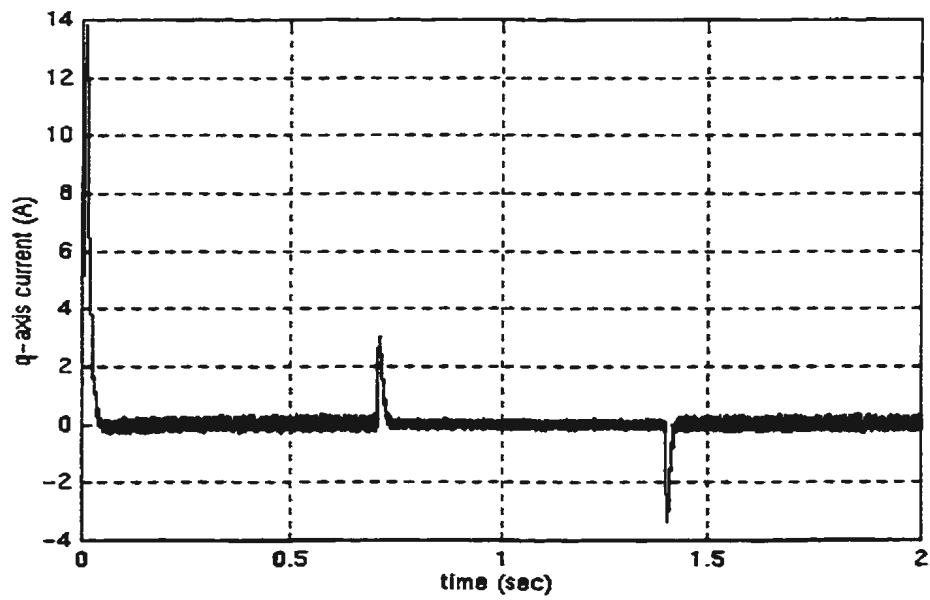


(l)

Figure 5.7: Drive responses for the step change in the reference speed at full load, (j) motor phase voltage during the step increase of speed and (l) motor phase voltage during the decrease of speed.



(a)



(b)

Figure 5.8: Drive responses for step change in the reference speed at no load, (a) speed response and (b) q-axis current.

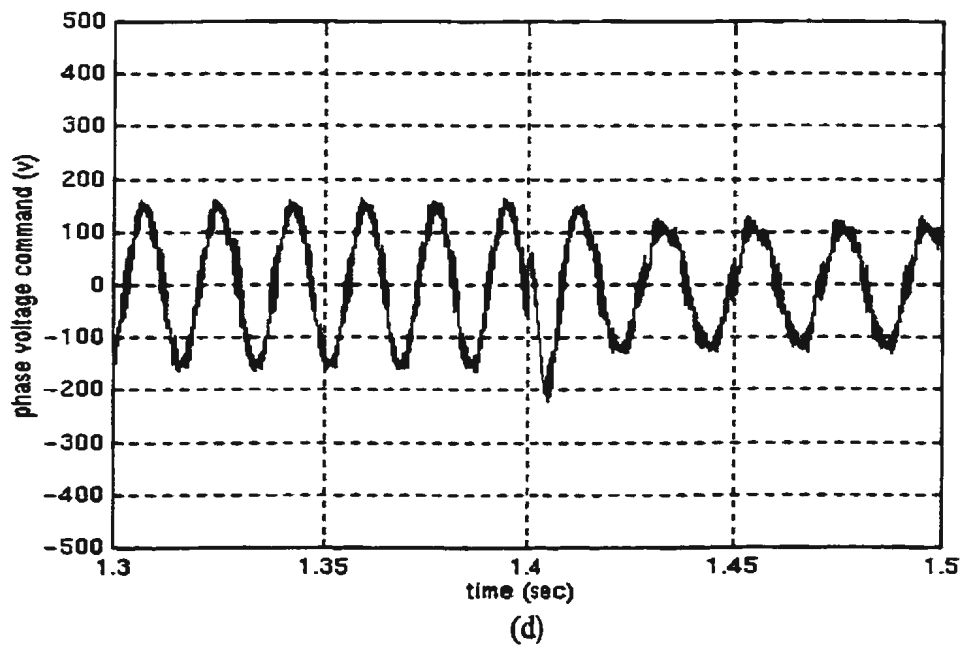
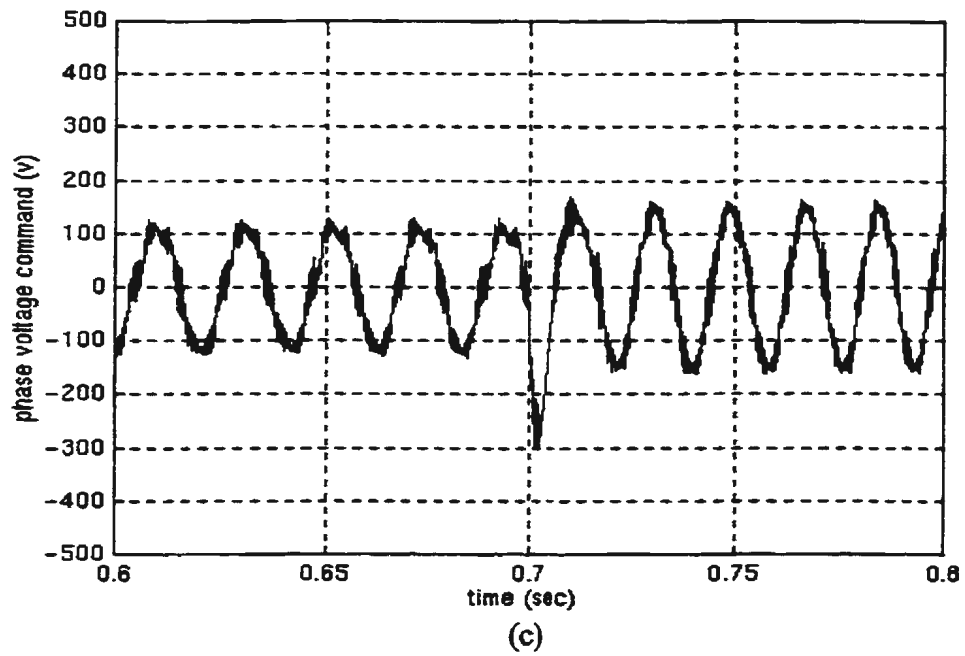


Figure 5.8: Drive responses for the step change in the reference speed, (c) voltage command during the step increase of speed and (d) voltage command during the step decrease of speed.

- Step change in the load

The ability to withstand disturbances in PMSM control system is another important feature. A step change in the motor load is considered as a typical external disturbance. A high performance control system should have a fast dynamic response in adjusting its control variables so that the system outputs affected by the load disturbances will recover to their original status as soon as possible. The dropped aptitude of the system output such as rotor speed and its recovering time are the important performance specifications.

Figure 5.9 (a) shows the speed response when the step change in the load is applied. The motor started at 50% load and the full load is applied after one second. The corresponding motor torque has emerged to balance the load at constant speed. Figure 5.9 (b) shows the q-axis current component that quickly followed the load applied to attain the equilibrium. Figure 5.9 (c) shows the phase voltage command during the change of the load. Figure 5.9 (d) shows the motor phase current that increased rapidly for the new load.

Similar results like those of Figure 5.9 were obtained with speed command at 150 rad/second. These are shown in the Figure 5.10

- Speed reversal:

The field oriented control of the PMSM drive can be operated in four quadrants like those in the dc motor. Figure 5.11 shows the system response for speed reversal. It is seen that the speed follows its reference command quickly. Figure 5.11 (a) shows the change from positive speed to negative speed. Figure 5.11(b) shows negative q-axis current.

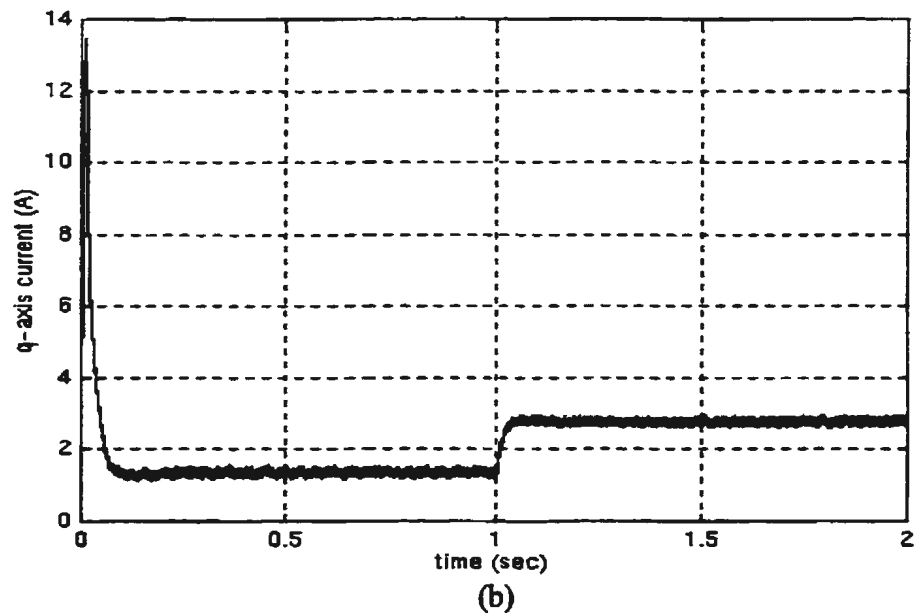
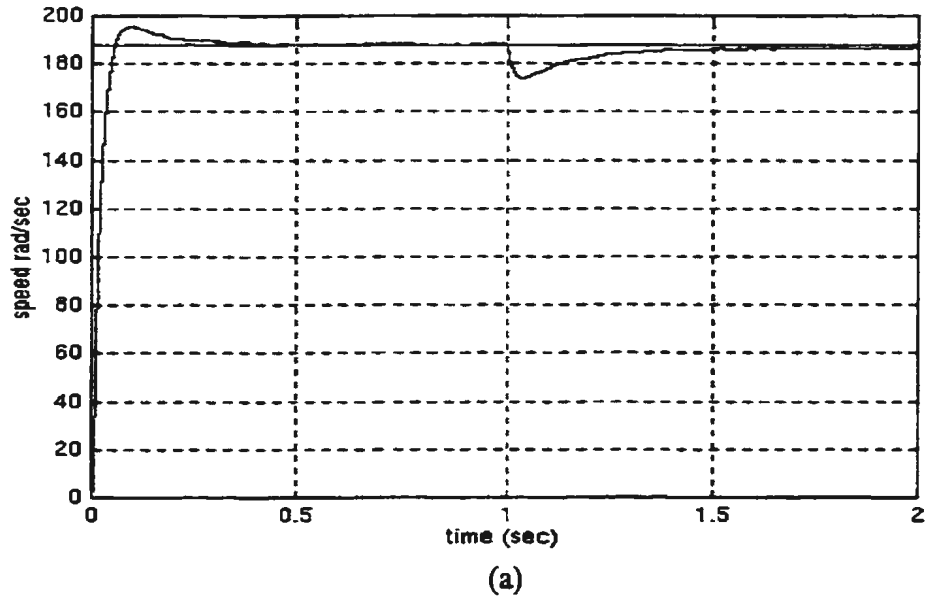


Figure 5.9: Drive responses for the step change in the load with speed command of 188 rad./sec., (a) speed response and (b)q-axis current.

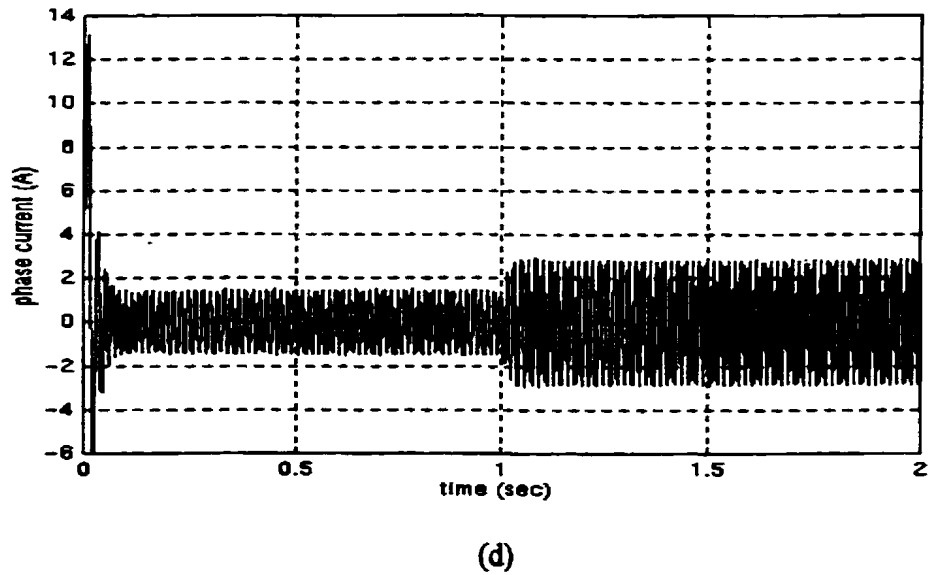
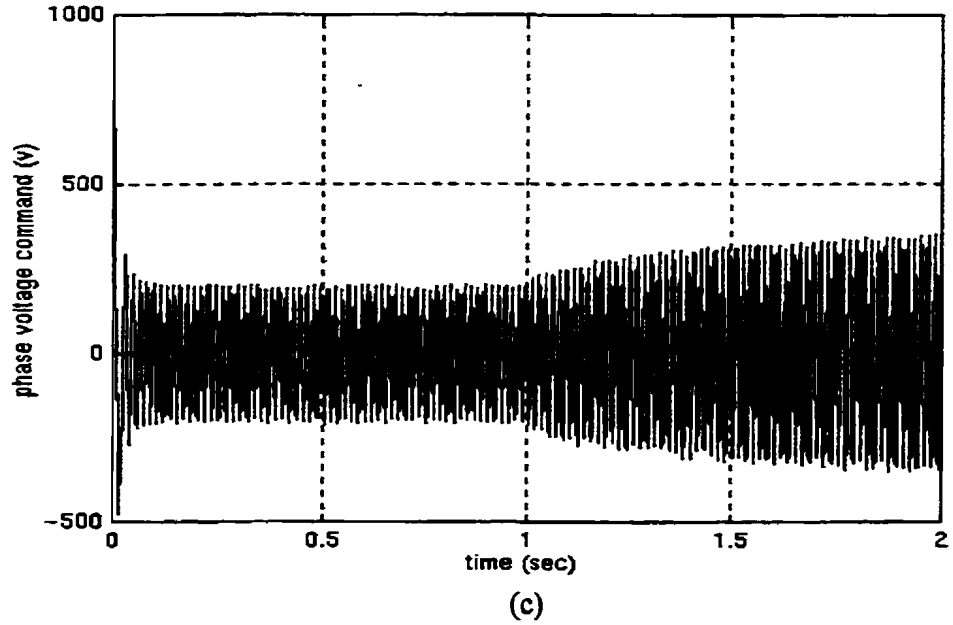


Figure 5.9: Drive response for the step change in load with speed command of 188 rad./sec., (c) phase voltage command and (d) motor phase current.

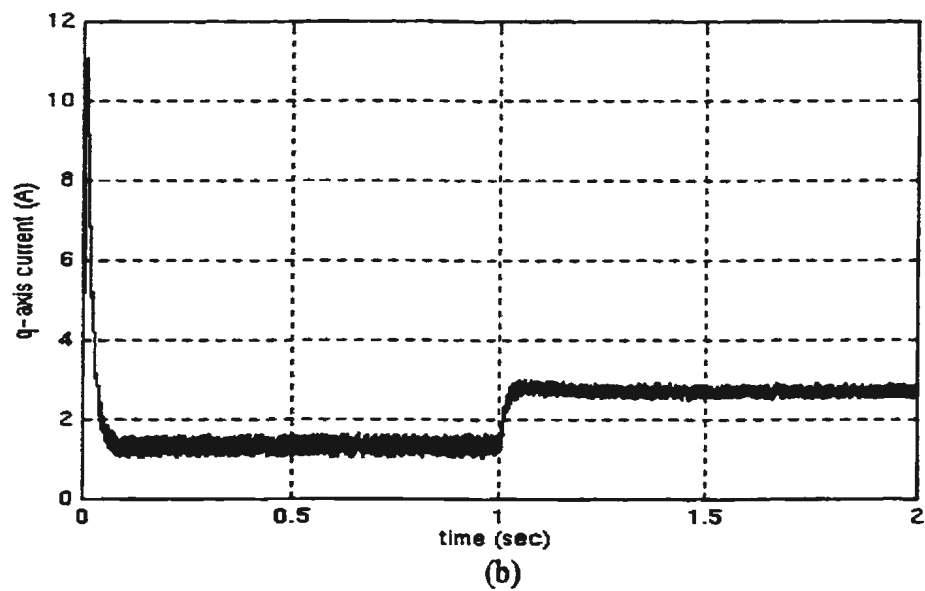
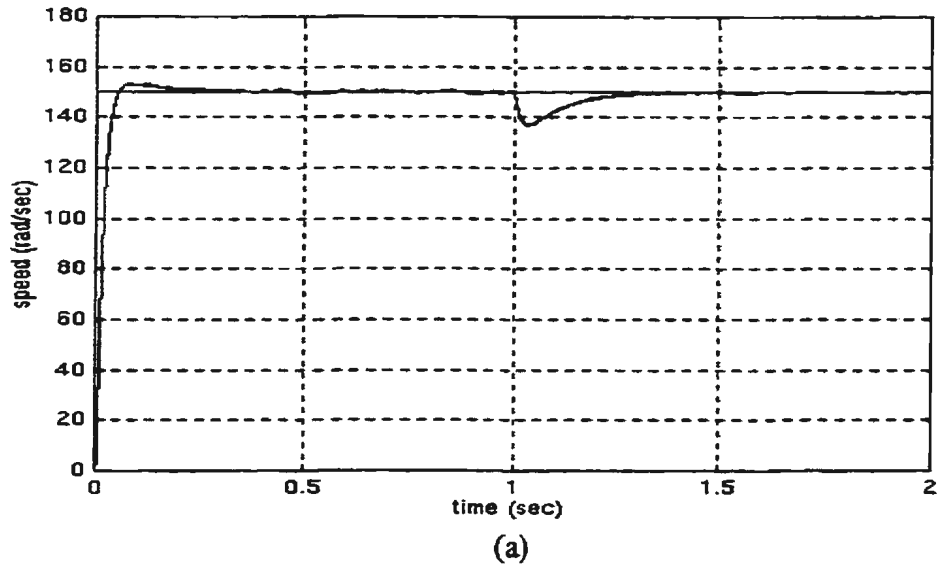


Figure 5.10: Drive responses for the step change in load with speed command of 150 rad./sec., (a) speed response and (b) q-axis current

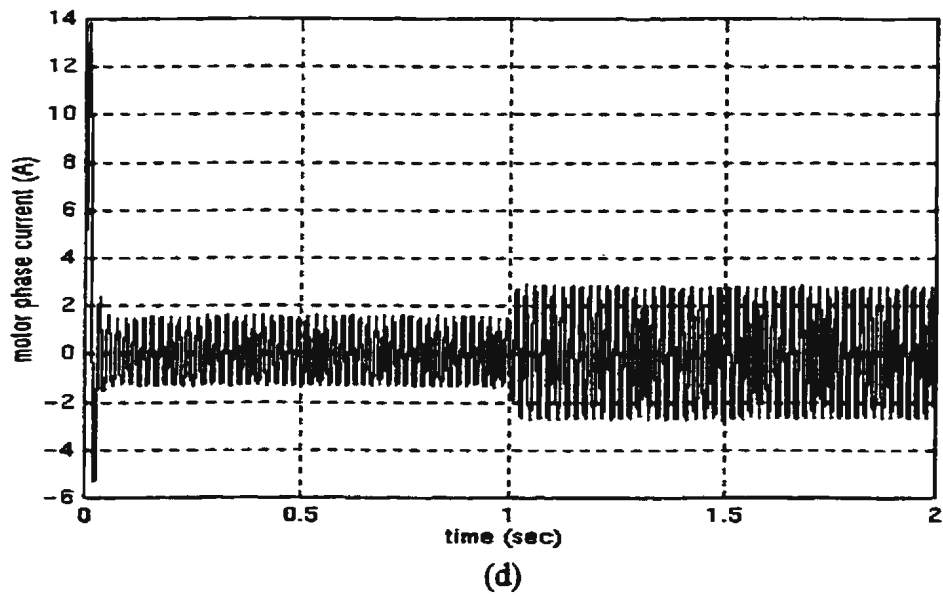
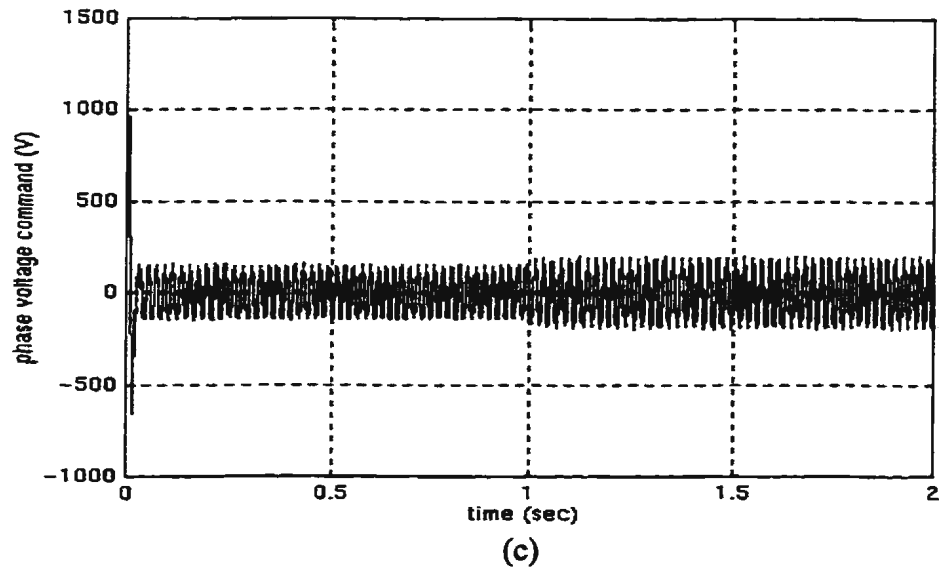
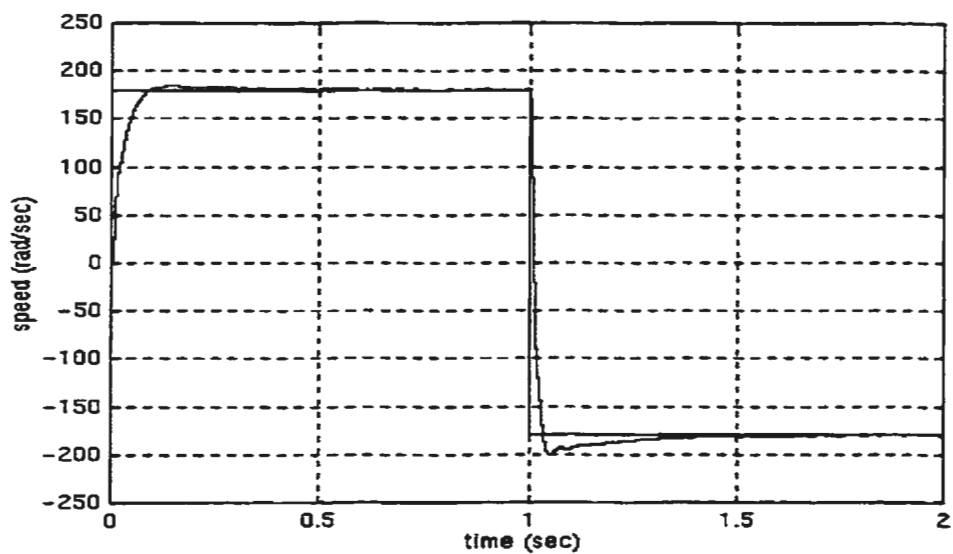
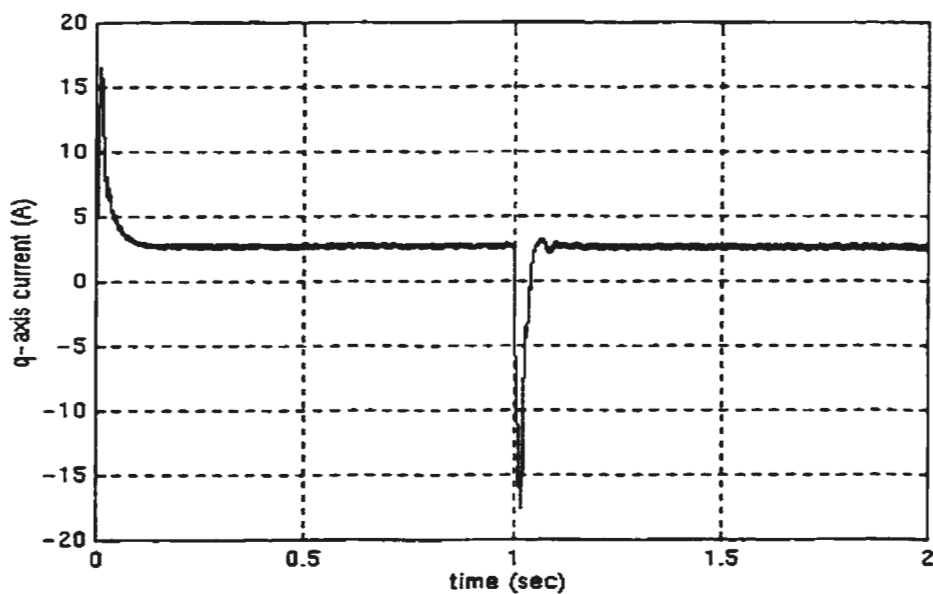


Figure 5.10: Drive responses for the step change in load with speed command of 150 rad./sec., (c) phase voltage command and (d) motor phase current.



(a)



(b)

Figure 5.11: Drive responses for speed reversal with speed command of 180 rad./ sec. to -180 rad./ sec., (a) speed response and (b) q-axis current.

5.3 Real-time implementation

5.3.1 Experimental set up.

The schematic of the experimental set up of the drive system is shown in Figure 5.12. The entire control scheme is implemented using the DSP controller board DS1102. The main processor of the board is based on TMS320C31 high speed main DSP and slave DSP TMS320E14. The description and details of this board are given in Appendix C. The motor currents are measured using Hall-effect sensors and fed to the board through the 12-bit A/D converters. The rotor position is sensed using incremental encoder. The output of the encoder is fed to the DSP board through built-in incremental encoder interface. Using 24-bit up down counter, the value of the rotor position θ_e is fed to the software for the purpose of co-ordinate transformation. The outputs from the board are in the form of 6-PWM pulses which are fed to the inverter through isolation and driving circuits. Since the controllers work in synchronous reference frame, the measured phase currents have to be transformed. The speed controller and current controllers as well as the co-ordinate transformation are implemented in software using high level C programming language (see Appendix D and Appendix E). The sampling times for speed and current loops are 1ms and 100 μ s, respectively. The C source file is compiled using TI compiler and downloaded to the DSP board using the dSPACE software.

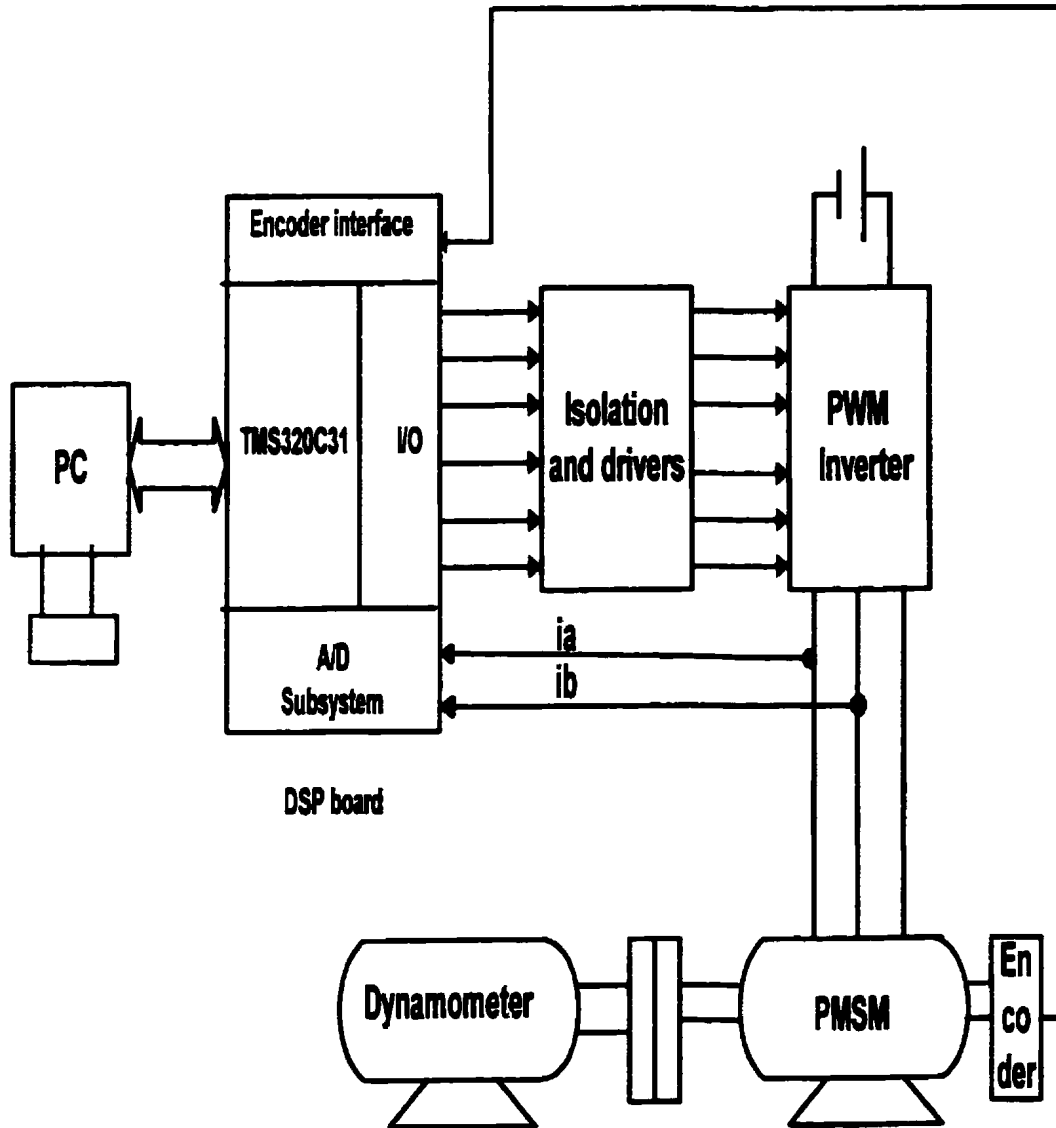


Figure 5.12: Experimental set up for PMSM

5.3.2 Experimental results

A series of the experimental investigations have been carried out to verify the validity of the multi-loop controls. These results were obtained by different tests including at no load and full load conditions. All the results were displayed through the D/A converters on the DSP board and recorded using digital oscilloscope. Figure 5.13(a) shows the speed response at full load with command speed of 150 rad./sec. The motor started with acceptable overshoot and it is noted that the motor speed follows its command value with nearly zero steady-state error. The motor phase voltage is shown in Figure 5.13 (b).

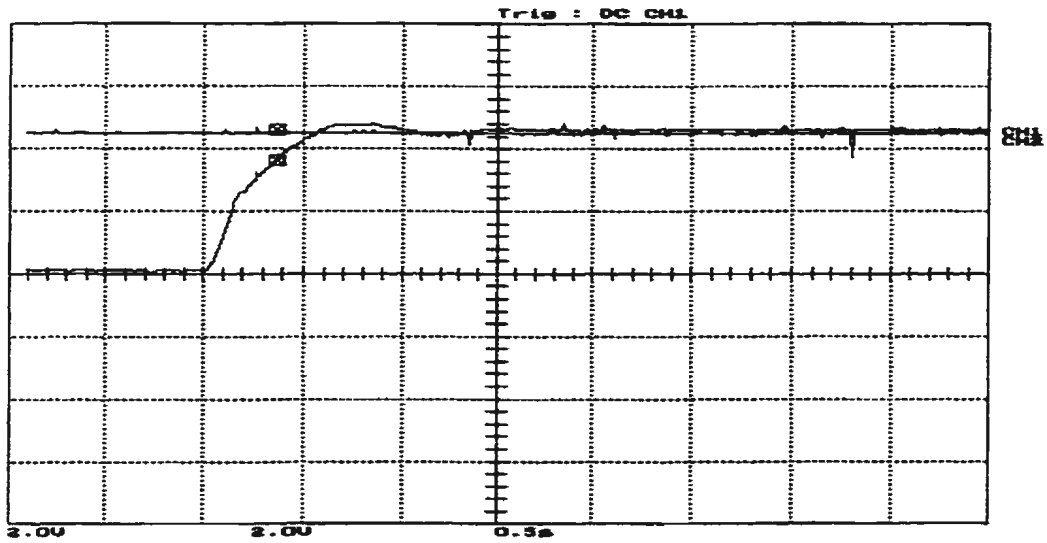
- For step change in the command speed condition

Figure 5.14(a) shows the step change in speed from 150rad./sec to 180rad./sec, then back to 150rad./sec at half load. It is seen that the rotor is accelerated and decelerated smoothly to follow its reference command. Figure 5.14(b) shows the q-axis current component that changed during the step up and step down of the speed and quickly returned to the steady state condition. Figure 5.15 (a) shows the step change in speed from 150rad./sec. to 180rad./sec. then to 150rad./sec. at full load. Figure 5.15(b) shows the phase current.

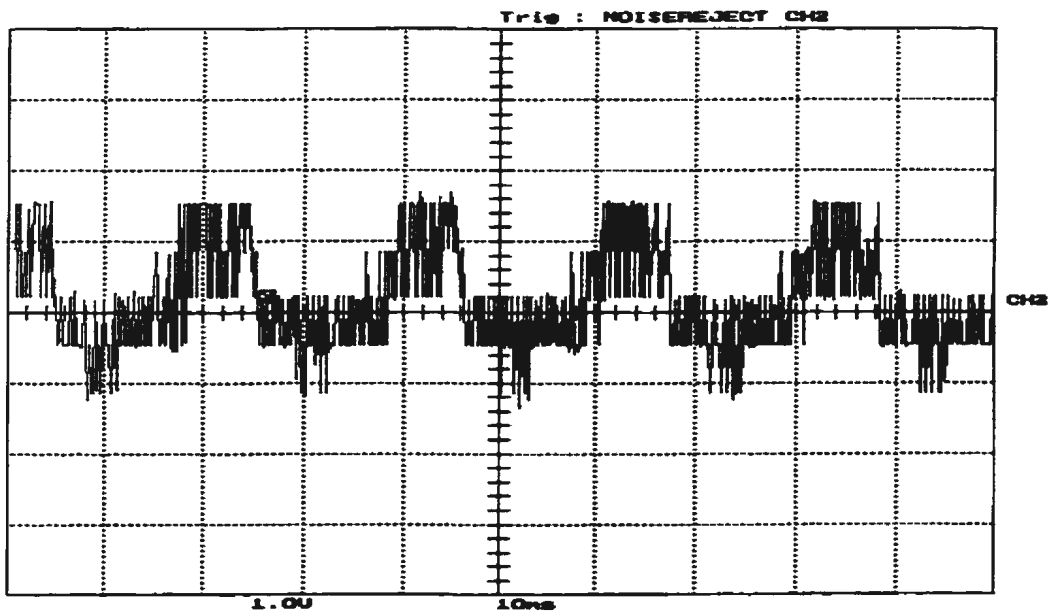
- For step change in the load condition

The motor started with half load with speed command of 150 rad./sec, and a full load is applied suddenly. Figure 5.16(a) shows the speed response during the step change in the load. The speed recovered quickly and followed its reference. Figure 5.16(b) shows the phase current during the change and the current increased to satisfy the load condition. Similar results were obtained as shown in figure 5.17 for the speed at 188 rad./sec. and step change in load from half load to full load.

In summary the experimental results showed that multi central strategy worked reasonably well for sudden changes in speed and loading commands for the laboratory 1hp permanent synchronous motor.

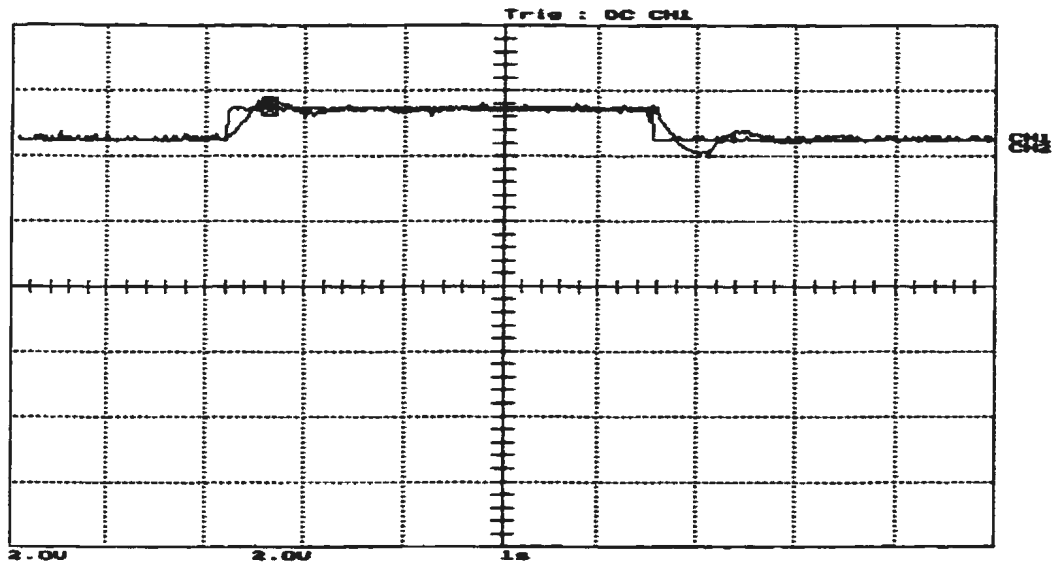


(a)

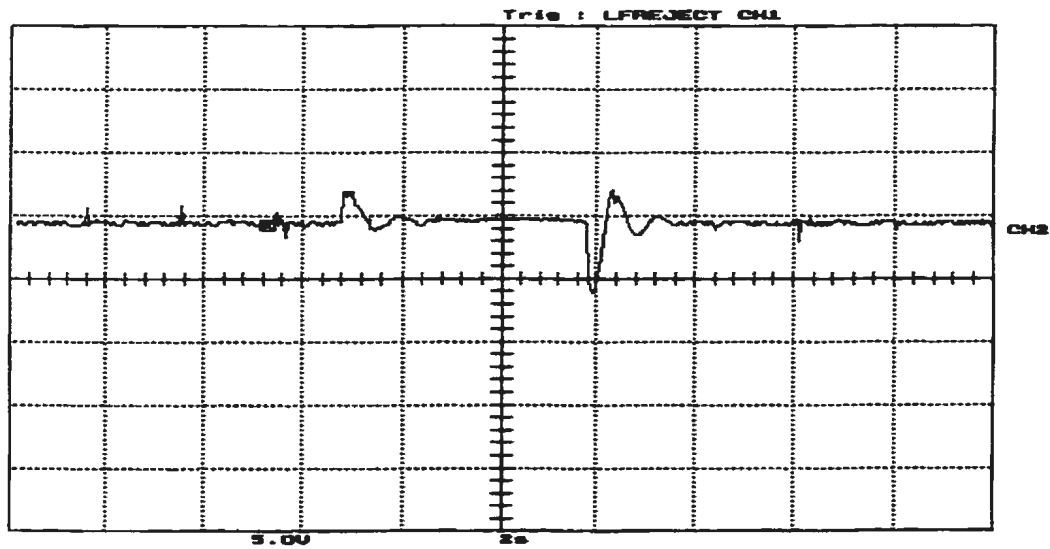


(b)

Figure 5.13: Drive responses at full load with speed command of 150 rad./sec., (a) speed response (speed scale 66.67 rad./sec/div) and (b) motor phase voltage (voltage scale 150 volt/div).

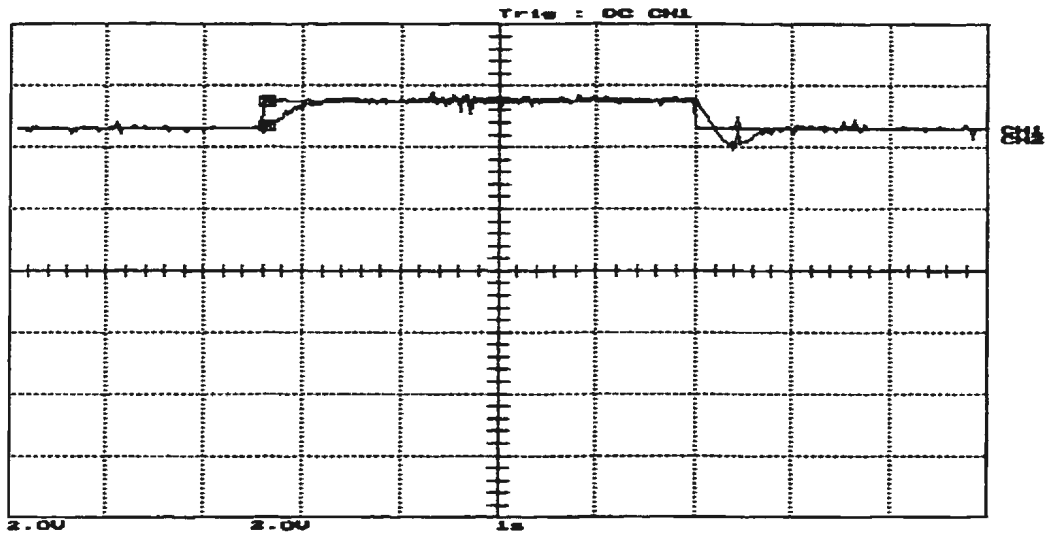


(a)

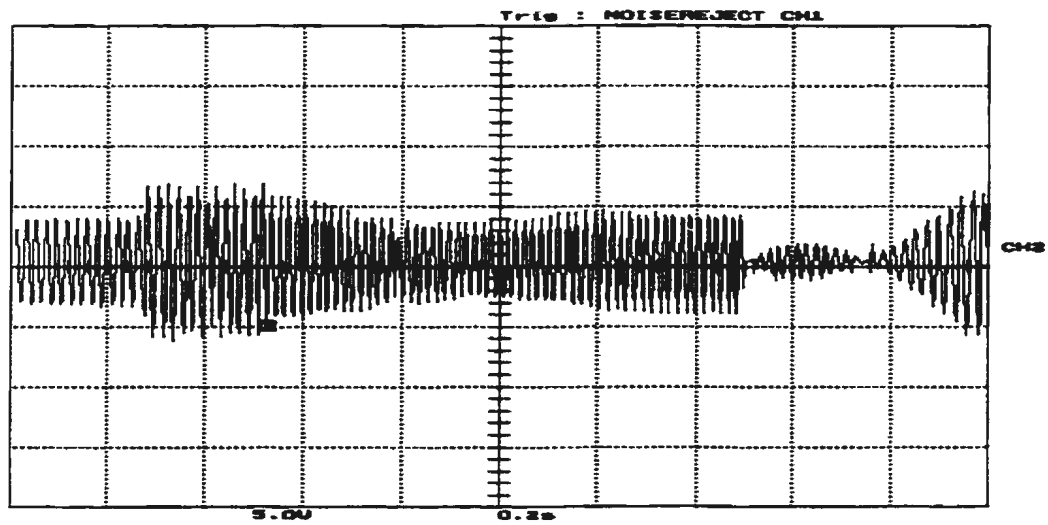


(b)

Figure 5.14: Drive responses for step change in the speed command at half load, (a) speed response (speed scale 66.67 rad./sec./div) and (b) q-axis current (current scale 1.25A/ div).

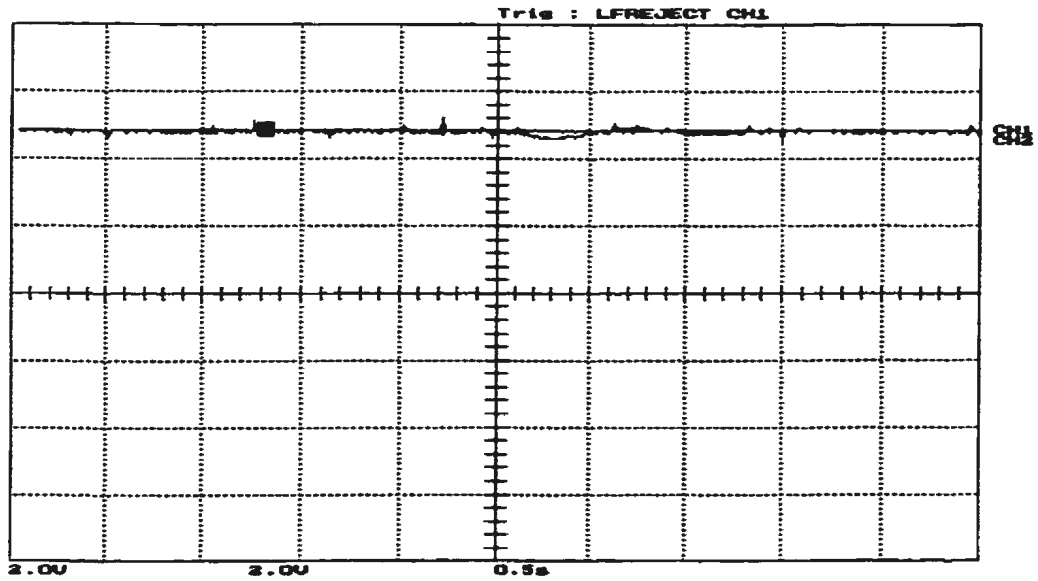


(a)

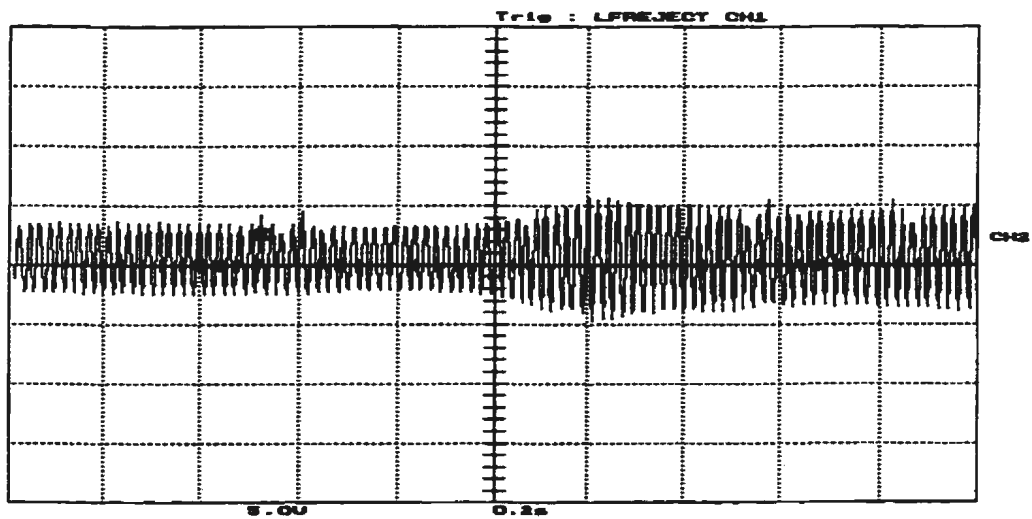


(b)

Figure 5.15: Drive response for step change in the command speed at full load, (a) speed response (speed scale 66.67 rad./sec./div) and (b) motor phase current (current scale 3A/div).

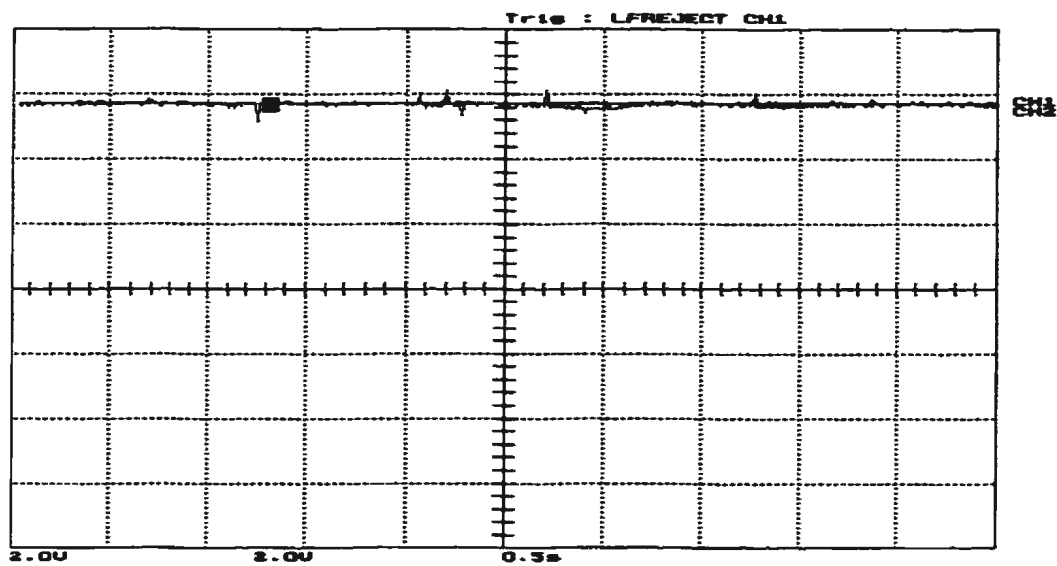


(a)

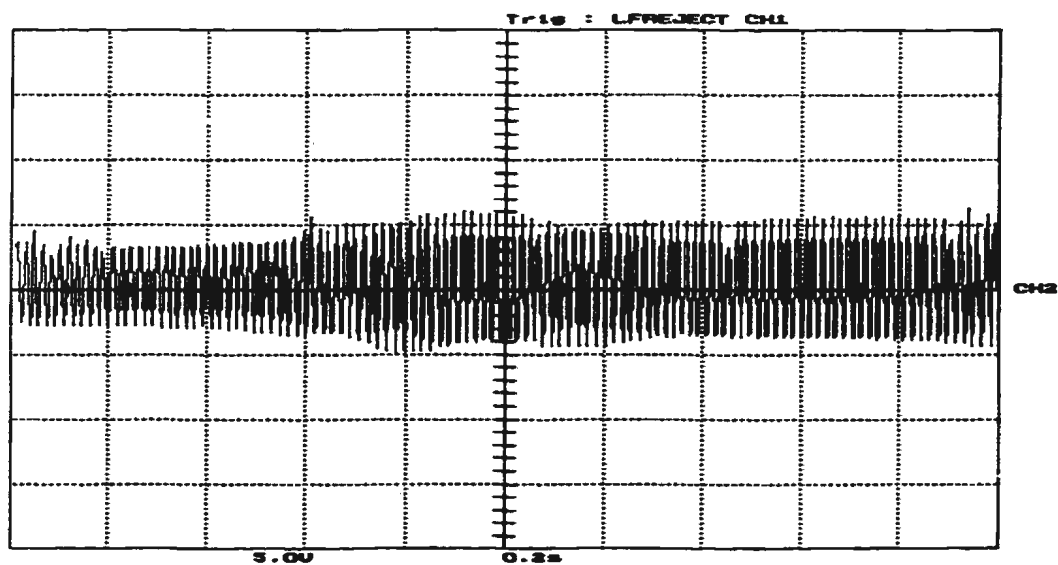


(b)

Figure 5.16: Drive response for step change in load with speed command of 150 rad./sec, (a) speed response (speed scale 66.67 rad./sec./div) and (b) motor phase current (current scale 3A/div).



(a)



(b)

Figure 5.17: Drive response for change in load with speed command of 188 rad/sec., (a) speed response (speed scale 66.67 rad/sec/div) and (b) motor phase current (current scale 3A/div).

Chapter six

Conclusion

This thesis explores the role of the permanent magnet synchronous motor in a drive system. A complete PMSM drive system has been developed. Analytical and experimental studies have been presented. The design of multi-loop control for interior type PMSM for high performance has been developed. Speed controller using synchronous reference frame PI regulator is employed as an outer loop. Moreover, two synchronous frame PI regulators are employed as inner loops to control the direct and quadrature axis current components of the motor. The controllers are based on the indirect field orientation.

General machine theory is systematically analyzed and the Park's transformation model has been presented. The torque expressions for the PMSM are derived. The PMSM drive system is developed using the PWM inverter system. The multi-loop control method of speed and current controllers is developed. Based on the transfer function, the parameters of each PI controller are determined. The simulation has been carried out using the field oriented vector control techniques for decoupling the direct and quadrature axis control quantities. By forcing the d-axis current component to zero has resulted in a linear model of the drive system in the rotating reference frame. Designs of the speed and current controllers were based on the linear model. The multi-loop control

method was applied to the 1 hp, 208V. laboratory permanent magnet synchronous motor. The computed results have shown fast responses with small overshoots. The simulation results have been successfully confirmed via laboratory implementation of the PMSM drive system. In this thesis a digital signal processor board DS1102 has been successfully used for on-line control of the PMSM drive.

The permanent magnet motors are now being increasingly used in high efficiency and high performance, industrial drives requiring constant speed, low noise and minimum maintenance. The use of voltage source PWM inverters made the permanent magnet synchronous motor ideally suitable for domestic and commercial air conditions. Japanese are one of major producers of the neodymium boron iron permanent magnet motors. The improved operational characteristics of the inverter-fed permanent magnet synchronous motor make these drives competitive in terms of overall production cost and economy.

- The application of the synchronous reference frame PI regulators for speed and current loops has shown the effectiveness of the multiple loop control of a PMSM drive.
- The speed and current responses have shown minimum overshoots and fast dynamic responses.
- The theoretical and experimental results have confirmed the efficacy of the proposed multiple loops control scheme.
- The proposed control scheme has useful application in the motor drives where the dynamic responses affect greatly the quality of the manufactured products.

References

- [1] M. A. Rahman and G.R. Slemon, "the promising applications of NdBFe magnets in Electrical Machines (invited)", *IEEE Trans. on Magnetics*, Vol. MAG-21, no.5, 1985, pp. 1712-1716.
- [2] A. R. Wheeler, "Comparison of electrical variable speed drives", Intl. Conf. on Power Electronics and Variable Speed Drives, *IEE conf. Publication*, no. 234, London, 1984, pp. 175-179.
- [3] E. Richter, T. J. E. Miller, T. W. Neumann and T. I. Hudson" The ferrite permanent magnet ac motor-a technical and economical assessment", *IEEE Trans. Industry Applications*, Vol. IA-21, no.4, May/June 1985, pp. 644-650.
- [4] V. B. Honsinger, " The fields and parameters of interior type ac permanent magnet machines", *IEEE Trans. on Power Apparatus and Systems*, Vol. PAS-101, no.4, April 1982, pp. 867-875.
- [5] M. A. Rahman, T. A. Little and G. R. Slemon, "Analytical models for interior-type permanent magnet synchronous motors", *IEEE Trans. on Magnetics*, Vol. MAG-21, no.5, September 1985, pp. 1741-1743.
- [6] T. Sebastian, G. R. Slemon and M. A. Rahman, "Design considerations for variable speed permanent magnet motors", *Proc. International Conf. on Electrical Machines*, 1986, pp. 1099-1102.

- [7] M. A. Rahman and P. Zhou, "Field analysis brushless permanent magnet synchronous motors", *IEEE Trans. on Industrial Electronics*, Vol. 43, no.2, April 1996, pp. 256-267.
- [8] R. J. Parker, R. J. Studders, "*Permanent magnets and their applications*", (John Wiley and Sons), 1962.
- [9] Chee-Mun Ong, "*Dynamic simulation of electrical machinery using Matlab/Simulink*", prentice hall, 1998.
- [10] M. A. Rahman, "High efficiency permanent magnet synchronous motors", *IEEE /IAS Conf. Record, Annual meeting*, 1979, pp. 561-564.
- [11] M. A. Rahman, "Permanent magnet synchronous motors- A review of the state of design", *Proceedings of ICEM, Athens*, Sep 1980, pp. 312-319.
- [12] F. Blashke, "The principle of field orientation as applied to the transvector closed control system for rotating field machines", *Siemens Review*, Vol. 34, May 1972, pp. 217-220.
- [13] K. Hasse, "On the dynamic behavior of induction machine driven by variable frequency and variable voltage sources", *ETZA, BD. 89, H. 4*, 1968, pp. 77-81.
- [14] P. Vas, "*Vector control of ac drives*", Prentice- Hall, Englewood Cliffs, New Jersey 1986.
- [15] R. Krishnan, "Selction criteria for servo motor drives", *IEEE Trans. on Industry Applications*, Vol. IA-23, no.2, March/April, 1987.
- [16] P. Pillay and R. Krishnan, "Modeling of permanent magnet motor drives", *IEEE Trans. Industrial Electronics.* , Vol.35, no.4, Nov. 1988, pp. 537-541.

- [17] P. Pillay and R. Krishnan, "Modeling, simulation, and analysis of permanent magnet motor drives, Part I: The permanent-magnet synchronous motor drive", *IEEE Trans. Ind. Applications*, Vol. 25, no.2, March/April 1989, pp. 265-273.
- [18] P. Pillay and Krishnan, "Modeling, analysis and simulation of a high Performance, vector controlled, permanent magnet synchronous motor drive", *IEEE/IAS Annual Meeting Conf. Record*, 1987, pp. 253-261.
- [19] P. Pillay, and Krishnan, "Control Characteristics and speed controller design for a high performance permanent magnet synchronous motor drive", *IEEE Trans. on Power Electronics*, Vol. 5, no.2, April 1990, pp. 151-159.
- [20] B. K. Bose and P. M. Szczesny, "A microcomputer-based control and simulation of an advanced IPM synchronous machines drive system for electric vehicle propulsion", *IEEE Trans. Ind. Electronics.*, Vol. 3, no. 4, Nov. 1988, pp. 547-559.
- [21] F. Harashima, S. Konodo, K. Ohnishi, M. Kajota and M. Susono, "Multimicroprocessor based control system for quick response induction motor drive", *IEEE Trans. Industry Applications*, Vol. IA-21, no.4, May/June 1985, pp. 602-608.
- [22] T. H. Liu and C. H. Liu, "A Multiprocessor-based fully digital control architecture for permanent magnet synchronous motor drives", *IEEE Trans. on Power Electronics*, Vol. 5, no.4, Oct. 1990, pp.413-422.
- [23] P. Pillay, C. R. Allen and R. Budhabhathi, "DSP-Based vector and current controllers for a permanent magnet synchronous motor drive", *IEEE/IAS Annual Meeting Conf. Record*, Seattle, Washington, 1990, pp. 539-544.
- [24] M. L. Majenc, C. Villanueva and J. Hector, "Study and implementation of hysteresis controlled inverter on a permanent magnet synchronous machines", *IEEE*

- Trans. on Industry Applications*, Vol. IA-21, no.2, march /April 1985, pp. 408-413.
- [25] H. Le Huy and L. A. Dessaint, "An adaptive current control scheme for PWM synchronous drives: Analysis and simulation", *IEEE Trans. on Power Electronics*, Vol.4, no.4, , October 1989, pp. 486-495.
- [26] H. Le-Huy, K. Slimani and P. Viarouge, " Analysis and implementation of a real-time predictive current controller for permanent magnet synchronous servo drives", *IEEE Trans. on Industrial Electronics*, Vol. 41, no.1, February 1994, pp. 110-117.
- [27] D. M. Brod and D. W. Novotny, "Current control of VSI-PWM inverters", *IEEE Trans. on Industry Applications*, Vol. IA-21, no. 4, May/June 1985, pp. 562-570.
- [28] T. S. Radwan, M. A. Rahman, A. M. Osheiba and A. E. Lashine, "Performance of hybrid current controlled VSI fed permanent magnet synchronous motor drive", *IEEE power electronics specialists conference, PESC 96 record*, Vol. 1, June 23-27, Baveno, Italy, 1996, pp. 951-957.
- [29] P. C. Krause, "*Analysis of Electric Machinery*", McGraw Hill, 1986.
- [30] D. M. Triesenberg, "*Electric Power Systems*", Purdue University, 1978.
- [31] T. A. Lipo, "Recent progress in the development of solid state ac motor drives", *IEEE Trans. on Power Electronics*, Vol.3, no. 2, April 1988, pp. 105-117.
- [32] M. H. Rashid, "*Power electronics circuits, devices and applications*", second edition, Prentice Hall, 1993, pp.376-378.
- [33] J. Vithayathil "*Power Electronics Principles and Application*", McGraw-Hill, 1995, pp. 333-362.

- [34] Controller for synchronous ac drive running on DS1101, application notes preliminary document version 1.0, *dSPACE, Digital signal processing and control engineering, GmbH*, August 17, 1992.
- [35] Y. Murai, T. Watanabe and H. Iwasaki, "Waveform distortion and correction circuit for PWM inverter with switching lag-times", *IEEE-IAS Conf. Record*, 1985, pp. 436-441.
- [36] Simulink, The Math Works Inc., 1993.

Appendices

Appendix A

Permanent magnet synchronous motor design data

A 3-phase, 1hp, 208V, 3A, permanent magnet synchronous motor was tested in the laboratory. The magnet is samarium cobalt type with magnetic flux constant of 0.3 volts/rad./sec. The parameters of the motor is given as

Rated power = 1hp

Number of poles = 4

Stator resistance $r_s = 1.93 \Omega$

q-axis inductance $l_q = 0.07957 \text{ H}$

d-axis inductance $l_d = 0.04244 \text{ H}$

Rotor inertia constant $J_m = 0.003 \text{ kg.m}^2$

Viscus coefficient $B_m = 0.0008 \text{ N.m / rad/ sec.}$

Appendix B

Subsystem description

This Appendix presents the details of the subsystem blocks for the simulink model as shown in Figure D. Figure D.1 shows the multiple feedback loop controls. The inputs will be d-q axis current components of the motor and it will be compared with d-q axis current commands. They are employed as an inner loop, the speed sensed from the motor, which will be compared with the reference speed and is employed as outer loop of the system. These will generate d-q voltage commands. Figure D.2 shows these voltage commands converted by Park's transformation to variables a, b, c voltage commands. Figure D.3 shows that voltage commands compared with triangular wave and the output is three logic states N_A , N_B , N_C . Figure D.4 represents the inverter and the input will be the three logic states and dc voltage V_B and the output is the actual voltage to the motor. Figure D.5 shows the inverse Park's transformation to generate d-q axis motor voltages. Figure D.6 shows the permanent magnet synchronous motor voltage equation and the output will be d-q axis current components, rotor position and speed. These outputs will be fed to Figure D.1 as feedback for the multi-loop control to compare with d-q axis current components and speed commands. Figure D.7 shows the conversion from d-q axis current to the actual currents of the motor using Park's transformation.

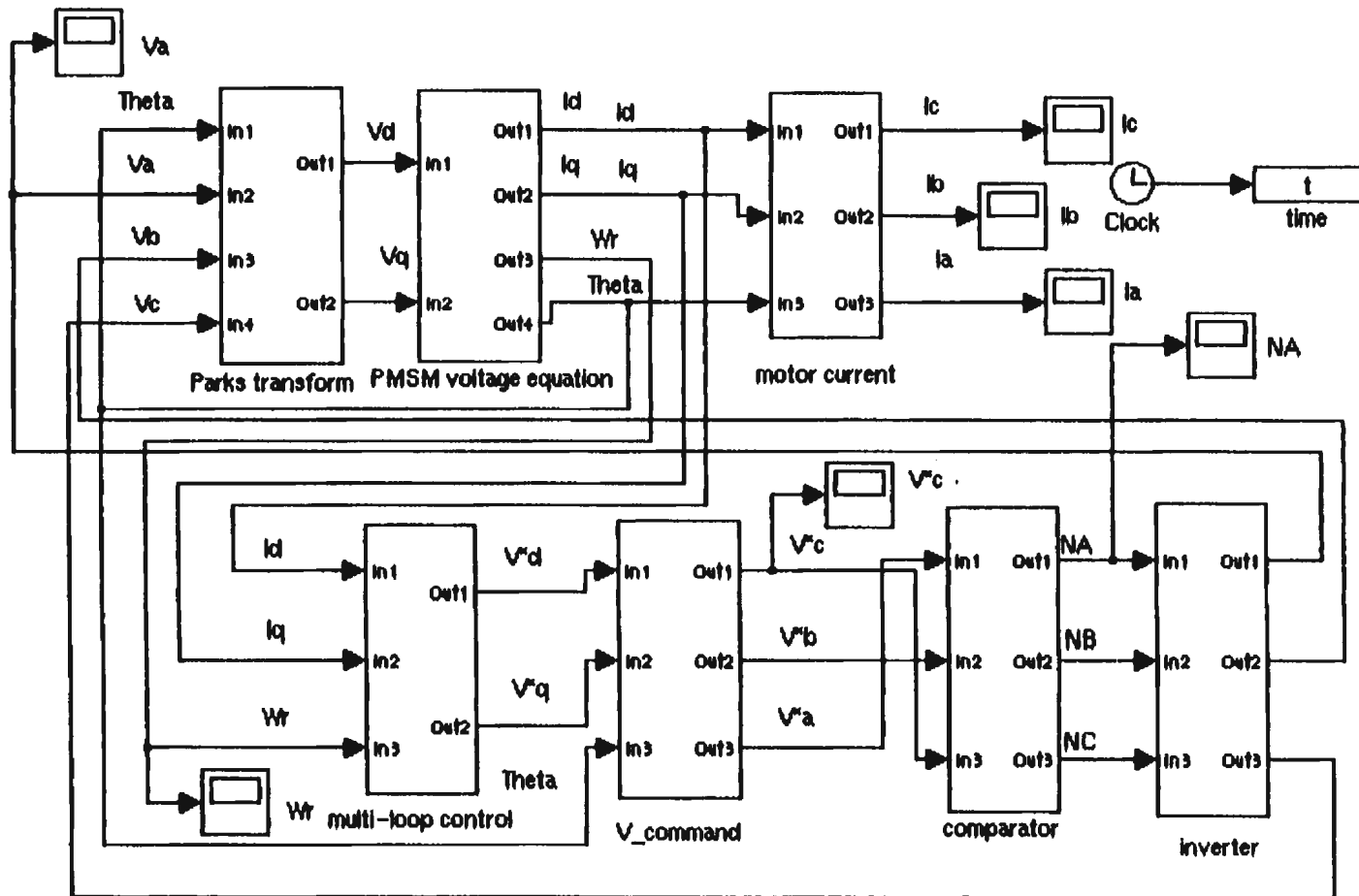


Figure D: Simulink model of the drive system

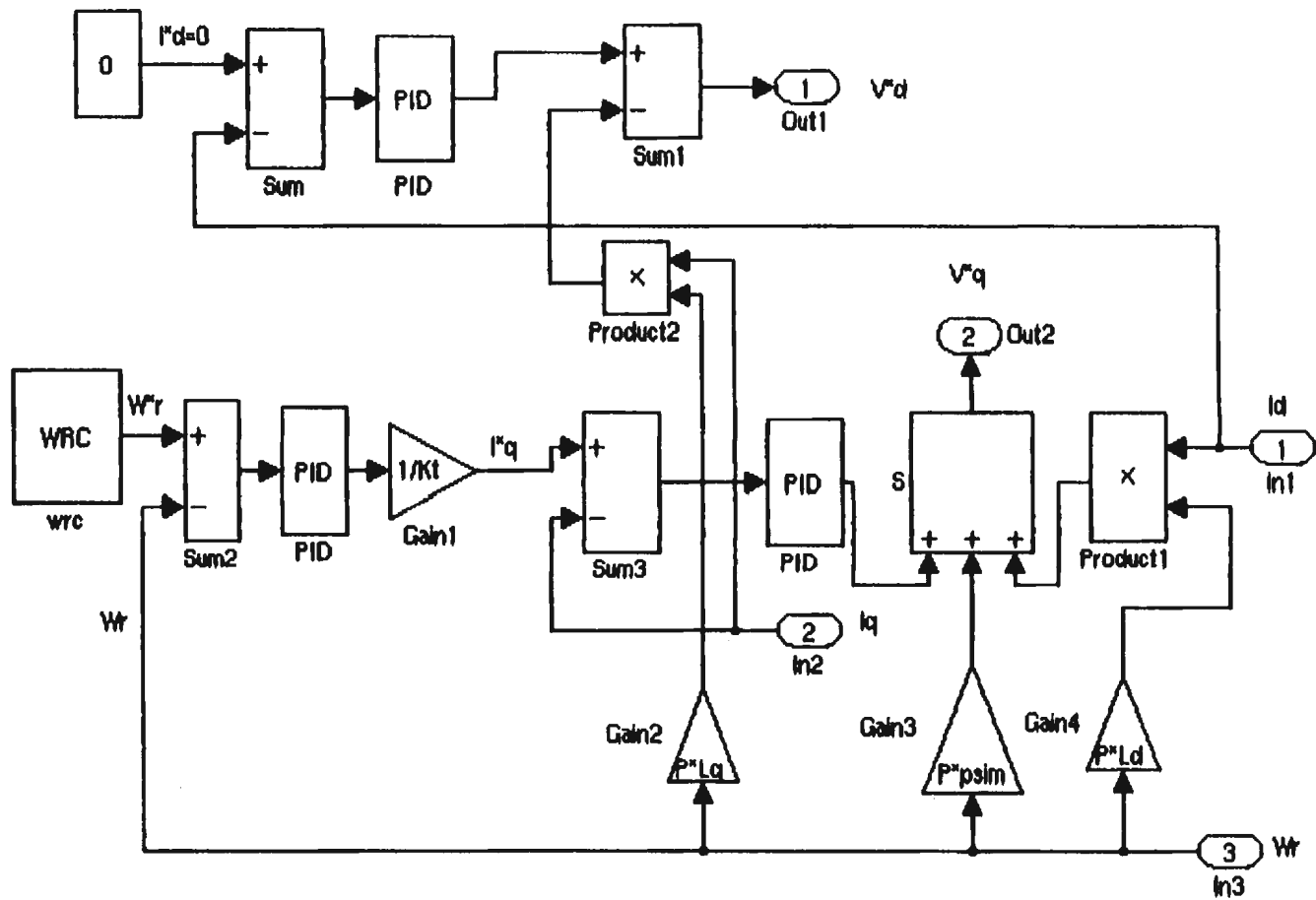


Figure D.1: Multi-loop control subsystem.

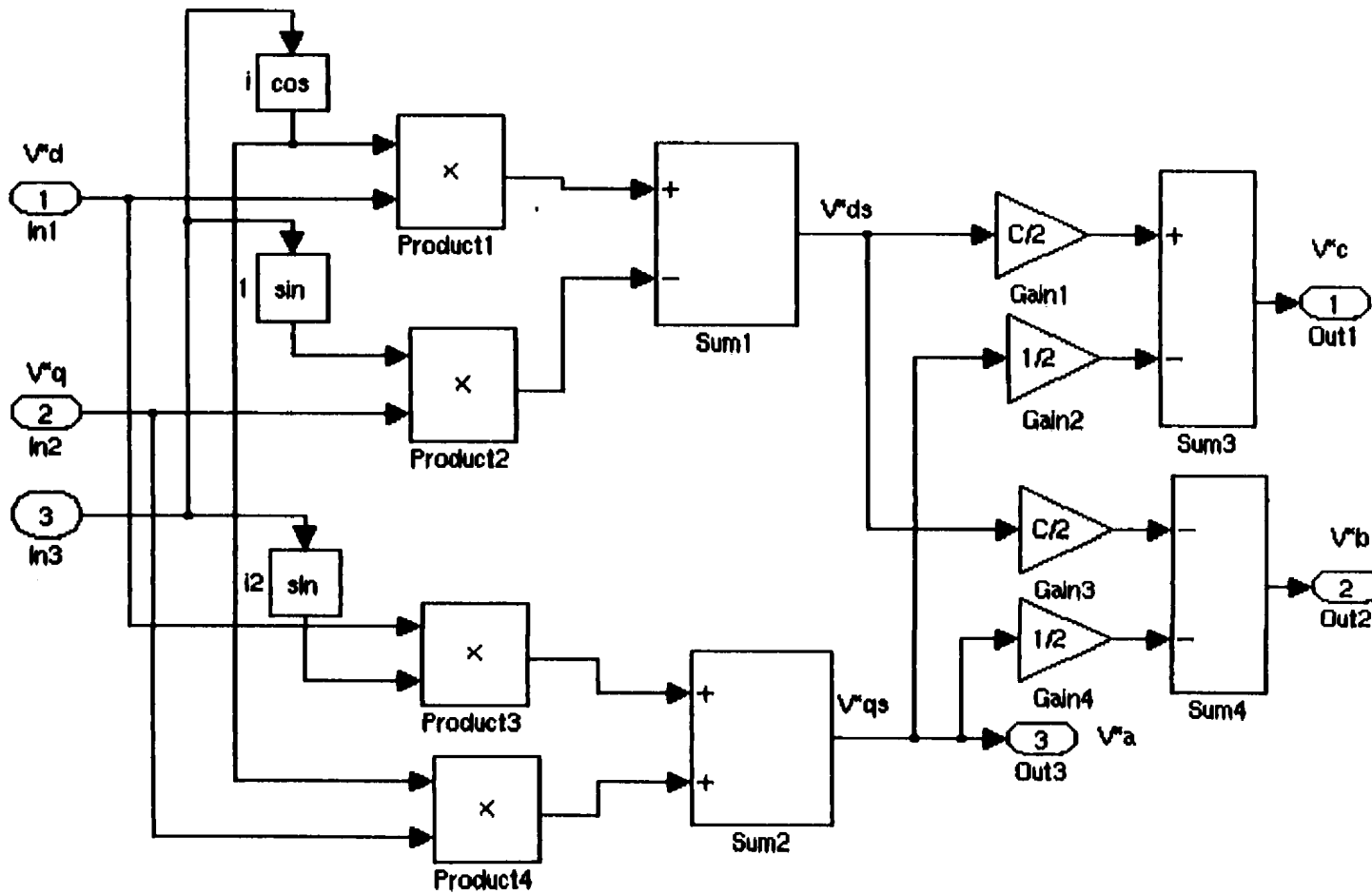


Figure D.2: $V_command$ subsystem

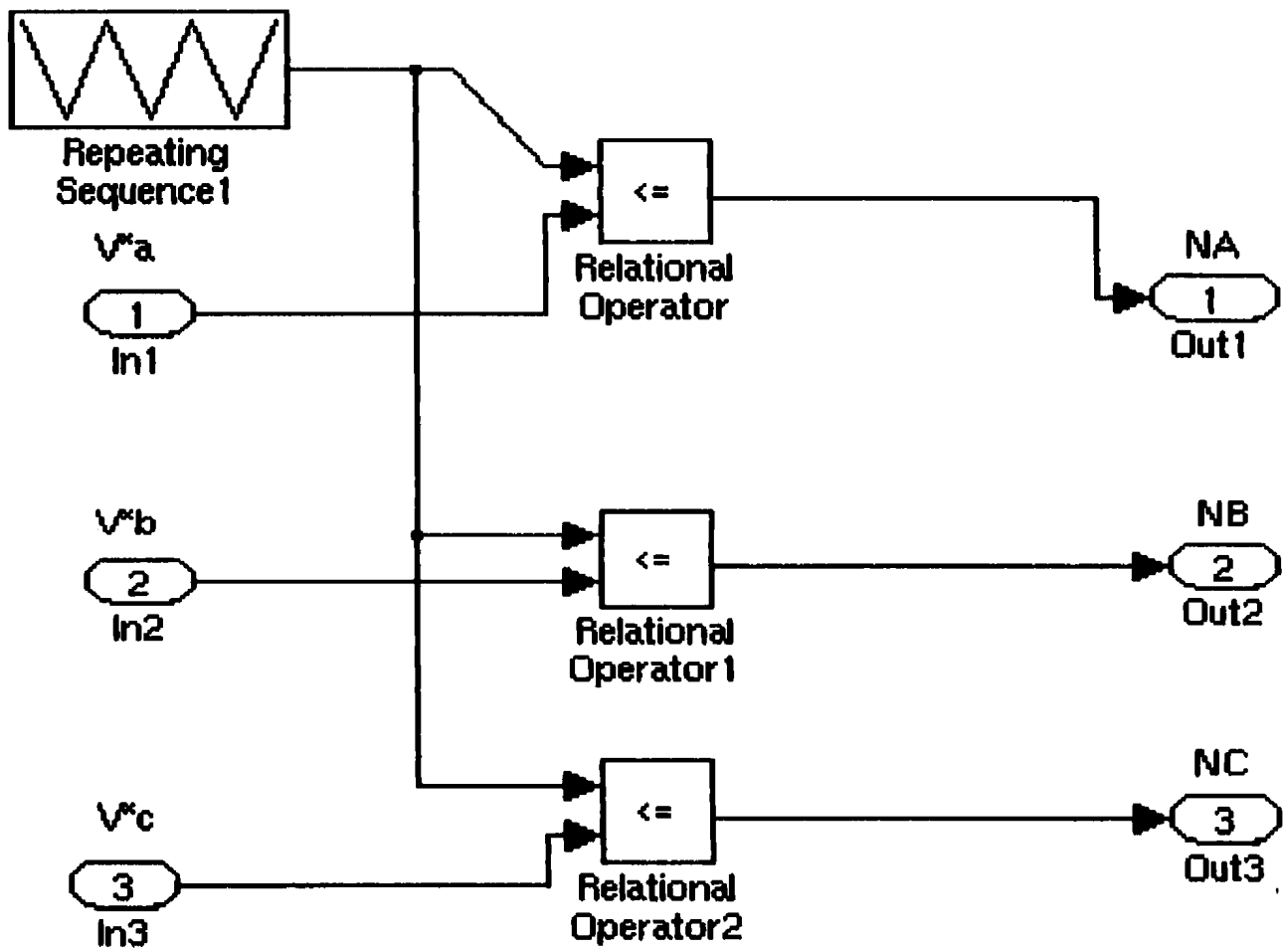


Figure D.3: Comparater subsystem

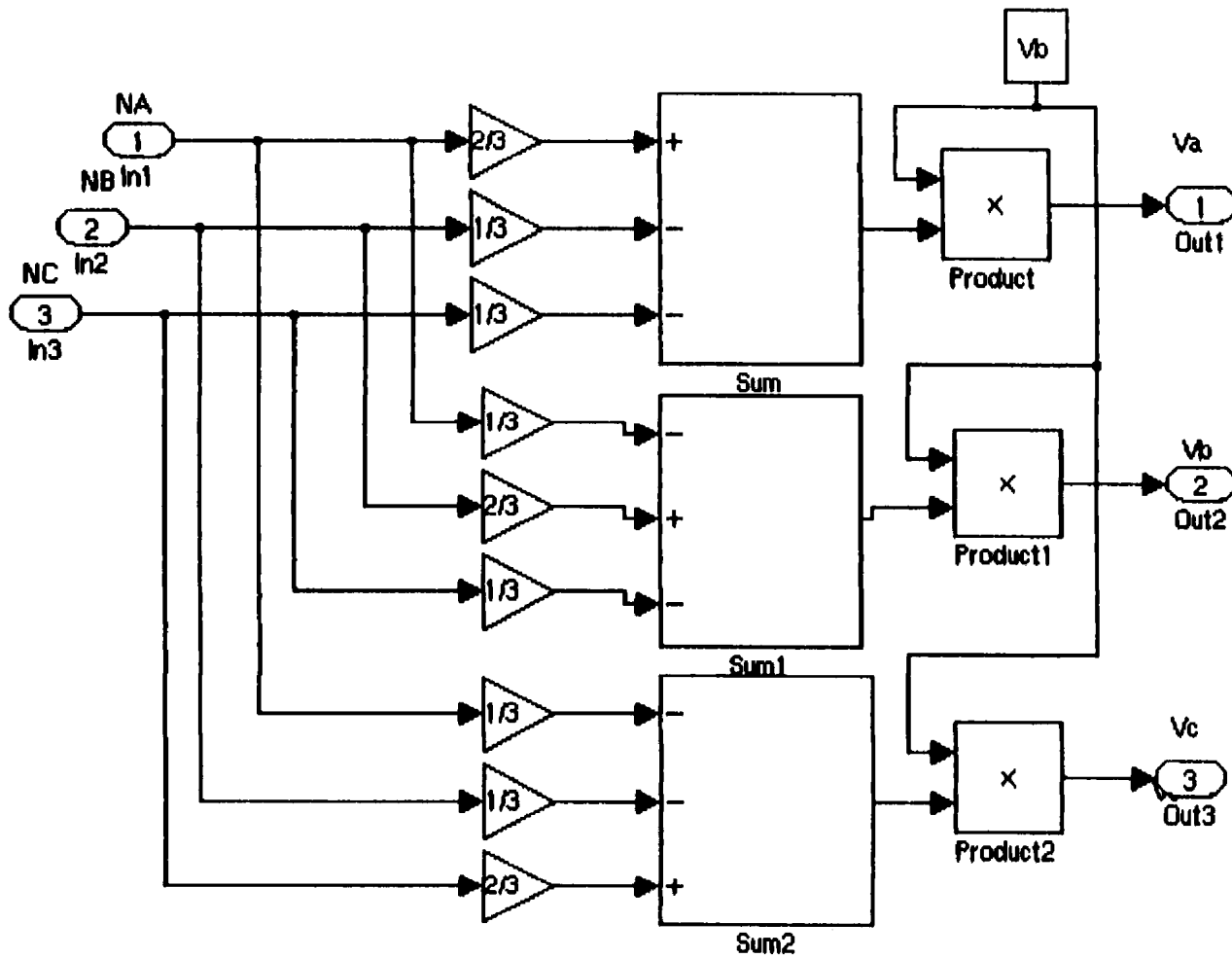


Figure D.4: Motor voltage subsystem

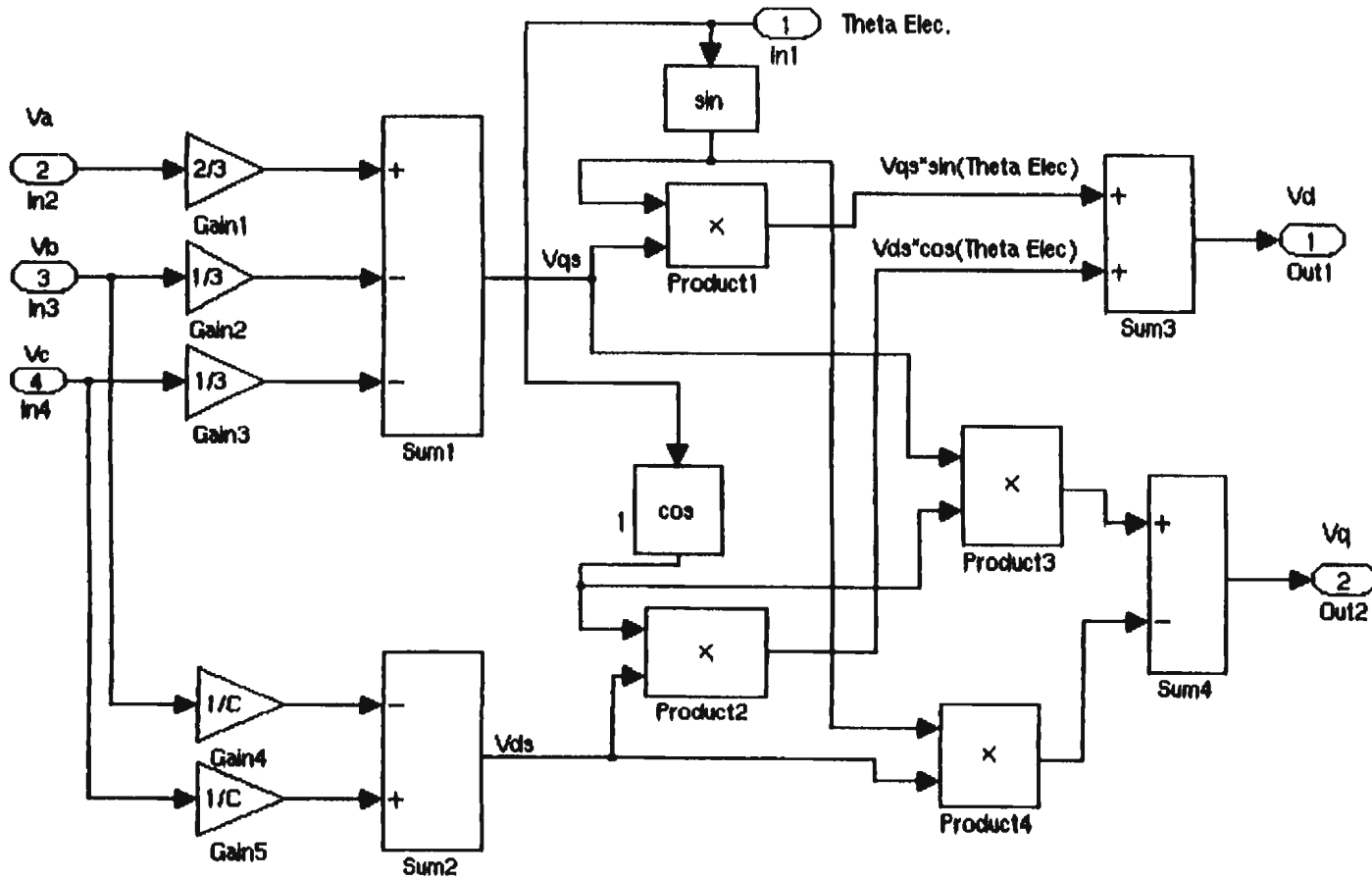


Figure D.5: Park's transformation subsystem

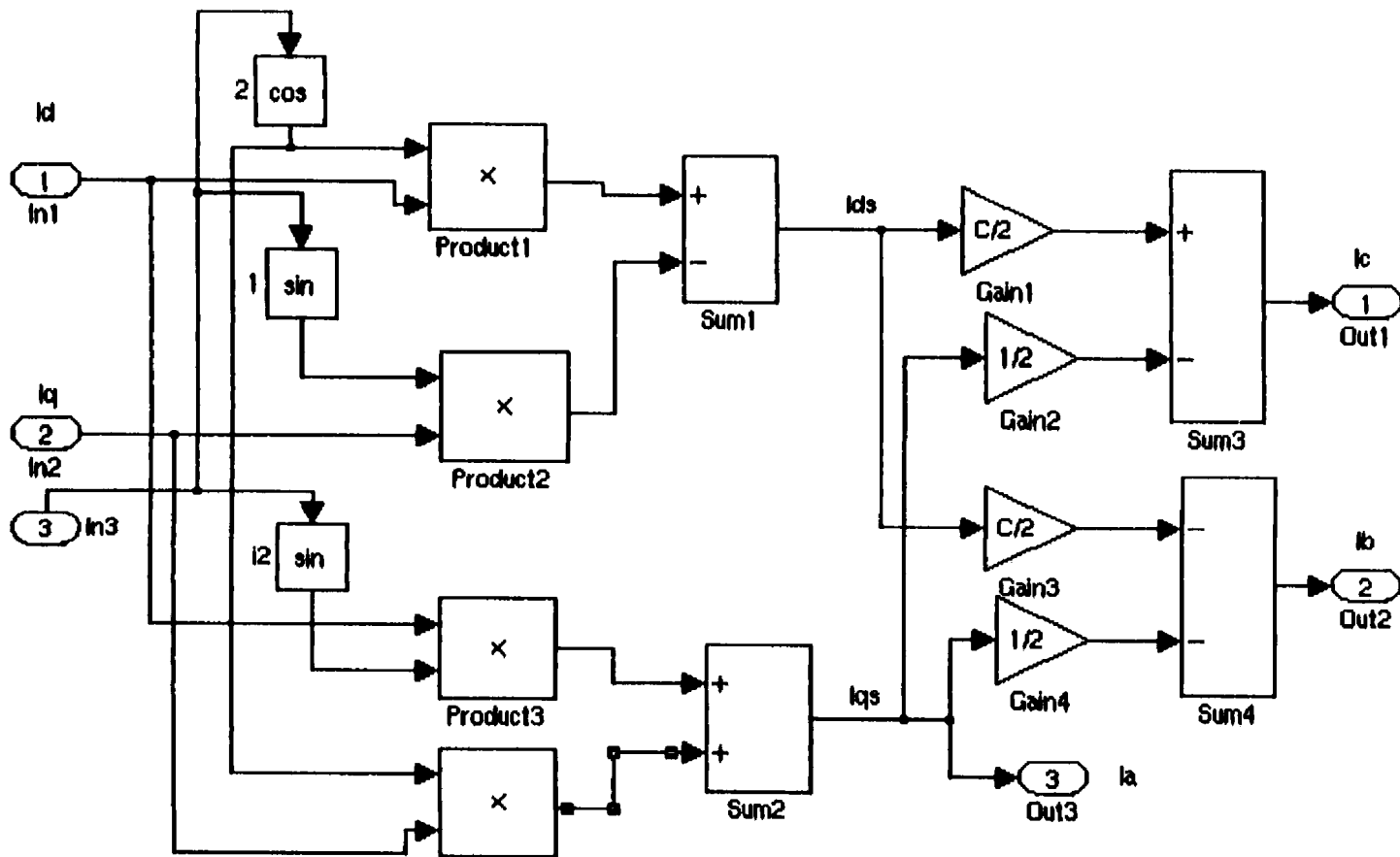


Figure D.7: Motor current subsystem

Appendix C

dSPACE DS1102 controller board

- **The main processor.**

The TMS320C31 third generation floating point DSP is a high performance member of Texas Instruments' TMS320 family of VLSI digital signal processors. It performs parallel multiply and arithmetic logic unit (ALU) operations on integers or floating point.

Some key features of the TMS320C31 are:

- 50 ns single cycle instruction execution time
- Two 1k*32-bit dual access on chip data RAM blocks
- 64*32-bit instruction cache
- 32-bit instruction and data words, 24-bit addresses
- 40/32-bit floating point/ integer multipliers and ALU
- 32-bit barrel shifter
- Eight 40-bit accumulators
- Two independent address arithmetic units
- DMA controller for concurrent DMA and CPU operation
- Four external interrupts
- Two 32-bit timers

- **Incremental encoder sub-system**

The DS1102 contains two incremental sensor interfaces to support optical incremental as shown in Figure C.1. Each interface contains line receivers for input signals. A digital noise filter which eliminates spikes on the line, a quadrature decoder which converts the sensed phase information to count-up and count-down pulses, a 24-bit counter which holds the current position of the sensor and a 24-bit output latch are included in the system. The minimum encoder state width is 120ns resulting in a maximum count frequency of 8.3 MHz.

- **A/D subsystem**

The DS1102 contains two types of A/D converters

- Two 16-bit auto-calibration sampling A/D converters with integrated sample/holds and the conversion time is 10 μ s.
- Two 12-bit sampling A/D converters with integrated sample/ holds and a conversion time of 3 μ s.

- **D/A subsystem**

The DS1102 contains a quad 12-bit D/A converter with programmable output voltage ranges. The D/A subsystem consists of four registers, a mode register and strobe bit in the input/output control register (IOCTL). The DACs have single ended voltage outputs with ± 10 V span. The return lines of the outputs are connected to the system ground. For applications requiring an emergency shut-down a DAC reset feature has been implemented which can be used to force all output voltages to zero.

- **Digital I/O subsystem**

The DS1102's digital subsystem is based on the TMS320P14 digital signal processor. Besides a 16-bit fixed point DSP core, it has a bit-selectable parallel I/O port, four timers, six PWM circuits, four capture inputs and a serial interface. The TMS320P14 contains firmware making all on-chip peripherals accessible by the TMS320C31. After power up the DSP executes an I/O server firmware residing in its built-in program PROM. This PROM has been augmented by an external program RAM providing a program download feature which allows application specific DSP programs to be executed in parallel to TMS32C31.

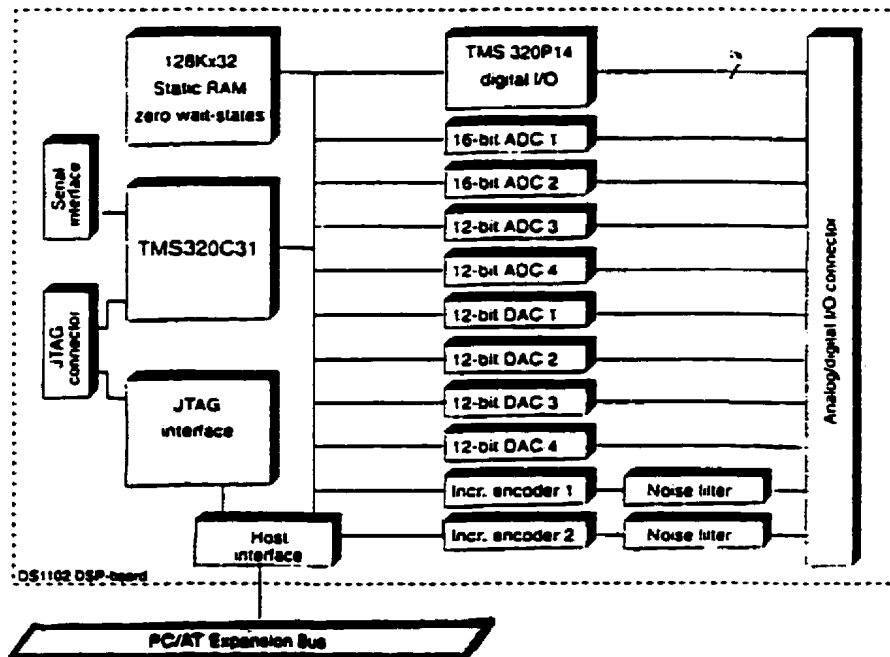


Figure C.1: Block diagram of the DS1102 DSP board

Appendix D

C programs on DSP board

The high level language C program is written to implement and control the drive system of PMSM on the DSP controller board. The program will read the motor phase currents by the analog to digital converters A/D on the DS1102 controller board. The rotor information is read by incremental encoder channel. The program then processes the control algorithm and writes the outputs to the digital output board and D/A converters.

The second program is written to change the drive speed from the computer keyboard. The command speed is entered from the keyboard and downloaded to the DSP board.

The programs are compiled with the help of TI C compiler and Borland C compiler. Then the object codes are downloaded to the controller board using the dSPACE software loader program.

Appendix E

Program listing

```

/*****Implementation of PMS motor drive under vector control*****/
/*****Filename saad.c*****/

#include"brtenv.h"
#include"math.h"
#define TS      1.000e-4      /*****sampling period ***/
#define WRCC   150          /**reference speed*****/
#define KP     .2           /**proportional gain*****/
#define KI     1.1         /**Integral gain*****/
#define KPQ    55
#define KIQ    .005
#define KPD    300
#define KID    10
#define psi    .313
#define LD     .04244
#define LQ     .07957
#define K_T    1.065        /*****K_T=1/kt*****/
#define SQR3   1.732        /**** square root of3****/
#define TCC    1000.        /***TCC=1/N*TS*****/
#define PI     3.14159      /*****pi*****/
#define INCG   3216.990877  /*****encodergain*****/
#define P      2            /*number of pairpole****/
#define M      130         /* triangularamplitude**/
#define TC     2.e-4       /* half period oftrig.**/
#define f_trg  2500.       /* triangularfreesquency*/
#define band   .06        /* some hysteresisband**/
#define IDC    0.0
#define one_3  .333333
#define one_r3 .57735
long int i,N=0,NA,NA1,NB,NB1,NC,NC1,IO;
double i_a, i_b, i_c,THI,TH, WR=0.0, DW2, DW1=0.0, TEC=0.0,IQC;
double VQ=0.0, VD=0.0, VQC, VDC, DIQ2, DID2, DIQ1=0.0, DID1=0.0;
double id, iq, VAC, VBC ,VCC, TH1=0.0, TH2=0.0, TH3,TH4, THE, WRC,x,y;
double D_errorA, D_errorB, D_errorC, delta_wrc, time=0.0,
ic,test_start;

/****error flag for chkerror31 at last dual-port memorylocation*****/

int *error = (int *) (DP_MEM_BASE+DP_MEM_SIZE-1);

/*****timer0 interrupt service routine*****/

ISR_t0()
{
begin_isr_t0(*error);
ds1102_ad_start();
i_a=10.5*ds1102_ad(3);
i_b=10.5*ds1102_ad(4);
}

```

```

i_c=-(i_a+i_b);
THI=ds1102_inc(1);
TH=THI*INCG;
test_start=dp_mem[1].f;
/*test_start=ds1102_ad(1);*/
if(test_start==0){
i=ds1102_inc_read_index(1);
    if(i>0){
        ds1102_inc_clear_counter(1);
        if(TH>0) TH2=TH2-2.*PI;
        if(TH<0) TH2=TH2+2.*PI;
    }
}
if(N>=10){
    TH1=TH2;
    TH2=TH;
    N=0;
    TH3=TH2-TH1;
    TH4=TH3;
    if(TH4<0.0) TH3=TH3+2.*INCG;
    WR=TH3*TCC;
}
delta_wrc=dp_mem[0].f;
WRC=WRCC+delta_wrc;
if(WR>1.1*WRC){
    WR=WRC;
}
if(WR<0.0){
    WR=WRC;
}
N+=1;
THE=P*TH;
DW2=WRC-WR;
TEC=TEC+(KP+KI*TS)*DW2-KP*DW1;
DW1=DW2;
if(WR>.5*WRC){
    if(fabs(TEC)>3.) TEC=3.;
}
else {
    if((TEC>45.) || (TEC<30.)) TEC=40;
}
x=cos(THE);
y=sin(THE);
iq=one_3*x*(2*i_a-i_b-i_c)+one_r3*y*(i_b-i_c);
id=one_3*y*(2*i_a-i_b-i_c)+one_r3*x*(i_c-i_b);
IQC=TEC*K_T;

DIQ2=IQC-iq;
VQ=VQ+(KPQ+KIQ*TS)*DIQ2-KPQ*DIQ1;
DIQ1=DIQ2;
DID2=IDC-id;
VD=VD+(KPD+KID*TS)*DID2-KPD*DID1;
DID1=DID2;
VQC=VQ+P*WR*(psi+LD*id);
/* if(VQC>100) VQC=100; */
/* if(VQC<0) VQC=100; */

```

```

VDC=VD-iq*WR*P*LQ;
/* if(abs(VDC)>2) VDC=0;*/
VAC=VQC*x+VDC*y;
VBC=-.5*VQC*x-.5*VDC*y+.5*SQR3*VQC*y-.5*SQR3*VDC*x;
VCC=-(VAC+VBC);

/*****PWM controller algorithm*****/

D_errorA=VAC;
D_errorB=VBC;
D_errorC=VCC;

/*****triangular wave generation*****/

if(time<=TC){
    ic=M-time*(4.*M*f_trg);
}
else if(time<=2.*TC){
    ic=-M+(time-TC)*(4.*M*f_trg);
}
else time=0.0;
time+=TS;

/*****

if(VAC>0.0){
    if(D_errorA>ic+band) NA=1;
    else NA=0;
}
else NA=0;
    if(VAC<0.0){
        if(D_errorA<ic-band) NA1=1;
        else NA1=0;
    }
    else NA1=0;
if(VBC>0.0){
    if(D_errorB>ic+band) NB=1;
    else NB=0;
}
else NB=0;
    if(VBC<0.0){
        if(D_errorB<ic-band) NB1=1;
        else NB1=0;
    }
    else NB1=0;
if(VCC>0.0){
    if(D_errorC>ic+band) NC=1;
    else NC=0;
}
else NC=0;
    if(VCC<0.0){
        if(D_errorC<ic-band) NC1=1;
        else NC1=0;
    }
    else NC1=0;
ds1102_da(3,.003*WRC);
ds1102_da(4,.003*WR);

```

```

IO=NA+2*NC1+4*NB+32*NA1+64*NC+128*NB1; /* Output signals from I/O*/
  ds1102_p14_write_io_register(0,0,IO);
  service_trace();
  end_isr_t0();
}

/*****

main()
{
  init(); /*init DAC mode, calibrate ADCs */
  init_slave_DSP_digital_i_o(); /* initialize i/o port as output
*/
  *error=NO_ERROR; /* initialize overload error flag
*/
  dp_mem[0].f=0.0; /* init 1st dp-mem loc for type
float */
  dp_mem[1].f=0.0; /* init 2nd dp-mem loc for typr
float */
  ds1102_inc_clear_counter(1); /* clear incremental encoder
counter */
  start_isr_t0(TS); /* initialize sampling clock timer
*/

  while(*error==NO_ERROR); /* background process */
}

/*****initialization of digital I/O port as output*****/

init_slave_DSP_digital_i_o()
{
  ds1102_p14_pin_io_init(0x00e7);
}

```

```

/*****Filename saad1.c*****/
/* dspeed.c for change speed command from the keyboard*****/

#include <stdlib.h>
#include <stdio.h>

#include <clib.h>          /* Host-DSP interface library include file
*/

#define DP_MEM_OFFS      0          /* use first dual-port memory address
*/

unsigned int board_index;
float speed,delta_speed;
void close_and_exit (int error_code)
{
    DSP_unregister_host_app();
    exit(error_code);
}

void write_dual_port_memory (UInt32 address, UInt32 value)
{
    int error;
    error = DSP_lock_board(board_index);
    if(error != DSP_NO_ERROR)
    {
        printf("Error: can't lock board error = %d.\n\n",error);
        close_and_exit(5);
    }
    error = DSP_write_dual_port_memory(board_index, address, value);
    DSP_unlock_board(board_index);
    if(error != DSP_NO_ERROR)
    {
        printf("Error %d writing the DSP board's dual-port memory !\n\n",
            error);
        close_and_exit(5);
    }
}

void main (int argc, char *argv[])
{
    int error;

    printf("\n dspeed  ``change speed reference from key
board...''\n\n");

    if(argc != 2)
    {
        printf("Usage: dspeed board\n\n");
        exit(1);
    }

    error = DSP_register_host_app("dspeed");
    if(error != DSP_NO_ERROR){
        switch(error){
            case DSP_DEVICE_DRIVER_NOT_FOUND:
                printf("\nDevice Driver not installed.\n");

```

```

        break;
    case DSP_VXD_NOT_LOADED:
        printf("\nVirtual device driver not installed.\n");
        break;
    case DSP_NO_FREE_HOST_APP_IDX:
        printf("\nNo free host application index.");
        break;
#ifdef NET
    case DSP_NET_ERROR:
        printf("\nNetwork error.");
        break;
#endif
    default:
        printf("\nDSP_register_host_app: error code %d\n",error);
        break;
    }
    exit(1);
}

error = DSP_board_index(argv[1], &board_index);
if(error != DSP_NO_ERROR)
{
    printf("\nBoard %s not registered, error = %d.\n",
        argv[1], error);
    close_and_exit(2);
}

/* initialize output signal with 0.0 */
write_dual_port_memory(DP_MEM_OFFS,
    DSP_cvt_ieee_to_ti((Float32) 0.0));

/* set output signal to speed */
do{
    printf("\n please enter the delta_speed in rpm...\n");
    scanf("%f", &delta_speed);
    speed=delta_speed*0.104719755;
    write_dual_port_memory(DP_MEM_OFFS,
        DSP_cvt_ieee_to_ti((Float32) speed));
} while (delta_speed!=0.0);
printf("Press RETURN to abort ...\n");
rewind(stdin);
getchar();

/* reset output signal to 0.0 */
write_dual_port_memory(DP_MEM_OFFS,
    DSP_cvt_ieee_to_ti((Float32) 0.0));

close_and_exit(0);
}

```

